AFOSR - TR - 75 - 1559

APPROVED FOR PUBLIC RELEASE, DISTRIBUTION UNLIMITED

ALEX(02)-TR-75-01-PART A

SOURCE STUDIES IN THE NEAR- AND FAR-FIELD

SEMI-ANNUAL TECHNICAL REPORT NO. 4 - PART A
1 NOVEMBER 1974 TO 30 APRIL 1975

Prepared by
Lawrence S. Turnbull, James C. Battis, David Sun
and Alan C. Strauss

TEXAS INSTRUMENTS INCORPORATED
Equipment Group
Post Office Box 6015
Dallas, Texas 75222

Contract No. F44620-73-C-0055
Amount of Contract: $294,749
Beginning 23 April 1973
Ending 30 June 1975

Prepared for

AIR FORCE OFFICE OF SCIENTIFIC RESEARCH

Sponsored by

ADVANCED RESEARCH PROJECTS AGENCY
Nuclear Monitoring Research Office
ARPA Program Code No. F10
ARPA Order No. 1827

30 May 1975

Acknowledgment: This research was supported by the Advanced Research Projects Agency, Nuclear Monitoring Research Office, under Project VELA-UNIFORM, and accomplished under the direction of the Air Force Office of Scientific Research under Contract F44620-73-C-0055.

APPROVED FOR PUBLIC RELEASE, DISTRIBUTION UNLIMITED

ALEX(02)-TR-75-01-PART A

SOURCE STUDIES IN THE NEAR- AND FAR-FIELD

SEMI-ANNUAL TECHNICAL REPORT NO. 4 - PART A
1 NOVEMBER 1974 TO 30 APRIL 1975

Prepared by
Lawrence S. Turnbull, James C. Battis, David Sun
and Alan C. Strauss

TEXAS INSTRUMENTS INCORPORATED
Equipment Group
Post Office Box 6015
Dallas, Texas 75222

Contract No. F44620-73-C-0055
Amount of Contract: $294,749
Beginning 23 April 1973
Ending 30 June 1975

Prepared for

AIR FORCE OFFICE OF SCIENTIFIC RESEARCH

Sponsored by

ADVANCED RESEARCH PROJECTS AGENCY
Nuclear Monitoring Research Office
ARPA Program Code No. F10
ARPA Order No. 1827

30 May 1975

Acknowledgment: This research was supported by the Advanced Research Projects Agency, Nuclear Monitoring Research Office, under Project VELA-UNIFORM, and accomplished under the direction of the Air Force Office of Scientific Research under Contract F44620-73-C-0055.

ABSTRACT

Examination of the seismic source from both the near- and far-fields has been undertaken. Using a discrete Fourier transform (DFT) and a maximum entropy spectral estimator on near-field acceleration data produced corner frequency and low frequency level estimates. This latter estimator eliminates leakage, thereby obtaining more accurate values for the high frequency end, with better roll-off values and definition of side lobes. When the maximum entropy spectral estimator was applied to data from the Parkfield earthquake and the Bear Valley event of June 22, 1973, the lower frequency level was lower than that from the DFT in all cases.

Using spectral fitting procedures on fundamental mode surface wave data from two central California events, generally close agreement was obtained with source mechanism solutions from bodywaves. For the Bear Valley earthquake of June 22, 1973, the seismic moment obtained from the surface wave data was an order of magnitude smaller than that obtained from acceleration data. In an effort to reduce the scatter in M_s - m_b plots for an earthquake population, several attempts were made to reduce the variance in M_s. Both demultipathing and correcting for the radiation pattern had no effect. It was concluded that the variance of m_b is the controlling factor. Finally, theoretical higher mode surface wave spectra was generated for a double couple source in a layered half space. Both the Rayleigh and Love wave higher mode spectra were found to vary shape dramatically as a function of source depth.

TABLE OF CONTENTS

LIST OF FIGURES

LIST OF FIGURES
(continued)

LIST OF FIGURES
(continued)

LIST OF FIGURES
(continued)

LIST OF FIGURES
(continued)

LIST OF FIGURES
(continued)

LIST OF TABLES

SECTION I

SPECTRAL ESTIMATES OF NEAR-FIELD ACCELERATION

A. INTRODUCTION

The results of the analysis of the Bear Valley Earthquake of June 22, 1973 using the Haskell moving dislocation model (Turnbull and Battis, 1974) demonstrate the high degree of non-uniqueness of the source parameters solution for a given event using this source representation. In this study three equally satisfactory solutions, judged solely on the quality of the velocity waveform fit, were found. Two of the solutions were essentially the same except for a shift in epicentral location of 2 kilometers. The third solution, however, was radically different in both dip angle and dislocation amplitude. Without externally imposed restrictions on the source structure, such as fault plane solution, seismic moment and fault dimensions, it is obvious that fault models generated with the Haskell model cannot be considered as valid indicators of the true source structure of an event.

While fault plane solutions cannot generally be obtained from near-field acceleration data alone, using techiques of spectral analysis in conjunction with a source model, such as that given by Brune (Brune, 1970), one can obtain estimators of the seismic moment and corner frequency. These, in turn, provide an estimate of source dimensions and total dislocation which can be used to limit the range of solutions derived from time domain waveform modeling of the earthquake source.

Therefore, in an effort to limit the degree of non-uniqueness of the Haskell source model, and to analyze the consistancy of the source parameters between time domain and frequency domain representations of the earthquake source, a program of spectral analysis of the available near-field acceleration data was implimented. The initial results from this work, using the discrete Fourier transform, were given in a previous report (Turnbull and Battis, 1974). However, they have subsequently been found to be in error. This section will discuss this error, and its effects on the results, and additional techniques adapted during this report period to provide better spectral estimation from near-field acceleration data.

B. FAST FOURIER TRANSFORM SPECTRAL ESTIMATOR

The discrete Fourier transorm (DFT) technique for obtaining a spectral estimator is well documented and no discussion of the theory will be given here. It was this form of analysis which was initially programmed for the spectral analysis of near-field acceleration data (Turnbull and Battis, 1974). In this program the autocorrelation function of the data was calculated as an intermediate step in the process, with the amplitude spectra being evaluated by Fourier analysis of the autocorrelation estimator. The rational for utilizing this system was that the appropriate filtering process could be judged more accurately on the basis of the behavior of the autocorrelation function than directly from the acceleration data.

The use of the autocorrelation function to determine the filtering characteristics proved satisfactory. However, a programming error associated with the normalization of the autocorrelation function induced errors in the evaluated amplitude spectra. These errors take the form of a scale factor dependent on the time gate of the analyzed signal, specifically

$$A(f) = A^{*}(f) / (\sqrt{T/2})$$

where $A(f)$ is the correct amplitude, $A^{*}(f)$ is the original calculated amplitude and T is the signal duration. The effect is to reduce the observed amplitudes and thus the low frequency level of the spectra. However, no change in the spectral shape occurs.

We have previously reported on the source parameters of 18 earthquakes derived from DFT spectral analysis of accelerometer data (Turnbull, et al., 1974b). As no change in the spectral shape occurs from this error, the evaluated corner frequencies (f_o) are still valid. The low frequency level (Ω_o), being improperly scaled, does change, in turn affecting the estimated seismic moment for each event.

The calculated seismic moments have been corrected and are given in Table I-1. In all cases, the seismic moments have been reduced and generally conform better with other estimates.

C. MAXIMUM ENTROPY SPECTRAL ESTIMATOR

The use of the DFT for spectral estimation from near-field acceleration data has one prominent drawback effecting the spectral evaluation of source characteristics. Windowing effects, in the form of power leakage from one frequency to another, produce high levels of noise in the DFT spectrum (Figures I-1, I-2, and I-3). A common example of this effect is the spurious side lobes which occur in the DFT spectrum of a pure sinusoid. This condition can be corrected by smoothing the spectrum, but this, in turn, reduces the prominence of any spectral peaks. In addition, since the smoothing process can be seen as a weighted averaging process on the spectrum, the accuracy of the calculated amplitudes within some localized bandwidth can be biased by a prominent peak or hole in the spectra located near this frequency band of interest.

Both effects of windowing are of importance when one is attempting to evaluate the spectral parameters which are considered characteristic of the earthquake source, specifically the corner frequency, f_o, and low frequency level, Ω_o. From previous work in this area, it would appear that the most consistent method of determining the corner frequency is to locate the maximum

TABLE I-1

CORRECTED PARAMETERS FROM SPECTRAL ANALYSIS OF NEAR-FIELD ACCELEROGRAM DATA

(PAGE 1 OF 5)

Event/Site	M_L Local Magnitude	R Hypocentral Distance (km)	Corner Frequency f_o (Hz)	Low Frequency Spectral Level Ω_o (cm-sec)	Seismic Moment M_o (dyne-cm)
Bear Valley (6-22-73)	3.5				
Station 2		10.6	2.7	0.0152	1.75×10^{22}
Station 4		10.9	2.3	0.005	6.48×10^{21}
Station 7		11.2	2.0	0.043	5.36×10^{22}
Station 8		11.1	2.2	0.063	7.47×10^{22}
San Fernando Earthquake Series (2-9-71)					
Main Shock	6.6				
Pacoima Dam		16.4	0.60	8.33	1.5×10^{25}
Orion Boulevard		28.5	0.60	4.42	1.39×10^{25}
First Street		46.1	0.73	1.06	5.48×10^{24}
Figueroa Street		46.1	0.93	0.913	4.75×10^{24}

TABLE I-1

CORRECTED PARAMETERS FROM SPECTRAL ANALYSIS OF NEAR-FIELD ACCELEROGRAM DATA
(PAGE 2 OF 5)

Event/Site	M_L Local Magnitude	R Hypocentral Distance (km)	Corner Frequency f_o (Hz)	Low Frequency Spectral Level Ω_o (cm-sec)	Seismic Moment M_o (dyne-cm)
Aftershocks Recorded At Pacoima Dam					
Event 1	5.5	18.0	5.0	0.021	4.07×10^{22}
Event 4	4.9	15.0	4.3	0.009	1.34×10^{22}
Event 10	4.8	12.0	5.5	0.009	1.24×10^{22}
Event 11	5.4	12.0	3.0	0.057	7.46×10^{22}
Event 16	4.4	7.0	6.7	0.005	3.84×10^{21}
Event 30	4.6	17.0	3.7	0.008	1.52×10^{22}
Kern County (6-21-52)	7.7				
Pasadena		126.9	0.94	0.520	7.25×10^{24}
Taft		41.4	1.3	0.647	2.94×10^{24}
Hollywood Stage B		120.3	0.90	0.367	4.87×10^{24}

TABLE I-1

CORRECTED PARAMETERS FROM SPECTRAL ANALYSIS OF NEAR-FIELD ACCELEROGRAM DATA
(PAGE 3 OF 5)

Event/Site	M_L Local Magnitude	R Hypocentral Distance (km)	Corner Frequency f_o (Hz)	Low Frequency Spectral Level Ω_o (cm-sec)	Seismic Moment M_o (dyne-cm)
Borrego Mountain (4-8-68)	6.5				
El Centro		67.3	0.50	2.37	1.75×10^{25}
San Diego		107.3	0.72	0.46	5.40×10^{24}
San Onofre		134.3	0.72	0.37	5.40×10^{24}
Parkfield (6-27-66)	5.6				
Station 2		58.6	1.4	1.07	6.89×10^{24}
Station 5		56.1	2.0	0.36	2.22×10^{24}
Station 8		83.7	2.3	0.165	1.51×10^{24}
Station 12		53.5	2.2	0.039	2.32×10^{23}
Temblor		59.6	2.6	0.24	1.55×10^{24}
Western Washington (4-13-49)	7.1				
Seattle		57.7	1.2	0.496	3.13×10^{24}
Olympia		16.9	1.1	1.26	2.33×10^{24}

TABLE I-1

CORRECTED PARAMETERS FROM SPECTRAL ANALYSIS OF NEAR-FIELD ACCELEROGRAM DATA (PAGE 4 OF 5)

Event/Site	M_L Local Magnitude	R Hypocentral Distance (km)	Corner Frequency f_o (Hz)	Low Frequency Spectral Level Ω_o (cm-sec)	Seismic Moment M_o (dyne-cm)
Puget Sound (4-29-49)	6.5				
Olympia		60.9	1.1	0.47	3.13×10^{24}
Helena, Montana (10-31-35)	6.0				
Helena		5.82	2.4	0.094	5.90×10^{22}
North West, California (9-11-38)	5.5				
Ferndale		55.1	2.4	0.73	4.33×10^{23}
North West, California (2-9-41)	6.6				
Ferndale		103.6	1.6	0.079	8.98×10^{23}

TABLE I-1

CORRECTED PARAMETERS FROM SPECTRAL ANALYSIS OF NEAR-FIELD ACCELEROGRAM DATA (PAGE 5 OF 5)

Event/Site	M_L Local Magnitude	R Hypocentral Distance (km)	Corner Frequency f_o (Hz)	Low Frequency Spectral Level Ω_o (cm-sec)	Seismic Moment M_o (dyne-cm)
Northern, California (9-22-52)	5.5				
Ferndale		43.2	1.3	0.20	9.56×10^{23}
Wheeler Ridge (1-12-54)	5.9				
Taft		42.8	1.4	0.10	4.75×10^{23}

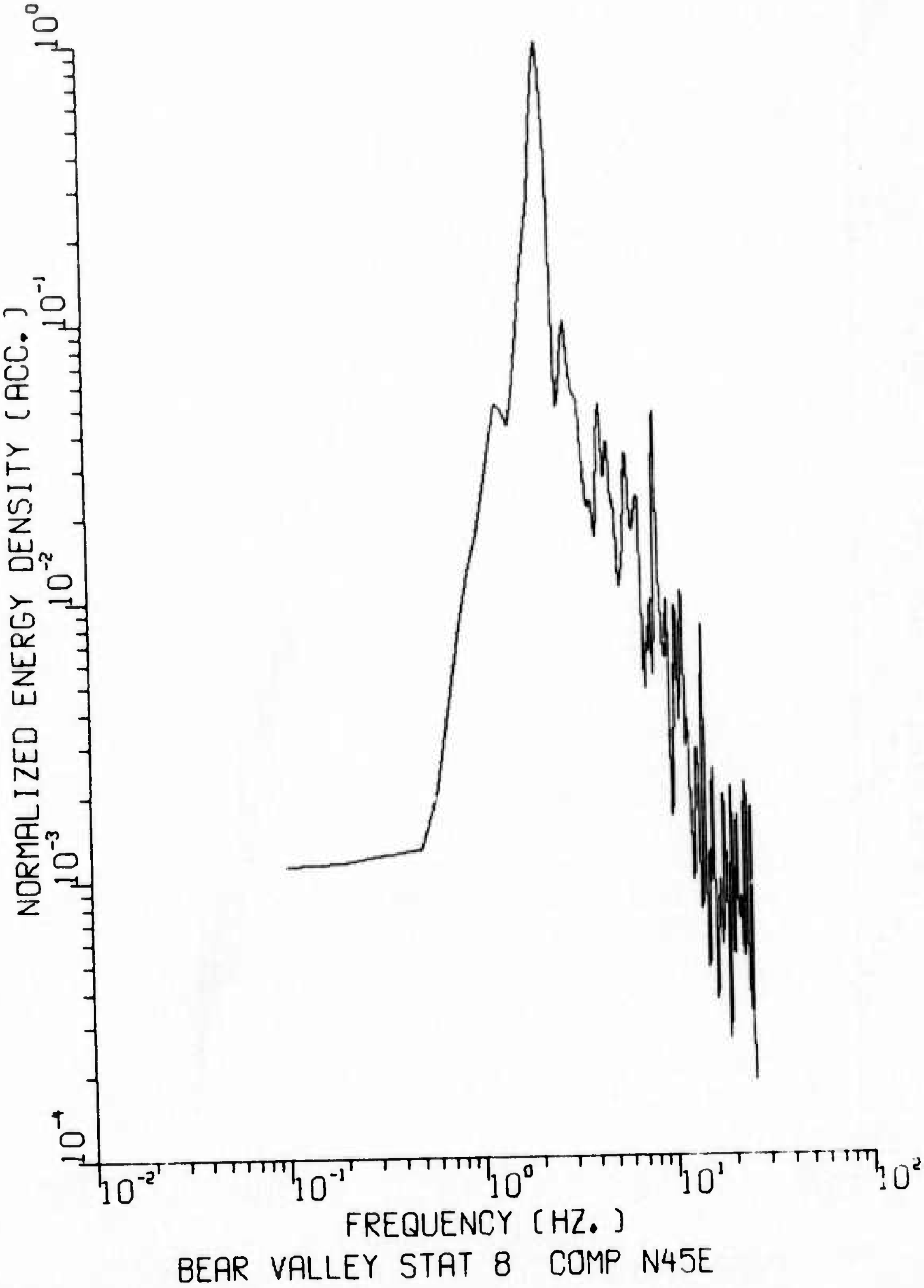

FIGURE I-1

NORMALIZED DFT ACCELERATION ENERGY DENSITY SPECTRUM FOR N45°E COMPONENT OF STATION 8; BEAR VALLEY EARTHQUAKE OF JUNE 22, 1973 (HIGH PASS FILTER CORNER FREQUENCY AT 0.7 Hz)

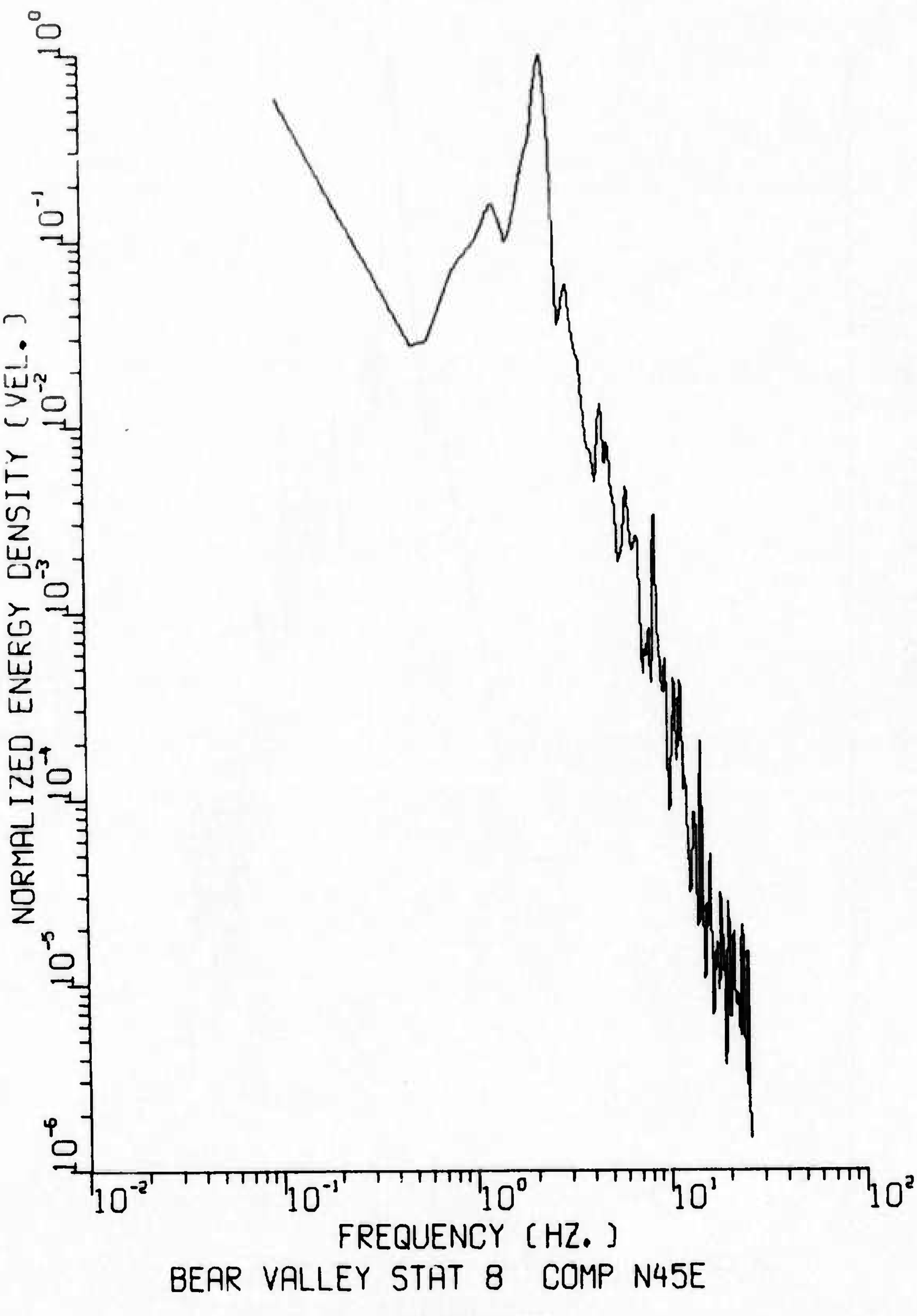

FIGURE I-2

NORMALIZED DFT VELOCITY ENERGY DENSITY SPECTRUM FOR N45°E COMPONENT OF STATION 8; BEAR VALLEY EARTHQUAKE OF JUNE 22, 1973 (HIGH PASS FILTER CORNER FREQUENCY AT 0.7 Hz)

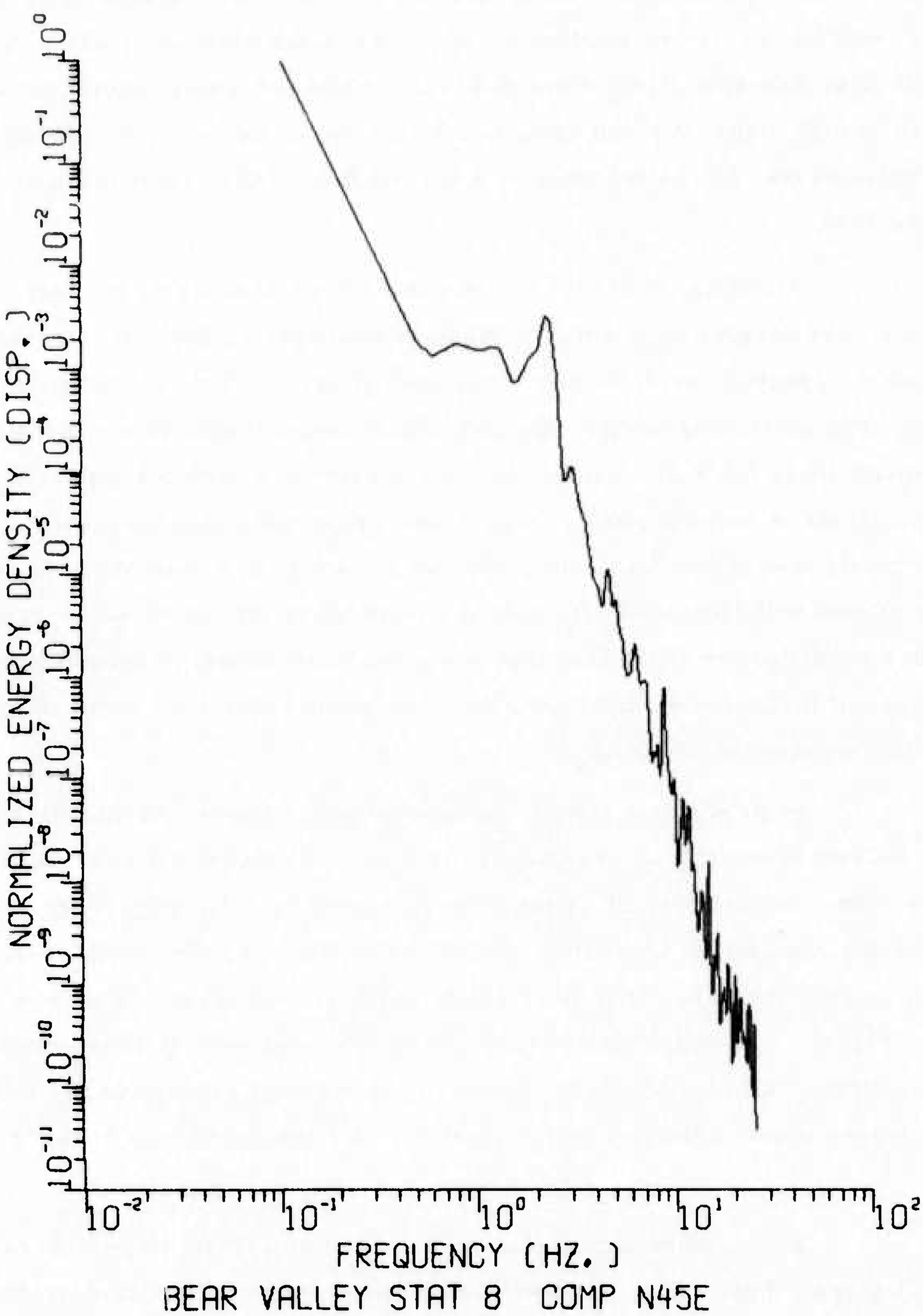

FIGURE I-3

NORMALIZED DFT DISPLACEMENT ENERGY DENSITY SPECTRUM FOR N45°E COMPONENT OF STATION 8; BEAR VALLEY EARTHQUAKE OF JUNE 22, 1973 (HIGH PASS FILTER CORNER FREQUENCY AT 0.7 Hz) peak in the velocity spectrum. However, if a smoothed DFT spectrum is used, the peak will be lowered in amplitude and its bandwidth widened, making the accurate determination of f_o more difficult. While not truely significant in the case of high signal to noise data, this effect can be important in low signal to noise cases such as station 2 or 4 for the Bear Valley earthquake of June 22, 1973.

Secondly, it is inherent in the methods of applying the instrument response correction to obtain a displacement spectra from acceleration data that the spectral level, as zero frequency is approached, should go to infinity. For an accelerometer, the instrument correction to obtain displacement spectrum is $(2\pi f)^{-2}$. If the acceleration spectrum does not approach zero amplitude at zero frequency in a manner producing a limited low frequency level, then at low frequency, the spectrum will be unbounded. Windowing effects will then boost Ω_o and, if smoothing is attempted on the spectrum, a further amplification of the low frequency level will occur. Depending on the degree of leakage and smoothing, this may greatly effect the estimation of seismic moment based on Ω_o.

In an effort to reduce the errors from leakage and smoothing the maximum entropy or Markov spectral estimator was adapted for near-field acceleration data analysis. This method, developed by John Burg (Burg, 1967) of Texas Instruments Incorporated, has the advantage over the standard DFT that, in theory, it has no windowing effects and thus no leakage (King, et al., 1974). Therefore, a smooth amplitude spectrum is obtained while maintaining high resolution. Of course, the accuracy of the spectral estimation is limited by the degree to which the processed signals match the hypothesis of the technique.

A simplified explanation of the maximum entropy spectral estimator is given below. More detailed examinations of the method and its comparison with other spectral analysis methods can be found in papers by

Barnard (1975), King, et al. (1974), Ulrych (1972), Burg (1968), and Lacoss (1971). The following is a summary of Section III of this report by King, et al.

The two basic equations of discrete power spectral evaluation (the square of the amplitude spectrum) are those which define the discrete autocorrelation function, $\phi(\tau)$, and the discrete power spectrum, P(f). These are given as

$$\phi(\tau) = \frac{1}{2T+1} \sum_{N=-T}^{T} X_N X_{N+\tau} \qquad (-\infty < \tau < \infty)$$

and

$$P(f) = \frac{1}{W} \sum_{\tau=-\infty}^{\infty} \phi(\tau) \cos(2\pi f \tau \Delta t), \qquad (0 \leq f \leq W = 1/2\Delta\tau)$$

where $\Delta\tau$ is the sampling period of the discrete time series. As $\phi(\tau)$ is known exactly for all lags, then the power spectrum has infinite resolution within the band limit W.

This requires that $\phi(\tau)$ be known exactly for all lags. As we are dealing with a finite data set, this does not hold. Any physically realistic values of $\phi(\tau)$ may be used to supplement the known values, but a criteria for judging what is a realistic value may be hard to determine. In many cases the data, X_N, beyond the known signal is defined as zero, producing a tapered autocorrelation function which introduces windowing effects. Depending on the transitory nature of the signal this may or may not be realistic.

The maximum entropy estimator takes a different approach and attempts to supplement the autocorrelation function in some "optimum" manner. This optimum manner chosen in the maximum entropy technique is that which maximizes the degree of disorder, or entropy, of the resulting power spectrum. Given N known lags of the autocorrelation function, the manner in which the N + 1 lag is evaluated while guaranteeing a non-negative definite autocorrelation function, and without modifying the known lags, turns out to be the same as the design of an N + 1 point prediction error filter $\{a\}$.

$$\begin{bmatrix} \phi(0) & \phi(1) & \cdots & \phi(N) \\ \phi(1) & \phi(0) & & \vdots \\ \vdots & & \ddots & \vdots \\ \phi(N) & \cdots & & \phi(0) \end{bmatrix} \begin{bmatrix} 1 \\ a_1^N \\ \vdots \\ a_N^N \end{bmatrix} = \begin{bmatrix} PE_N \\ 0 \\ \vdots \\ 0 \end{bmatrix}$$

The spectrum P(f), the maximum entropy spectrum, is then

$$P(f) = 2\Delta\tau\, PE_N \Bigg/ \left| \sum_{j=0}^{N} a_j e^{-2i\pi fj\Delta t} \right|^2 .$$

Consider the optimum N point prediction filter operating on the time series X_N producing an output $\hat{X}_N$. The difference in X_N and $\hat{X}_N$ is ϵ_N which is the output of the N + 1 point prediction <u>error</u> filter. Since the prediction filter is optimum in a least mean square sense, the expected value of the product of ϵ_N with any previous X_N is zero.

$$E[\epsilon_N X_i] = 0 \qquad (i = 1, N)$$

Suppose that the N point prediction filter was able to predict all the correlationed components of X_i. If this were true, then the N point filter would perform as well as an infinitely long prediction filter. The output of the N point filter applied to the original data, X, would be pure white uncorrelated random noise with a power density of $2\Delta\tau PE_N$. Thus, all spectral information of the original time series is contained in the prediction filter, and in effect, the autocorrelation function is extended to infinite lags. To recover the spectrum of the input time series, one need only divide the output power spectrum by the power response of the filter.

It should be noted that the power spectrum of the input time series is for the correlated part of the signal only. Thus, if one assumes that the uncorrelated part of the signal is due totally to noise, the spectrum represents the true signal.

In Figures I-4 to I-6 an example of the maximum entropy spectral estimates of the Bear Valley earthquake signal recorded by the N45 component at station 8 is shown. For comparison, Figures I-1 to I-3 show the spectra obtained for same signal using the DFT. In both cases, a high pass filter with a corner frequency of 0.6 Hz has been applied to the acceleration data. In addition, the maximum entropy displacement spectrum, calculated with the unfiltered data is given in Figure I-7.

It can readily be seen that the maximum entropy spectral estimator and the DFT are in general agreement on the spectral shape and amplitudes. As expected though, the maximum entropy spectra is considerably smoother. It appears, in a comparison of Figure I-6 and Figure I-7 that low frequency level has a drop in amplitude just before the corner frequency as would be expected from Archambeau's source model. However, more analysis of other events must be made before this can be confirmed.

Due to the elimination of leakage by use of the maximum entropy spectral estimator, two addition features of the spectral shape are more reliably estimated. First, in DFT, leakage will reduce the rate of high frequency roll-off. Without leakage, a better estimate of this value is attained. Secondly, the high frequency end of the spectrum is smoother and side lobes can be detected. No work with either of these features has been conducted for this report, and it has not been demonstrated that the side lobes are really those predicted by spectral source representations.

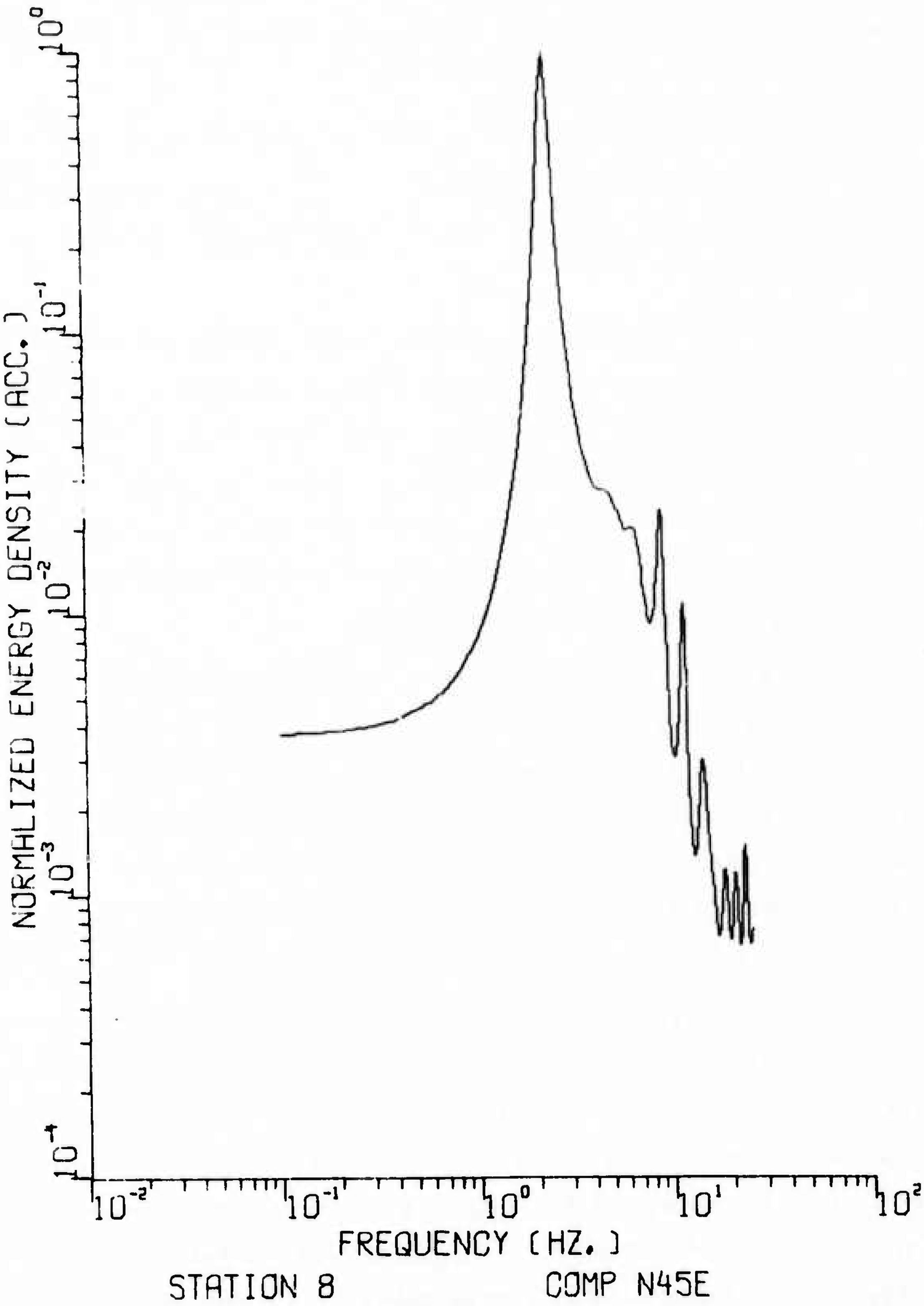

FIGURE I-4

NORMALIZED MAXIMUM ENTROPY ACCELERATION ENERGY DENSITY SPECTRUM FOR N45°E COMPONENT OF STATION 8; BEAR VALLEY EARTHQUAKE OF JUNE 22, 1973 (HIGH PASS FILTER CORNER FREQUENCY AT 0.7 Hz)

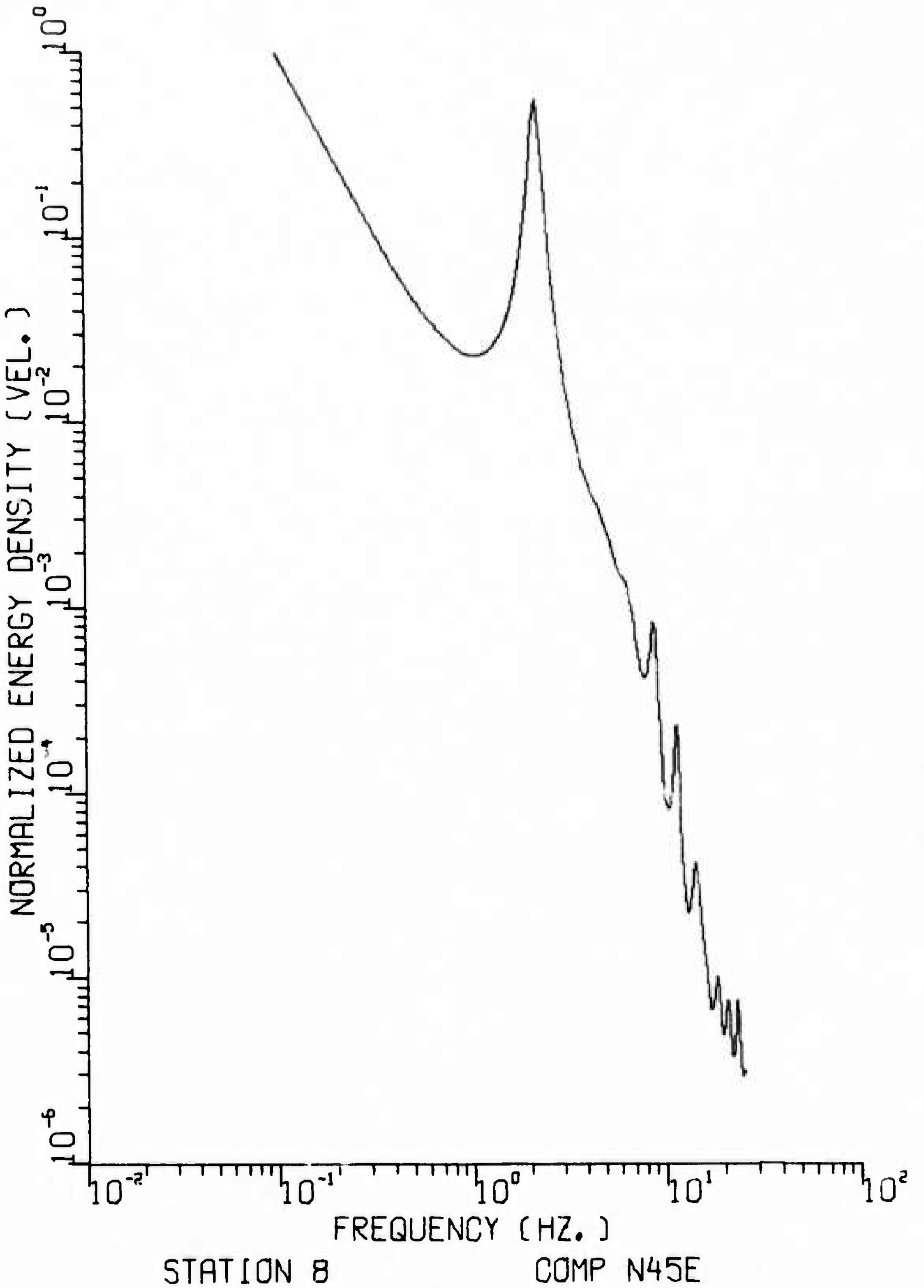

FIGURE I-5

NORMALIZED MAXIMUM ENTROPY VELOCITY ENERGY DENSITY SPECTRUM FOR N45°E COMPONENT OF STATION 8; BEAR VALLEY EARTHQUAKE OF JUNE 22, 1973 (HIGH PASS FILTER CORNER FREQUENCY AT 0.7 Hz)

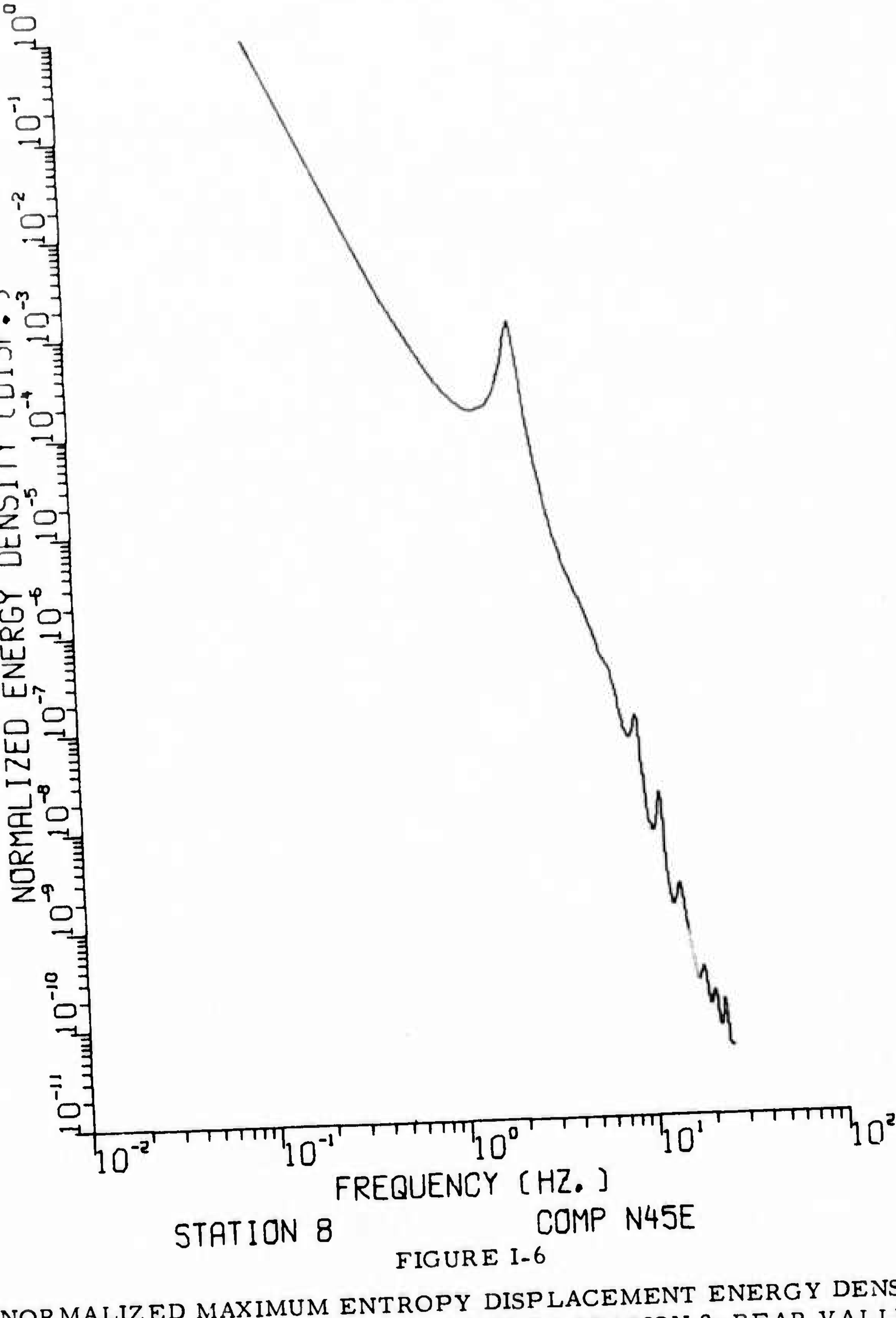

FIGURE I-6

NORMALIZED MAXIMUM ENTROPY DISPLACEMENT ENERGY DENSITY SPECTRUM FC ? N45°E COMPONENT OF STATION 8; BEAR VALLEY EARTHQUAKE OF JUNE 22, 1973 (HIGH PASS FILTER CORNER FREQUENCY AT 0.7 Hz)

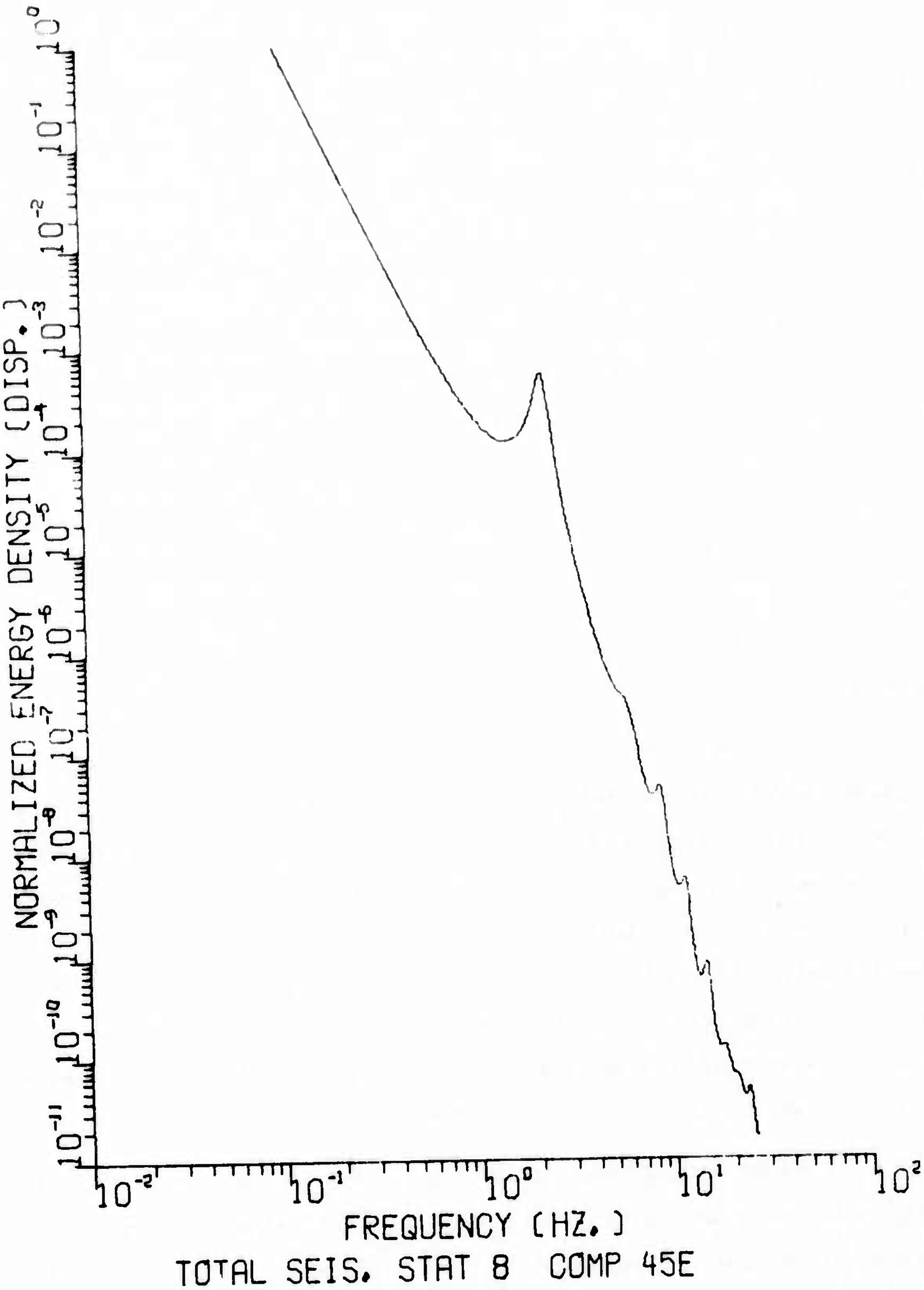

FIGURE I-7

NORMALIZED MAXIMUM ENTROPY DISPLACEMENT ENERGY DENSITY SPECTRUM FOR N45°E COMPONENT OF STATION 8; BEAR VALLEY EARTHQUAKE OF JUNE 22, 1973 (UNFILTERED SPECTRUM)

Finally, in Table 1-2 the source parameters of the Parkfield earthquake and the Bear Valley event of June 22, 1973 are given. The most important feature is the maximum entropy estimate of Ω_o as compared to those given in Table I-1. In all cases, the estimate is lower, probably resulting from the decreased leakage from zero frequency.

D. MODIFIED MAXIMUM ENTROPY SPECTRAL ANALYSIS

With either maximum entropy or DFT spectral estimation, the question of how best to incorporate instrument response corrections for obtaining displacement spectra from acceleration input data remains. Two standard approaches to this problem are twice integrating the acceleration data in the time domain to yield a displacement waveform, which is then Fourier analyzed or to perform the integration in the frequency domain by division of the acceleration spectra by the function $(2\pi f)^2$. These methods are theoretically analogus, but division in the frequency domain tends to be superior due to accumulating errors which exist with numerical integration in the time domain.

However, both methods cause errors in the estimation of the low frequency level, for the function $(2\pi f)^{-2}$ tends to infinity as frequency goes to zero. Then, if the acceleration spectral amplitudes do not tend towards zero in a manner which would yield a limit when the division is performed, the low frequency level of the displacement spectrum will also tend towards infinity. Since the behavior of the low frequency level of the displacement spectra is important in estimation of the seismic moment using Brune's model, and in the evaluation of various source models, such as Brune's model and Archambeau's model, it is important to eliminate this effect.

A new technique of spectral analysis which should eliminate this problem has recently been proposed by Robert Sax of Texas Instruments Incorporated (Sax, personal communications, 1975). This method is essentially a modification of the maximum entropy spectral estimator in which an N-point

TABLE I-2

MAXIMUM ENTROPY SOURCE PARAMETERS

PARKFIELD	f_o(Hz)	Ω_o	M_o
STATION 2	1.7	0.794	5.1×10^{24}
STATION 5	2.7 (6.3 P-Wave?)	0.2587	1.59×10^{24}
STATION 8	3.3	0.1123	1.03×10^{24}
TEMBLOR	2.7 (6.2 P-Wave?)	0.190	1.22×10^{24}

BEAR VALLEY	f_o(S)	f_o(P)	Ω_o	M_o
STATION 2	3.8	6.6	0.0083	9.5×10^{21}
STATION 7	2.8	6.8	0.025	3.1×10^{22}
STATION 8	2.4	6.4	0.0502	6.0×10^{22}

prediction filter is designed on the signal autocorrelation function. Though the mathematics of the method does not require it, the solution filter is presently restricted such that within the N-points the autocorrelation function is modeled only by poles. To achieve this, the instrument response, $(2\pi f)^{-2}$, must be removed as it will introduce zeros in the prediction filter. This technique guarantees a finite zero frequency amplitude and zero amplitude at infinite frequency for displacement spectra, conditions based on Brune's earthquake source mechanism model

As was previously discussed, the maximum entropy spectral estimator generates a prediction filter based on the data which can then be used to evaluate the spectrum. The prediction filter is essentially obtained by solution of the matrix equation:

$$Rf = G$$

where R is the autocorrelation spectra of the signal, f is the prediction filter and G is the autocorrelation function of a spike. It is G which causes the pre-whitening of the spectra. In Sax's modification of the maximum entropy spectral estimator, G is replaced by the autocorrelation function of the instrument response, with the poles removed, convolved with a spike.

At present the numerical methods used for this technique are under development. Successful results have been obtained on theoretical signals. When applied to real data, though, the calculations have been unstable. A more complete explanation of the theory and application will be given when the formulation of the method is complete, including a discussion of those techniques which insure stability.

E. CONCLUSIONS

Spectral estimates of near-field acceleration data were obtained using both a discrete Fourier transform (DFT) and a maximum entropy spectral estimator. For the former estimator, a scaling error had been found in our previous work. Correcting this error reduced our seismic moment estimates so as to agree more closely with those of other investigators. Since no change in spectral shape occurred, the corner frequency estimates were still valid.

Using the maximum entropy spectral estimator, we obtained general agreement on the spectral shape and amplitude level with the DFT estimate. As expected, the maximum entropy spectra is considerably smoother. Because this estimator eliminates leakage, a more accurate estimate of the higher frequency end is obtained, yielding better roll-off values and definition of side lobes. This estimator was applied to data from the Parkfield earthquake and the Bear Valley event of June 22, 1973; in all cases, the low frequency level was lower, probably resulting from decreased leakage.

Finally, work was begun on a modified form of the maximum entropy spectral estimator, in order to obtain a better estimate of the low frequency level. This method essentially involves an N-point prediction filter designed on the signal autocorrelation function. The technique guarantees a finite zero frequency amplitude and zero amplitude at infinite frequency for displacement spectra. Future development will include the numerical methods used for this technique and application to real data.

SECTION II

FAR-FIELD SOURCE STUDIES

A. INTRODUCTION

For the past several months, the examination of far-field spectra for source characteristics has been conducted along several lines of investigation. Surface wave data from the Bear Valley earthquake of June 22, 1973 were used to determine a source mechanism solution, and this solution is compared to that obtained from near-field data in Subsection B. The far-field solution to the central California earthquake of November 28, 1974 is also discussed in this subsection. In Subsection C, the results of an experiment to measure the effect of multipathing on surface wave magnitude measurements (M_s) and the scatter of M_s-m_b plots are discussed. Theoretical higher mode spectra are discussed in Subsection D, with particular emphasis on depth effects. Finally, in Subsection E, we summarize our results and discuss future plans.

B. FAR-FIELD SOURCE MECHANISM FOR TWO CALIFORNIA EARTHQUAKES

Using spectral fitting procedures previously described by Tsai (1972), Turnbull et al., (1973), and Turnbull et al., (1974a), we attempt to obtain source mechanism solutions to the June 22, 1973 and November 28, 1974 California earthquakes using the available VLPE and array data. The event description of the former is given in Table II-1, with the travel paths to the available stations shown in Figure II-1. We see from this figure that all of the travel paths are continental and lie to the east of the event. The vertical, transverse, and radial components recorded at these stations are given in Appendix A. Demultipathing procedures were applied to the data on the PDP-15 interactive graphics system (see Appendix B).

TABLE II-1

EVENT DESCRIPTION: THE BEAR VALLEY EARTHQUAKE OF JUNE 22, 1973

Event I. D. : BEV/622/73

Location : 36°35.4N, 121°11.6W

Magnitude : $m_b = 3.5$

Date : 06/22/73

Origin Time: 01:29:12.3

Recording Station	Location		Azimuth From Source	(km)
	Latitude	Longitude		
OGD	41.07N	74.62 W	68.3	4026.6
ALQ	34.94N	106.46 W	93.5	1343.6
LASA	46.69N	106.22 W	43.2	1672.5

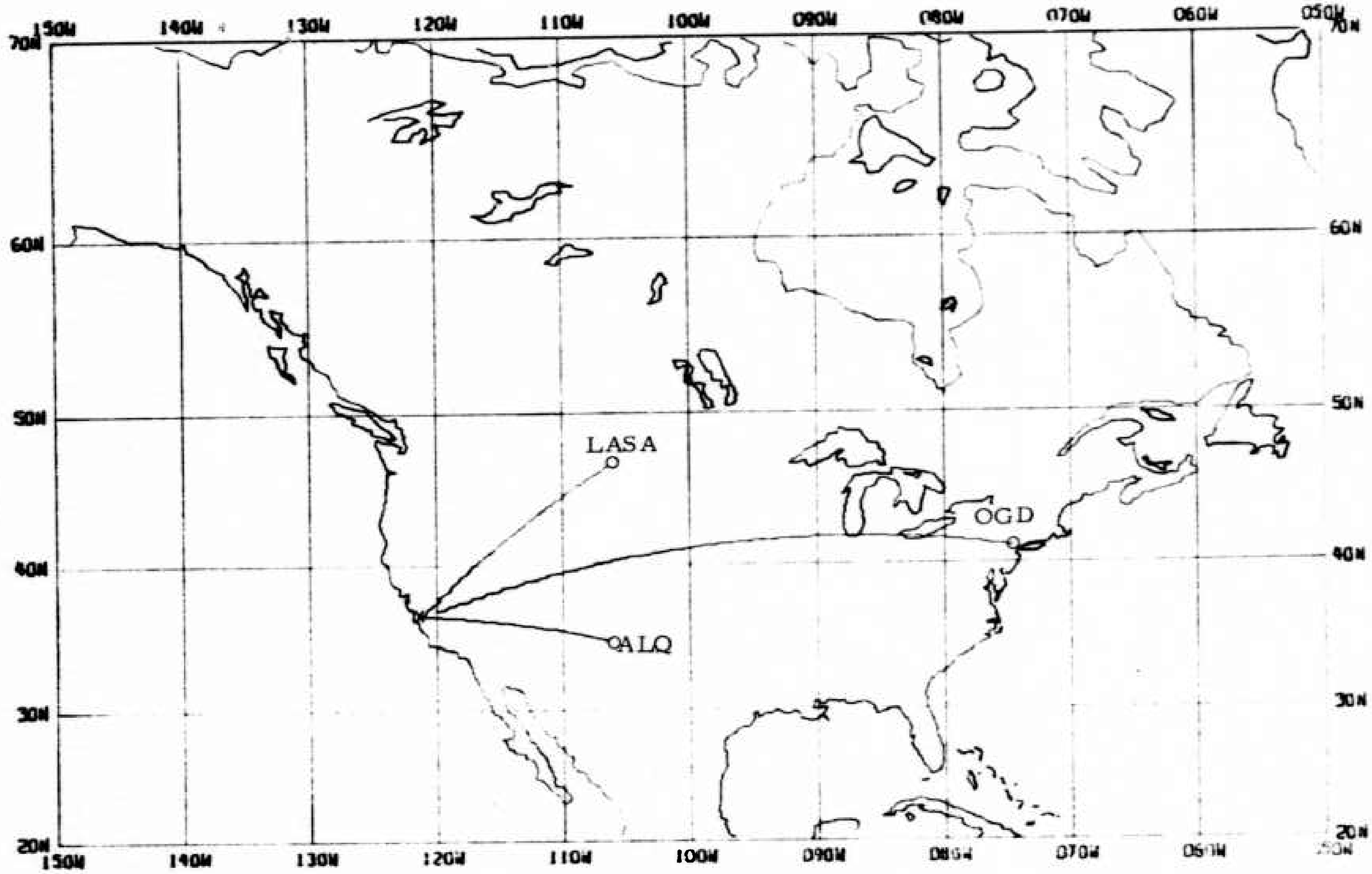

FIGURE II-1

TRAVEL PATHS TO THE AVAILABLE STATIONS FOR THE JUNE 22, 1973 EARTHQUAKE

In order to generate theoretical spectra to "fit" to the observed spectra, a layered half space is required which provides a fair approximation of the geologic structure in the source region. Although surveys are presently being undertaken to determine this structure, no definite estimate exists for this region. Helmberger (1975), using shear body waves, has determined a rough approximation for the structure to the east of the event in the source region. This is shown in Table II-2 below and in Figure II-2.

TABLE II-2

BEAR VALLEY EARTH MODEL-NORTHEAST OF FAULT

Layer Number*	Thickness(km)	V_p(km/sec)	V_s(km/sec)	ρ(gm/cc)
1	1.5	2.55	1.5	2.0
2	13.5	5.71	3.3	2.6
3	2.0	5.79	3.4	2.7
4	2.0	6.22	3.6	2.8
5	21.0	6.58	3.8	3.0

* Normal Gutenburg-Bullen for depths >40 km.

The Love and Rayleigh wave group and phase velocity dispersion of this model is shown in Figure II-3. Its main characteristic is higher velocities at the shorter periods than a normal Gutenberg-Bullen model (Turnbull, et al., 1974a).

The spectral fit obtained using this structure is shown in Figure II-4. We see that the fit is of "average" quality at best; this is due to the relatively small azimuthal spread of stations and the gross source structure approximation. The source parameter distributions are shown in Figure II-5, with source parameter estimates given in Table II-3. Considering the quality of the fit, the agreement between this solution and that obtained using acceleration data (Turnbull and Battis, 1974) is remarkable. The depth, dip, slip, and strike are in close agreement. The largest discrepancy occurred between the moments,

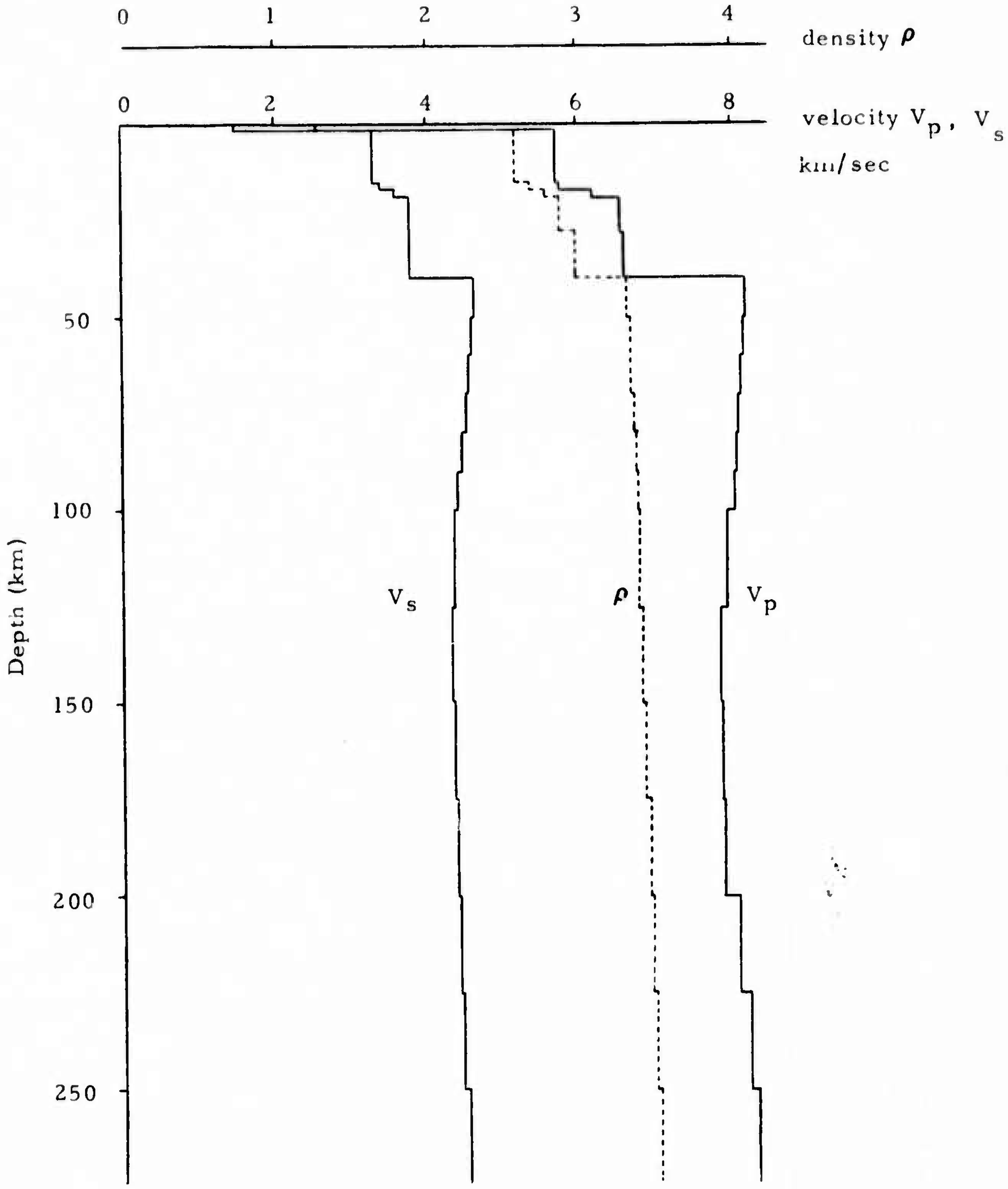

FIGURE II-2

BEAR VALLEY EARTH MODEL - NORTHEAST OF FAULT

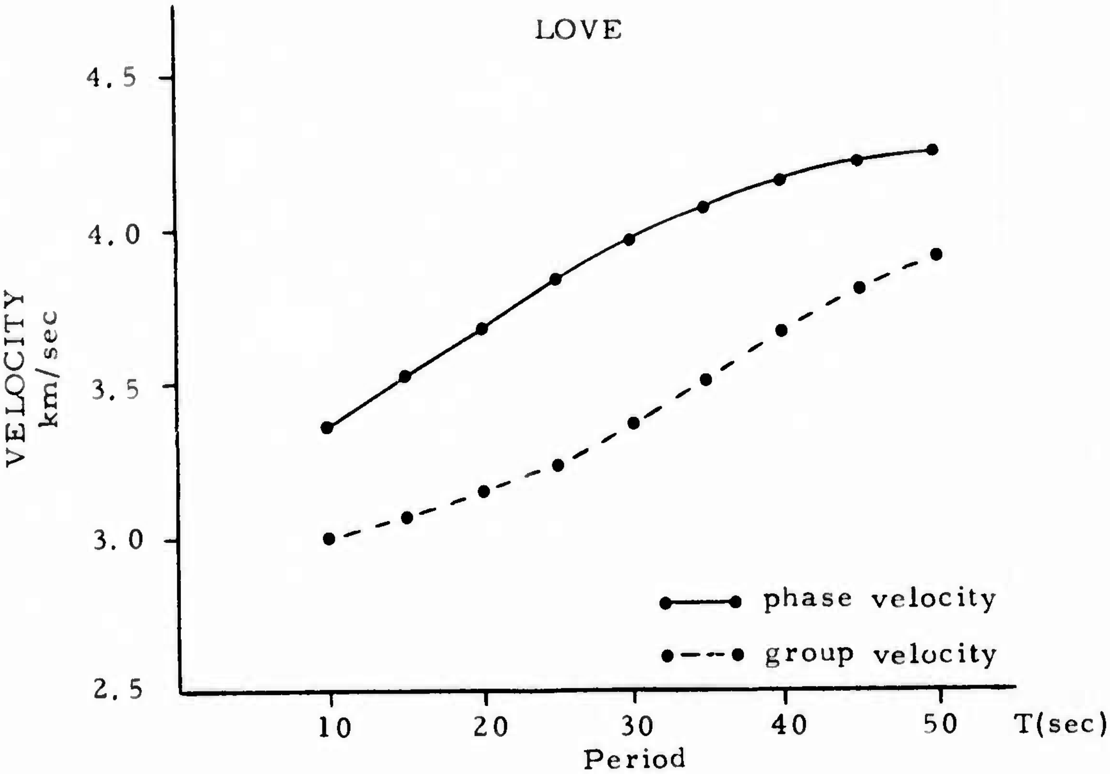

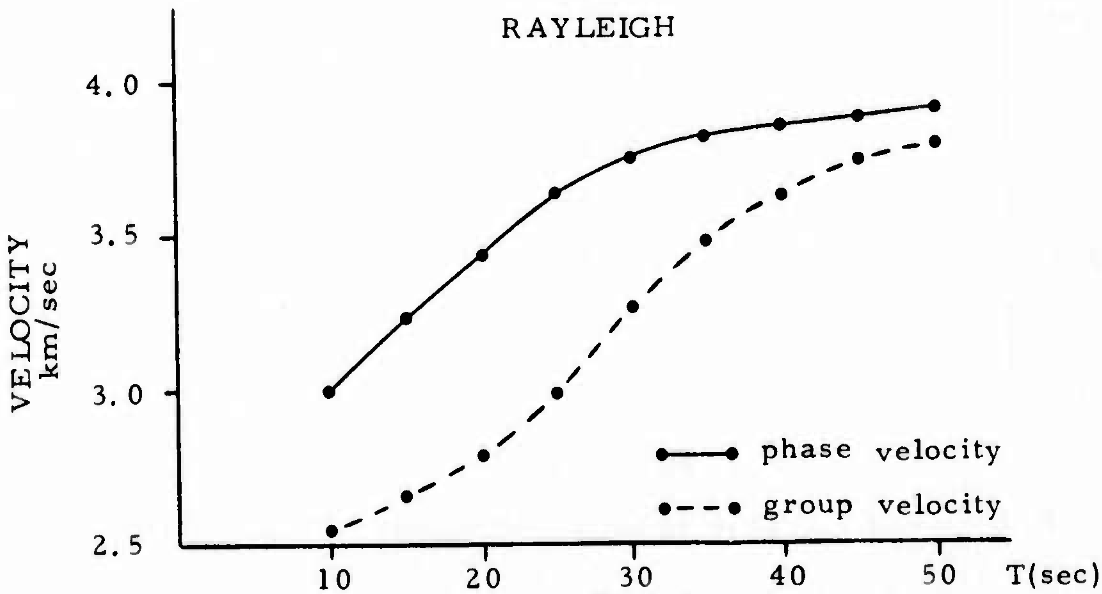

FIGURE II-3

LOVE AND RAYLEIGH WAVE DISPERSION FOR THE BEAR VALLEY EARTH MODEL

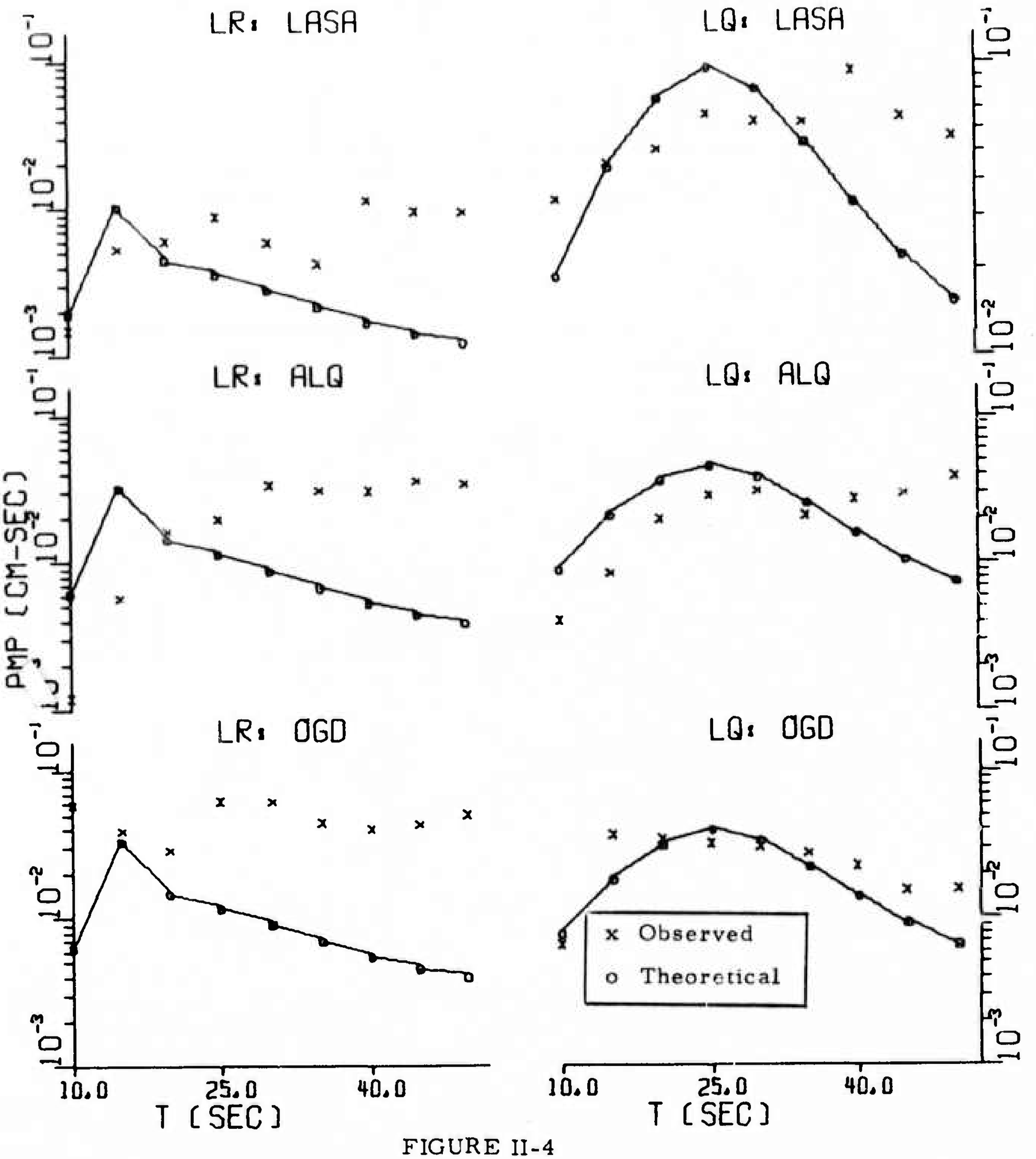

FIGURE II-4

SPECTRAL FIT - THE BEAR VALLEY EARTHQUAKE
OF JUNE 22, 1973

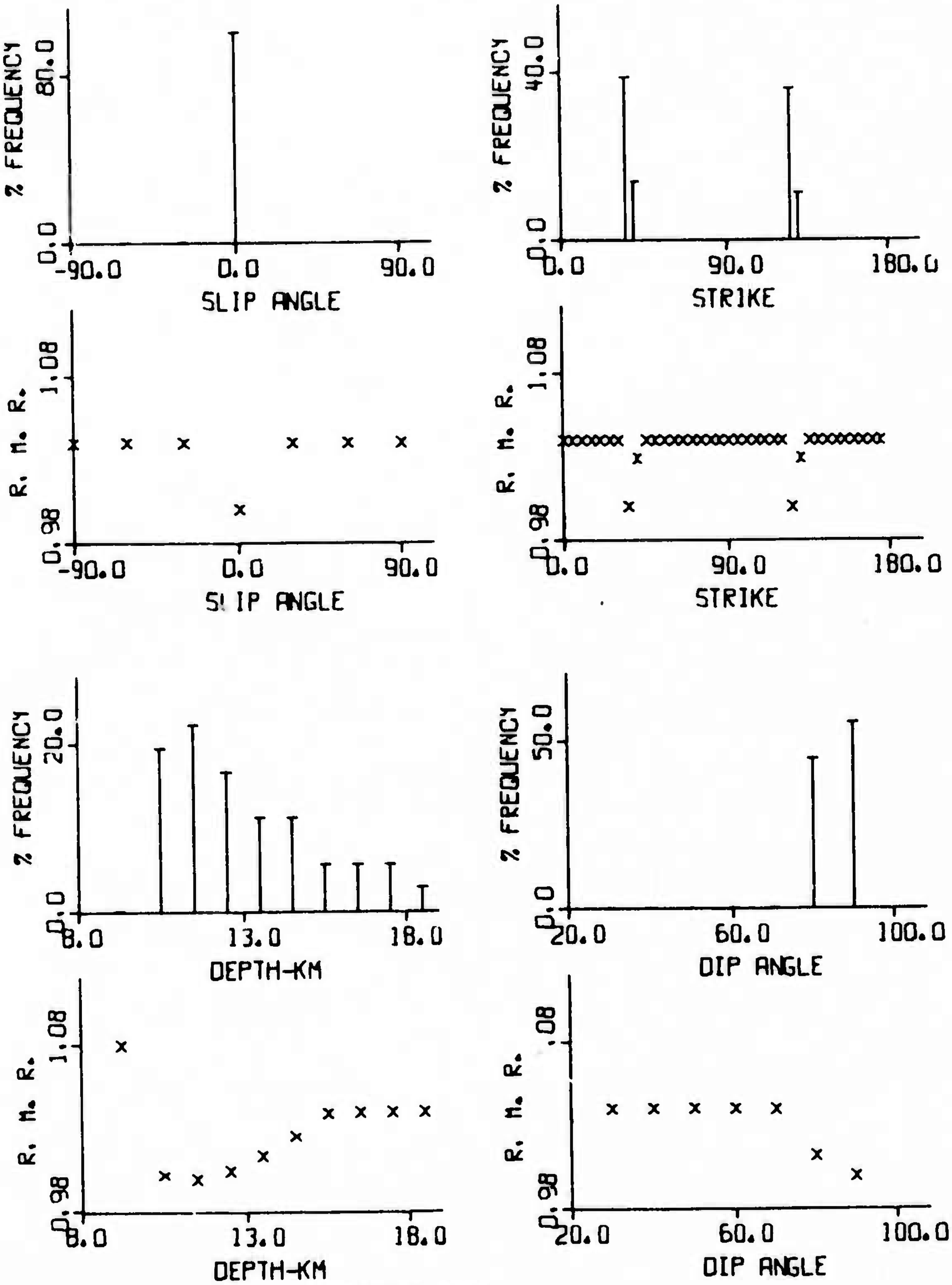

FIGURE II-5

SOURCE PARAMETER DISTRIBUTIONS FOR THE BEAR VALLEY EARTHQUAKE OF JUNE 22, 1973

TABLE II-3

ESTIMATES OF SOURCE PARAMETERS FOR BEAR VALLEY EARTHQUAKE OF JUNE 22, 1973

Solutions for Event: BEV/622/73

A. Solution by Minimum-Residual Criterion

Event I. D.	Optimal Solution				
	Depth h km	Dip Angle δ^{o}	Slip Angle λ^{o}	Strike $N\phi^{o}W$	Moment 10^{25} dyne-cm
BEV/622/73	11.5	90	0	55, 145	0.743×10^{-3}

B. Solution by Distribution-of-Minimum-Residual Criterion

Event I. D. / Source Parameter	Probable Range	% Confidence
h(km)	10.5 - 14.5	81
δ	90^{o} 80^{o}	55 45
λ	0^{o}	100
ϕ	55, 145	75

with the near-field moment being an order of magnitude larger. At this time, it is difficult to say whether this difference is a result of modeling inaccuracies or a real source property. Future studies will be concerned with a closer examination of this problem.

The second California earthquake, that of November 28, 1974, was analyzed using the same procedure. The event description is given in Table II-4, with the travel paths to the available stations shown in Figure II-6. The vertical, transverse, and radial components recorded at these stations are given in Appendix A. After demultipathing procedures were applied, we attempted to fit spectra recorded at stations whose travel paths lie to the east of the fault. This limitation was imposed because our source structure was only valid for that side of the fault. Future studies will use structures from both sides to take advantage of all of the available data.

The spectral fit obtained for this event is shown in Figure II-7. Again, we see that the fit is of "average" quality at best and for the same reasons. The source parameter distributions are shown in Figure II-8, with the source parameter estimates given in Table II-5. Comparing our results with those obtained by Johnson (1975) from body wave data, the agreement is again quite remarkable considering the quality of the fit. The depth is within a kilometer of his solution, with the fault nearly vertical and mostly strike-slip as is Johnson's. The strike direction is approximately 30 degrees different using the complementary solution. With a more accurate source structure, and utilization of all the available data, it is hoped that a better fit can be obtained. This future result will then be compared to more exact solutions obtained from body wave data.

C. THE EFFECT OF DEMULTIPATHING ON THE MINIMIZATION OF THE SURFACE WAVE MAGNITUDE (M_s) VARIANCE

In previous work by Turnbull et al., (1974b), the M_s-m_b discriminant was investigated with the objective of reducing the scatter of the

TABLE II-4

EVENT DESCRIPTION: THE CENTRAL CALIFORNIA EARTHQUAKE OF NOVEMBER 28, 1974

Event I. D.: CCA/332/74

Location : $36^{o}54.7$N, $121^{o}29.8$W

Magnitude : $m_b = 5.2$ (M_L)

Date : 11/28/74

Origin Time: 23:01:24.8

Recording Station	Location		Azimuth From Source	Δ(km)
	Latitude	Longitude		
LASA	46.69 N	106.22 W	44.5^{o}	1665.6
NORSAR	60.844N	10.887W	21.9^{o}	8341.3
TLO	39.86 N	4.02 W	43.2^{o}	9380.4
ALPA	65.233N	147.743W	-20.4^{o}	3589.4
KIP	21.42 N	158.02 W	-105.7^{o}	3914.0
ZLP	16.50 S	68.13 W	126.3^{o}	8139.0

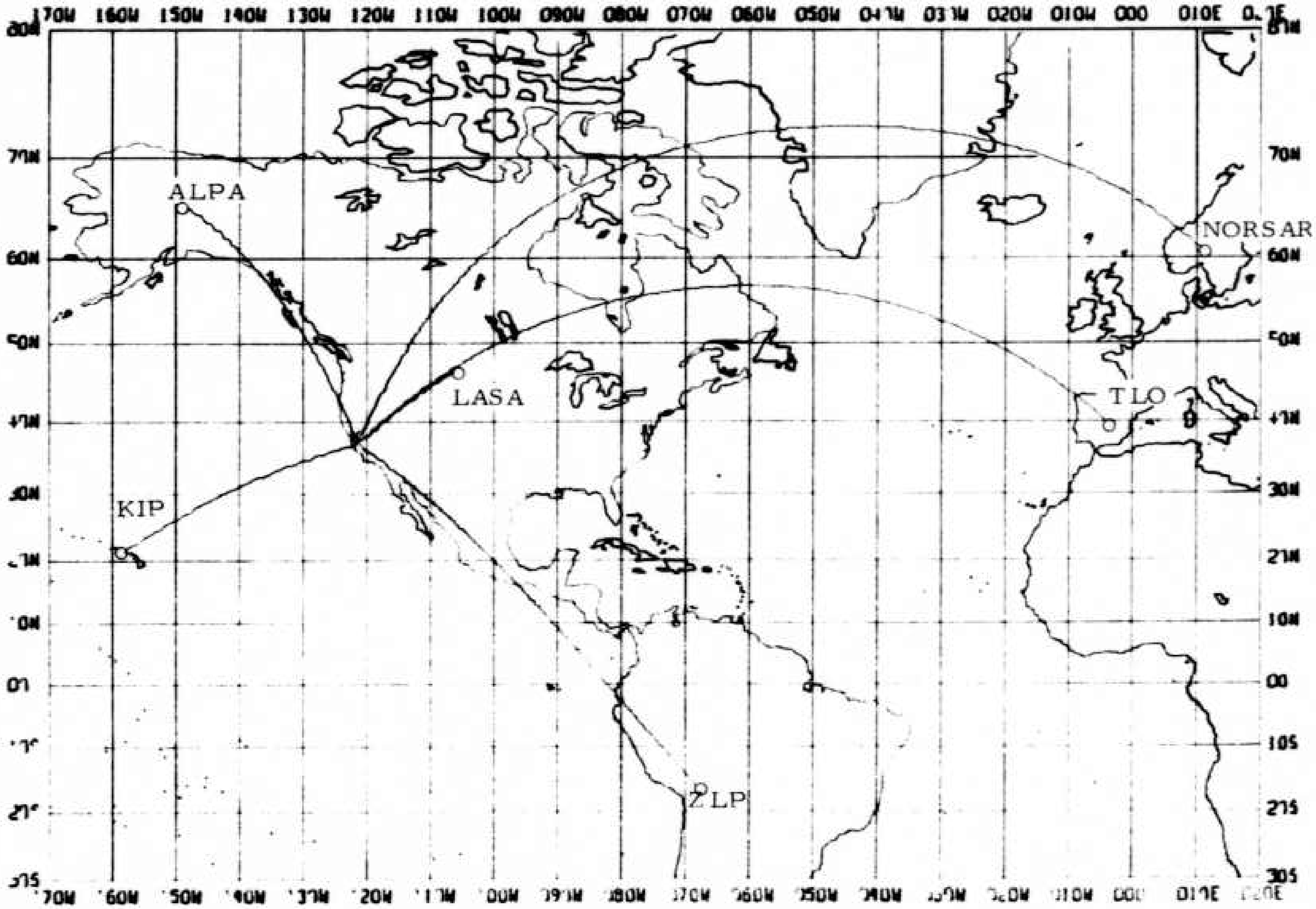

FIGURE II-6

TRAVEL PATHS TO THE AVAILABLE STATIONS FOR THE NOVEMBER 28, 1974 EARTHQUAKE

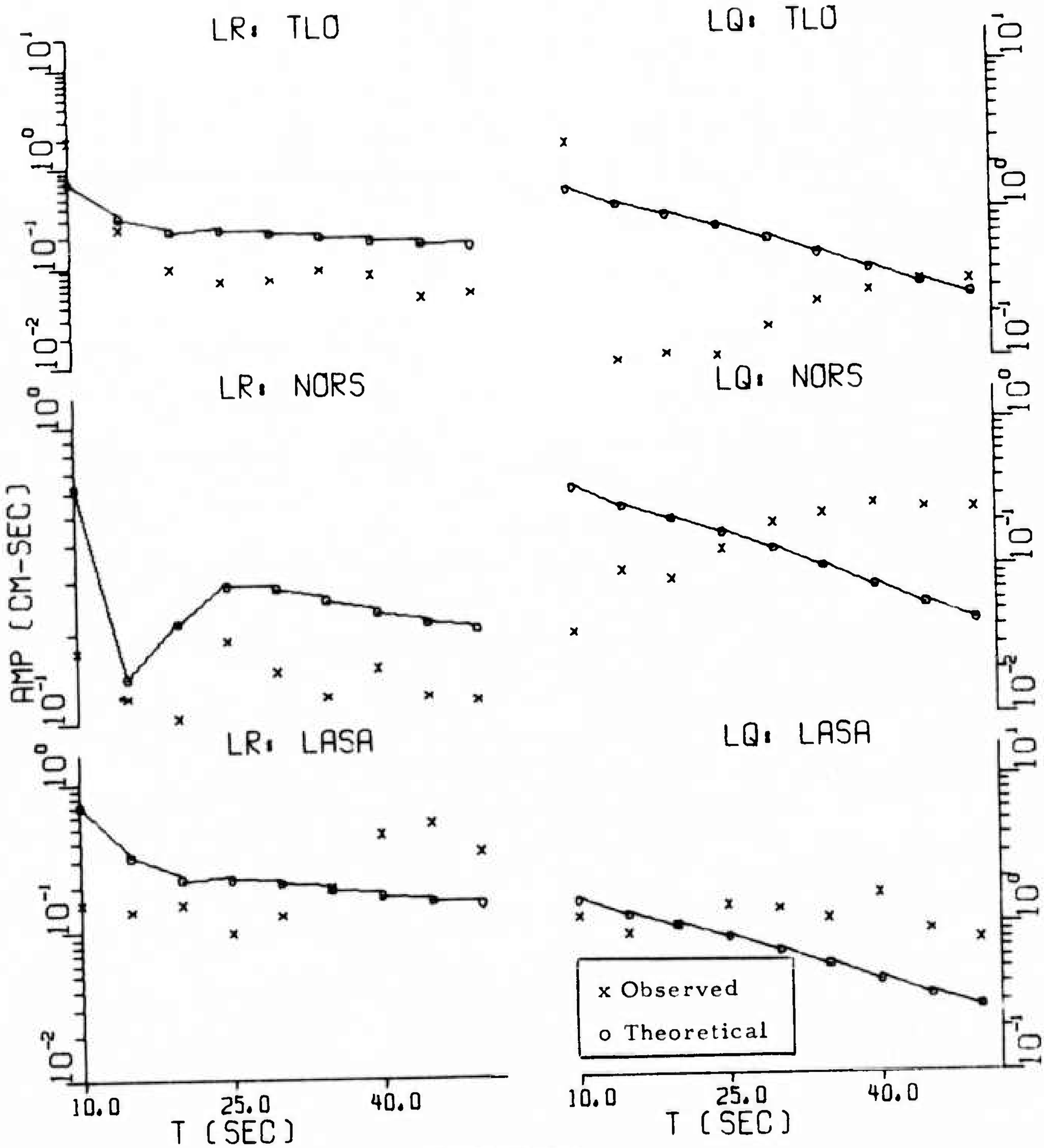

FIGURE II-7

SPECTRAL FIT - THE CENTRAL CALIFORNIA EARTHQUAKE OF NOVEMBER 28, 1974

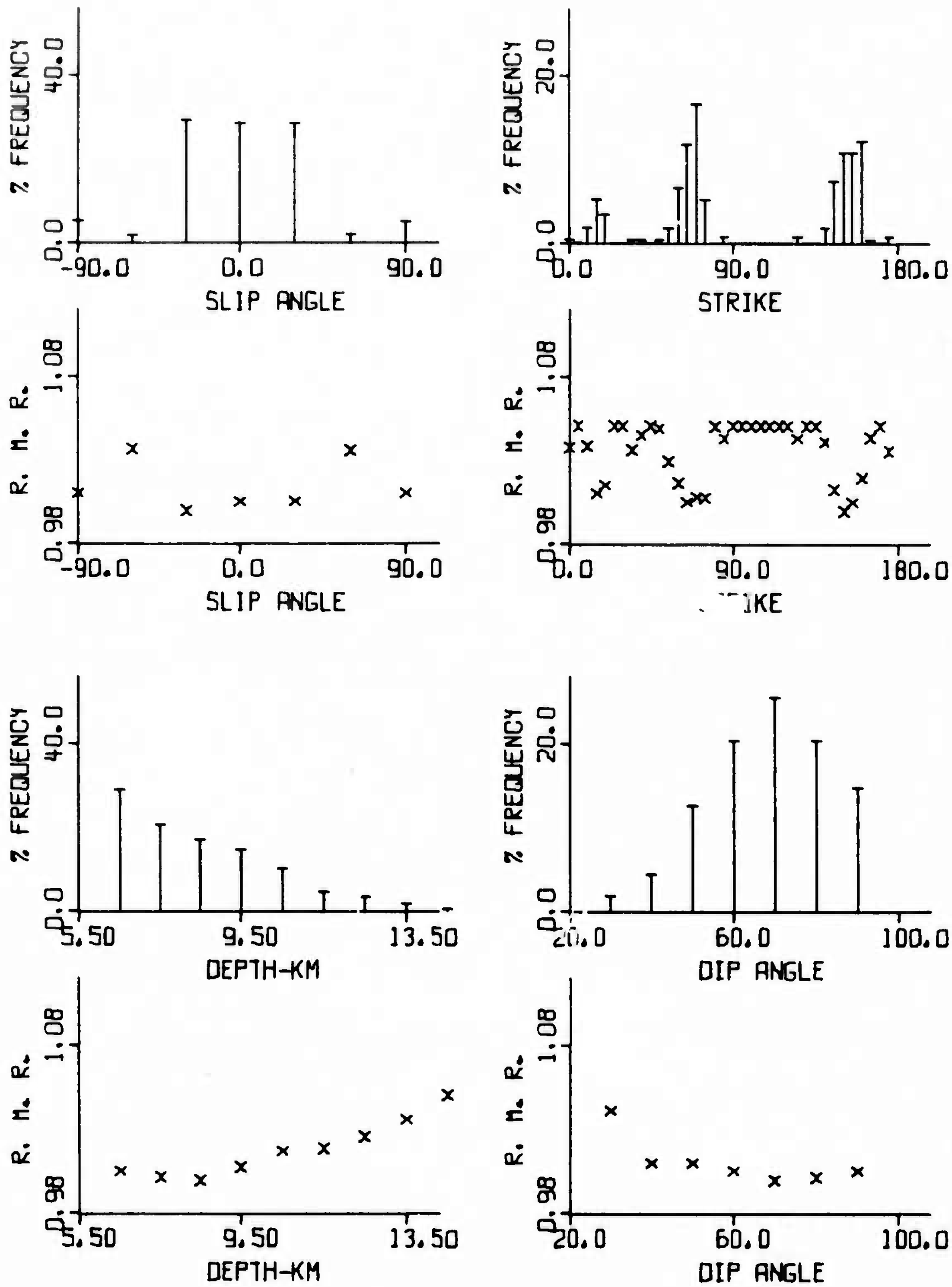

FIGURE II-8

SOURCE PARAMETER DISTRIBUTION FOR THE
CENTRAL CALIFORNIA EARTHQUAKE OF NOVEMBER 28, 1974

TABLE II-5

ESTIMATES OF SOURCE PARAMETERS FOR THE CENTRAL CALIFORNIA EARTHQUAKE OF NOVEMBER 28, 1974

Solutions for Event: CCA/332/74

A. Solution by Minimum-Residual Criterion

Event I. D.	Optimal Solution				
	Depth h km	Dip Angle δ^o	Slip Angle λ^o	Strike $N\phi^o W$	Moment 10^{25} dyne-cm
CCA/332/74	8.50	70	-30.0	30	0.522×10^{-1}

B. Solution by Distribution-of-Minimum-Residual Criterion

Event I. D. / Source Parameter	Probable Range	% Confidence
h(km)	6.50 - 10.50	91
δ	60 - 90	82
λ	-30 - 30	86
ϕ	20 - 35 105 - 120	42 40

earthquake population. The method of performing this reduction was to minimize the effect of the source mechanism radiation pattern and to obtain the M_s value at the same period for all events and all components.

A set of 66 Eurasian earthquakes recorded at three or more VLPE stations during 1972 and 1973 was selected for this investigation. Surface wave magnitude (M_s) measurements were first made manually on these records and the results averaged for each event. By averaging, it was hoped to reduce radiation pattern effects. Using M_s calculated from the vertical component Rayleigh wave and averaged at three or more stations, a standard deviation of $\sigma = 0.354$ was obtained (all values of σ given here were computed using a fitting technique which treats both variables as independent, and minimizes the perpendicular distance from the fitting line to the data points). This is almost identical to that obtained by Lambert, et al., (1974) for M_s from single stations. Using M_s calculated from both the Rayleigh and the Love waves, a standard deviation of $\sigma = 0.368$ was obtained, which is virtually the same.

Using the same data set, M_s measurements were made by using a spectral estimate at 20 seconds period. The vertical Rayleigh data obtained in this manner yielded a standard deviation of $\sigma = 0.369$. Using an M_s obtained from Rayleigh and Love waves yielded a standard deviation of $\sigma = 0.363$.

Thus, the two methods used previously (M_s averaging and computing M_s from spectral estimates) produced no improvement over the standard deviations computed from single-station data.

Another possible way to reduce the scatter about the mean value line could be to demultipath the data, accounting for path effects. The method used for demultipathing, incorporating a series of narrow-band filters, is outlined in Appendix B. Before processing of the data was initiated, the 66 events used previously were reviewed visually. Seven events were rejected due to either suspicion of being mixed or to the presence of malfunction (spikes, etc.) which would interfere with the narrow bandpass filtering. The net result was that the data base was reduced to 59 events consisting of 221 station-events (a station-event is one event as recorded at one station). The parameters of these events are listed in Table II-6. Due to time constraints, only the vertical component of the Rayleigh wave was processed for each station event.

The great-circle travel paths from event location to the VLPE stations are shown in Figure II-9 (the key to this figure is given in Table II-7). The event locations are placed in the center of regions which represent the events which were analyzed. Only those stations which recorded one or more events from a given region were used in constructing the travel path between that region and station.

Since the size of the data base was changed, it was necessary to recompute the standard deviations for the previously reported three or more stations average M_s and the spectral estimate M_s. We shall use as a reference the standard deviation for the case of M_s measured on the vertical component of the Rayleigh wave and averaged over three or more station M_s values. (All M_s data referred to below was measured at a period of 20 seconds.) The following cases summarize the results of this study.

- Figure II-10 illustrates the reference data set. The standard deviation for this set is $\sigma = 0.283$.
- Figure II-11 illustrates the case where M_s was computed from Love and Rayleigh wave average M_s values. The standard deviation of this set is $\sigma = 0.285$, which is essentially the same as the reference value of σ.
- Figure II-12 illustrates the case where M_s was computed from spectral estimates made from the vertical Rayleigh wave. The standard deviation of this set is $\sigma = 0.291$, which is slightly greater than the reference value of σ.

TABLE II-6

DEMULTIPATHED EVENT INFORMATION
(PAGE 1 OF 2)

EVNO	EVENT NAME	DATE	O.T.	LAT.N	LON.E	MB	DEP	IS	STATIONS
0031	LX-TAIWA-041	01/10/72	05.23.52	20.9	120.4	5.0	32	P	2,3,6
0036	LX-GRECE-048	01/12/72	13.51.20	35.0	23.5	4.9	48	P	4,6,7
0037	LX-EKAMC-049	01/1[illegible]/72	20.20.15	55.6	163.9	4.8	N	P	2,4,6,7
0039	LX-ESIBE-052	01/13/72	17.24.23	61.9	147.1	5.3	N	P	2,4,6,7
0043	LX-BRUSS-056	01/15/72	18.07.58	57.4	120.7	4.7	13	P	2,3,4,6
0062	LX-TAIWN-087	01/25/72	23.00.39	22.3	122.4	4.6	24	P	2,6,7
0073	LX-INDIA-101	01/28/72	10.26.54	26.6	66.3	5.9	N	P	2,3,4,6,7
0081	LX-NECHI-112	01/30/72	03.56.41	40.9	120.2	3.9	--	L	3,6,7
0087	LX-GRECE-121	02/02/72	21.19.49	38.9	21.2	4.6	44	P	3,4,6,7
0088	LX-CAUCA-124	02/03/72	02.29.22	40.0	48.4	5.1	39	P	3,4,6,7
0089	LX-YUANN-125	02/03/72	07.22.49	23.4	102.4	4.5	N	P	3,6,7
0095	LX-TIBET-132	02/04/72	14.08.22	30.4	84.6	5.2	18	P	3,6,7
0112	LX-TAIWN-153	02/08/72	03.37.52	19.3	122.0	5.7	50	P	3,4,6,7
0123	LX-KAMCH-167	02/11/72	21.36.17	56.1	162.9	4.6	44	P	3,4,6
0133	LX-KURIL-185	02/19/72	13.19.25	44.4	149.1	5.2	N	P	3,6,7
0134	LX-KURIL-186	02/19/72	13.54.46	44.6	149.1	5.4	50	P	3,6,7
0141	LX-HINDU-196	02/22/72	01.14.48	36.4	70.6	5.3	212	P	3,6,7
0286	LX-OKHOT-366	03/16/72	05.22.59	52.2	152.2	4.5	435	P	3,4,6
0294	LX-TADZH-375	03/17/72	09.17.11	40.1	69.7	5.2	26	P	3,4,6
0341	LO-TAIWA-433	06/08/72	09.14.08	21.1	120.2	5.4	N	P	1,6,8,9
0350	LO-CRETE-443	06/09/72	07.42.20	34.8	26.5	4.9	N	P	6,7,9
0472	LX-KURIL-596	07/11/72	06.58.21	48.4	154.5	5.2	62	P	1,4,6
0505	LX-KAMCH-635	07/17/72	08.28.52	55.0	159.6	5.3	N	P	4,5,8,9
0605	LX-BAIKL-757	08/09/72	19.42.17	53.0	107.5	5.1	N	P	4,8
0611	LX-MONGO-765	08/11/72	02.22.14	44.7	102.0	5.0	N	P	4,5,8
0653	LX-OEKAM-816	08/20/72	08.10.08	51.3	161.6	5.2	N	P	1,4,8
0710	LX-KURIL-890	11/06/72	16.22.16	43.7	147.5	4.5	49	P	2,6,8
0711	LX-TAIWA-892	11/07/72	06.40.36	22.7	120.0	5.4	22	P	2,6,8,9
0716	LX-TIWAN-898	11/08/72	14.25.43	23.9	121.6	5.5	27	P	2,6,8,9
0744	LX-TAIWA-940	11/21/72	02.47.14	23.8	121.6	5.7	14	P	2,6,8,9

TABLE II-6

DEMULTIPATHED EVENT INFORMATION
(PAGE 2 OF 2)

EVNO	EVENT NAME	DATE	O.T.	LAT.N	LON.E	MB	DEP	IS	STATIONS
0775	LX-IRAN -982	12/01/72	11.39.04	35.4	57.9	5.4	N	P	2,6,8,9
0776	LX-NECKM-983	12/01/72	21.15.52	54.9	162.0	4.8	N	P	2,6,8,9
0799	LX-KURIS+016	12/10/72	18.26.07	44.8	149.4	6.0	13	P	2,8,9
0818	LX-KURRE+036	12/12/72	09.03.56	44.1	151.0	5.7	38	P	1,2,8,9
0825	LX-KURIS+047	12/15/72	14.41.32	44.6	149.4	4.7	40	P	1,2,8,9
0828	LX-KURIS+051	12/17/72	09.18.34	44.7	149.2	5.7	50	P	1,2,8,9
0837	LX-KURIS+060	12/17/72	06.24.52	44.6	149.4	4.9	N	P	1,2,8,9
0859	LX-NECKM+091	12/25/72	18.55.58	53.0	159.4	5.7	52	P	1,2,5,6,8,9,11
0881	LX+CENAP+ 6	01/02/73	22.25.57	31.2	88.1	5.2	N	P	2,5,6,8,11
0890	LX+GTURP+ 17	01/05/73	05.49.17	35.8	21.8	5.3	N	P	6,9,11
0897	LX+GTURP+ 29	01/10/73	03.24.12	37.8	21.3	5.0	41	P	5,6,8,9
0918	LX+CENAP+ 59	01/19/73	15.10.02	32.7	68.3	5.0	30	P	2,6,8,9,10
0929	LX+CENAP+ 75	01/24/73	03.20.20	41.0	82.2	5.1	N	P	2,6,8,10,11
0937	LX+SKAMP+ 86	01/27/73	04.04.42	50.4	156.8	5.2	47	P	2,6,8,11
0946	LX+CENAP+ 99	01/30/73	11.10.12	42.7	94.3	4.3	N	P	2,8,11
0950	LX+CENAP+125	02/16/73	07.29.47	31.7	100.0	4.9	N	P	6,8,9
0956	LX+GTURP+134	02/19/73	18.10.00	40.2	33.9	4.5	22	P	6,8,9
0965	LX+CENAP+146	02/23/73	10.45.06	37.6	86.4	4.8	N	P	6,8,9,11
0966	LX+SIRAP+148	02/24/73	00.02.40	28.6	52.6	5.2	27	P	5,6,8
1008	LX+SKAMP+195	03/01/73	02.19.03	49.8	157.2	5.5	30	P	6,8,9,11
1039	LX+NKAMP+230	03/04/73	17.57.43	54.8	161.5	6.1	32	P	1,6,9,11
1065	LX+SKAMP+261	03/09/73	13.58.41	50.0	157.1	4.6	N	P	2,6,9,11
1080	LX+TWANP+277	03/11/73	14.53.07	21.0	120.2	4.8	32	P	1,2,6,8
1083	LX+SKAMP+281	03/12/73	11.14.23	50.1	156.7	5.7	49	P	1,2,6,8,9,11
1085	LX+SKAMP+283	03/12/73	19.39.21	50.8	157.1	6.1	54	P	1,2,6,8,9,11
1132	LX+TWANP+344	03/26/73	02.37.21	23.4	124.0	5.5	16	P	1,2,6,10,11
1166	LX+KURSP-418	04/04/73	21.50.54	43.4	147.7	5.2	N	P	1,2,4,7,8,11
1172	LX+KURSP-425	04/05/73	22.16.59	43.6	147.7	5.4	N	P	1,2,4,6,7.8
1180	LX+KURSP-433	04/06/73	00.01.56	43.7	147.6	5.3	N	P	2,6,8

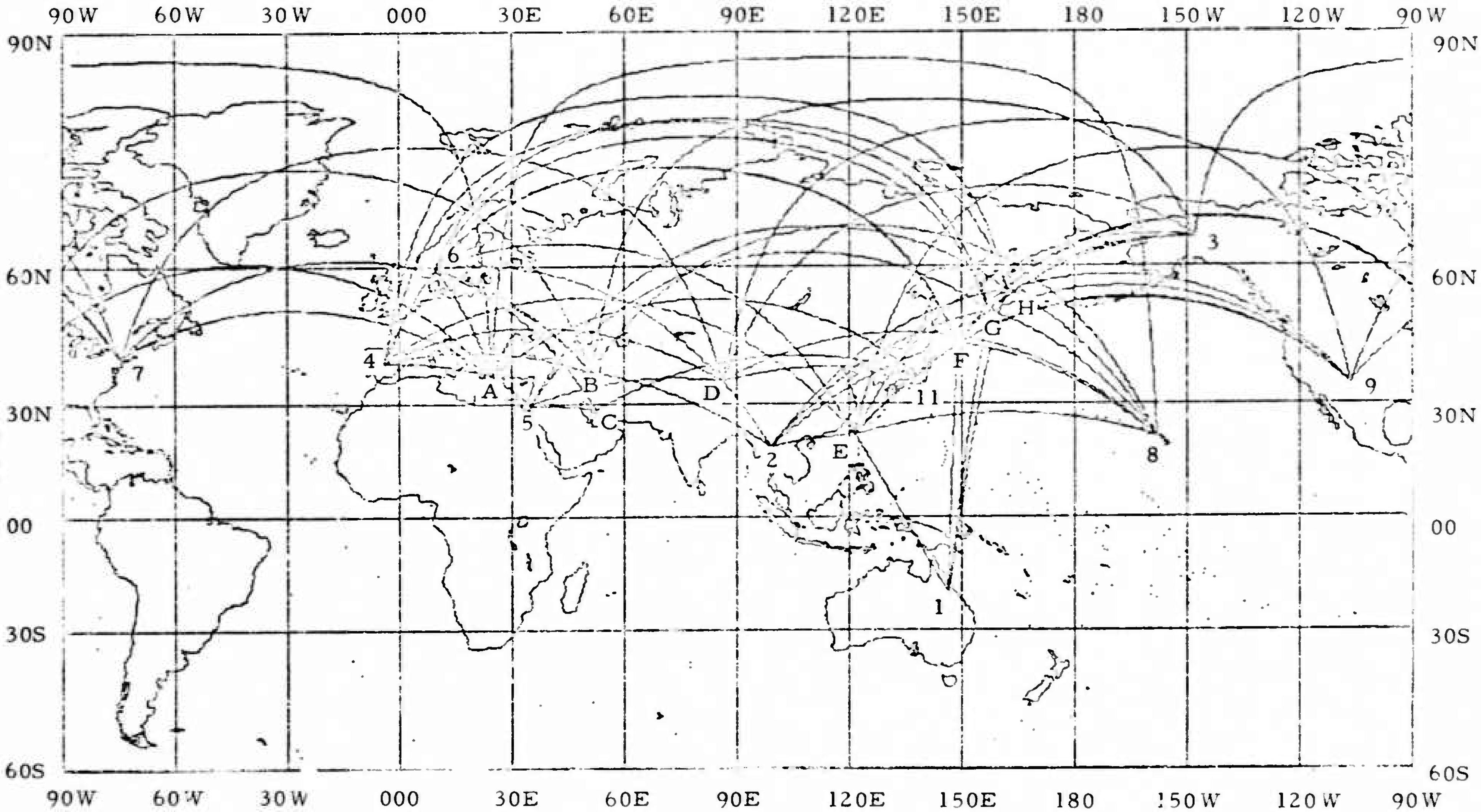

FIGURE II-9

GREAT-CIRCLE TRAVEL PATHS FOR DEMULTIPATHED EVENTS

TABLE II-7

KEY TO FIGURE II-9

LIST OF VLPE STATIONS

Station Number	Name	Station Coordinates	
		Latitude	Longitude
1	Charters Towers, Australia	20.09S	146.26E
2	Chiang Mai, Thailand	18.79N	98.98E
3	Fairbanks, Alaska	64.90N	148.01W
4	Toledo, Spain	39.86N	4.02W
5	Eilat, Israel	29.55N	34.95E
6	Kongsberg, Norway	59.65N	9.59E
7	Ogdensburg, New Jersey	41.07N	74.62W
8	Kipapa, Hawaii	21.42N	158.02W
9	Albuquerque, New Mexico	34.94N	106.46W
11	Matsushiro, Japan	36.54N	138.21E

LIST OF SEISMIC REGIONS

Station Designator	Name	Coordinates of Region Center	
		Latitude	Longitude
A	Greece - Turkey	37.1N	24.7E
B	Caspian Sea	37.7N	51.2E
C	Southern Iran	28.6N	52.6E
D	Central Asia	35.6N	86.2E
E	Taiwan	22.0N	121.4E
F	Kurile Islands	44.2N	148.8E
G	Southern Kamchatka	51.0N	157.3E
H	Northern Kamchatka	55.3N	162.0E

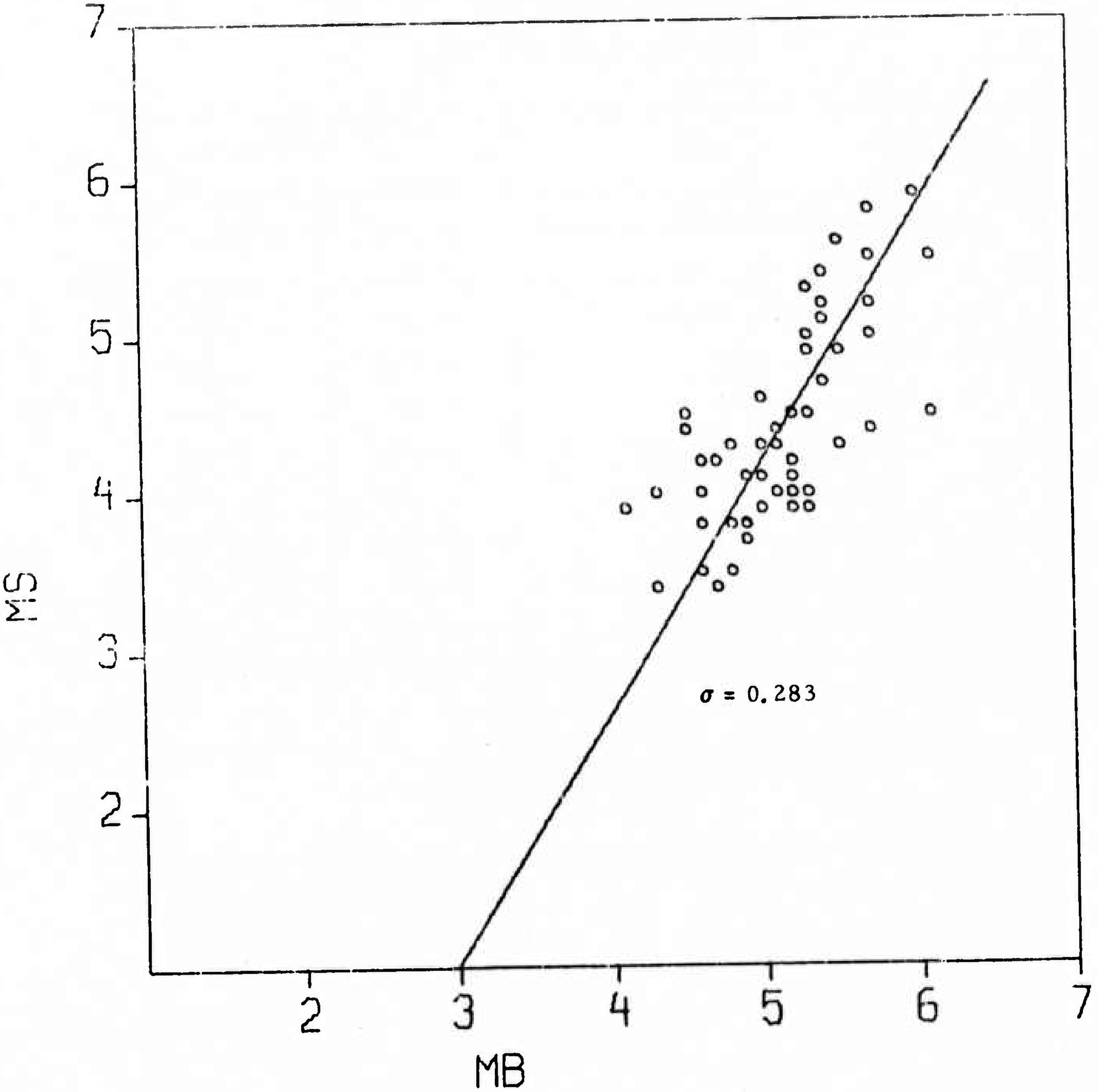

FIGURE II-10

REFERENCE DATA SET - MANUAL M_s MEASUREMENT AND STATION AVERAGED USING RAYLEIGH WAVE

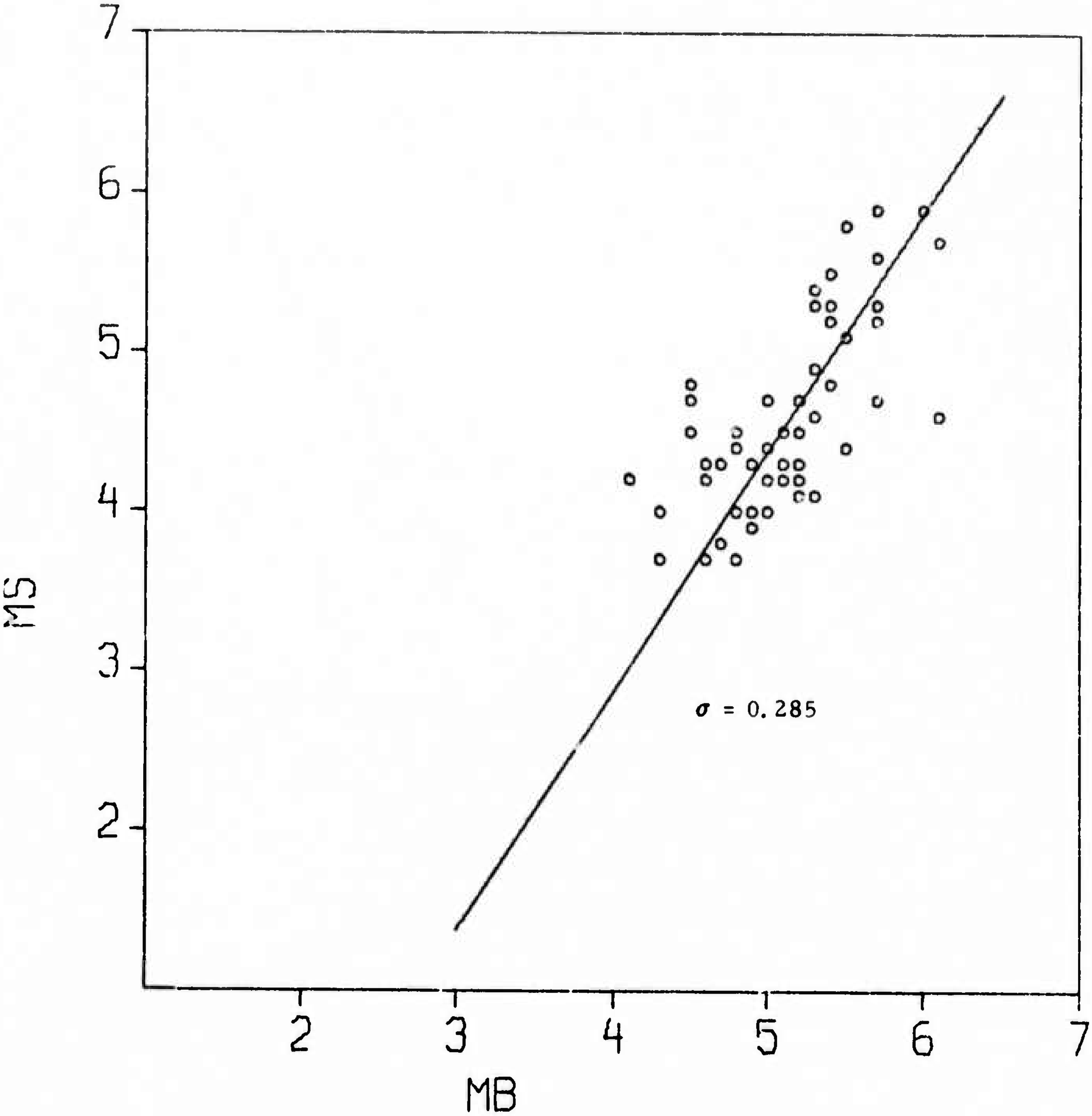

FIGURE II-11

MANUAL M_s MEASUREMENT AND STATION AVERAGED USING BOTH RAYLEIGH AND LOVE WAVES

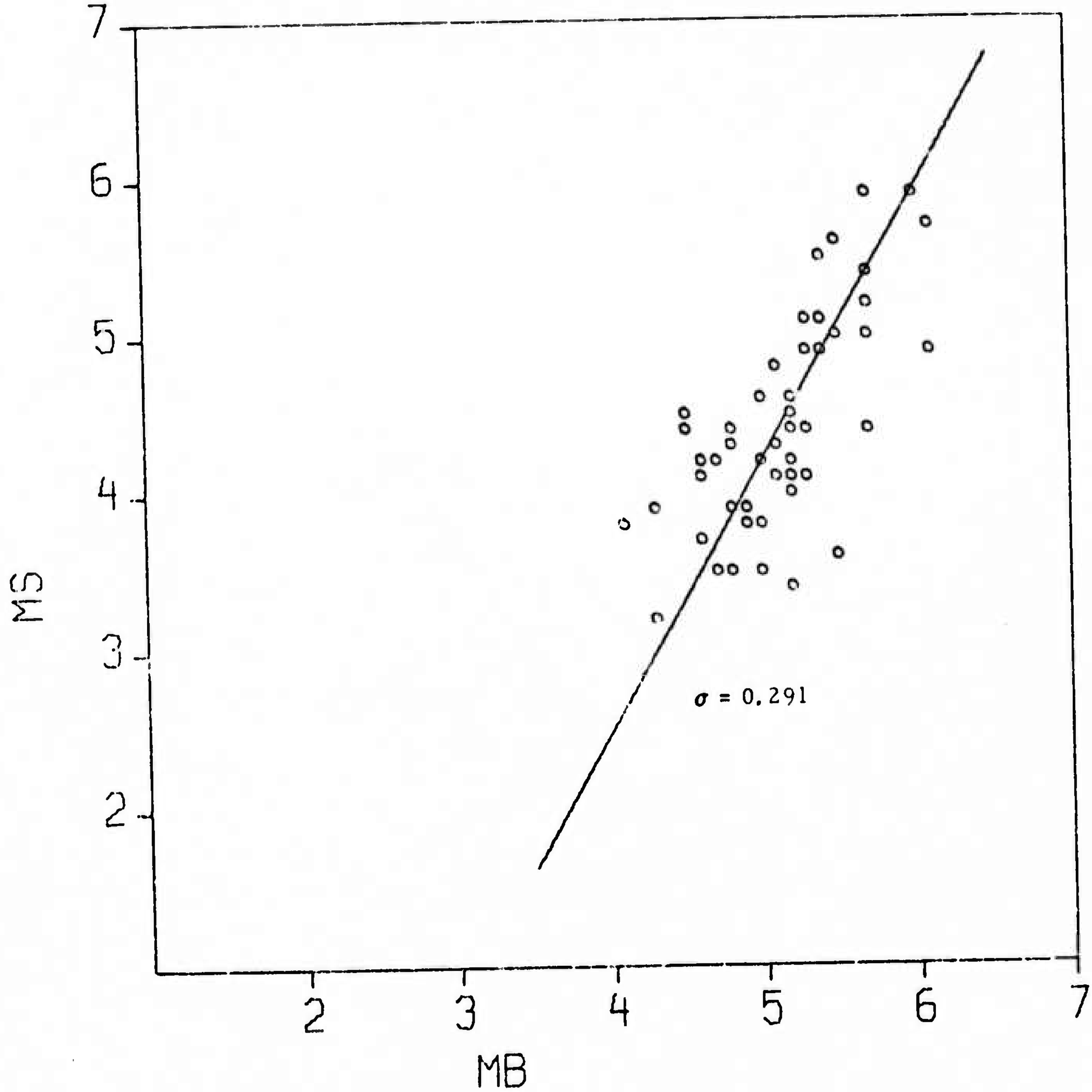

FIGURE II-12

SPECTRAL M_s ESTIMATE FROM RAYLEIGH WAVE

- Figure II-13 illustrates the case where M_s was computed from spectral estimates made from both the Love and vertical Rayleigh waves. The standard deviation of this set is $\sigma = 0.276$, which is slightly lower than the reference value of σ.

- Figure II-14 illustrates the case where M_s values were computed by the method of demultipathing as described in Appendix B. These M_s values are averages of all available station M_s values. The standard deviation of this set is $\sigma = 0.291$, which is slightly greater than the reference value of σ.

- Figure II-15 illustrates the case where an effort was made to remove the high and low station M_s values. For each event, the station M_s values derived from the demultipathing method were averaged and a standard deviation computed. Those station M_s values which were greater than one standard deviation from the average in absolute value were rejected. The average of the remaining station M_s values was then computed. The standard deviation of the resulting data set is $\sigma = 0.276$, which is slightly lower than the reference values of σ.

In addition to the above, standard deviations for the corresponding data sets at 30 second and 40 second periods were computed. These showed essentially no change from that of the 20 second data.

The above discribed data sets used m_b values as reported by PDE. Standard deviations for the data sets were also computed using NORSAR and LASA m_b values. These standard deviations were markedly higher than those using PDE m_b data.

Therefore, we have seen that the various methods of reducing the scatter in M_s-m_b plots as described above have not succeeded. This suggests that, for the case where PDE m_b values are used and all mixed events have been

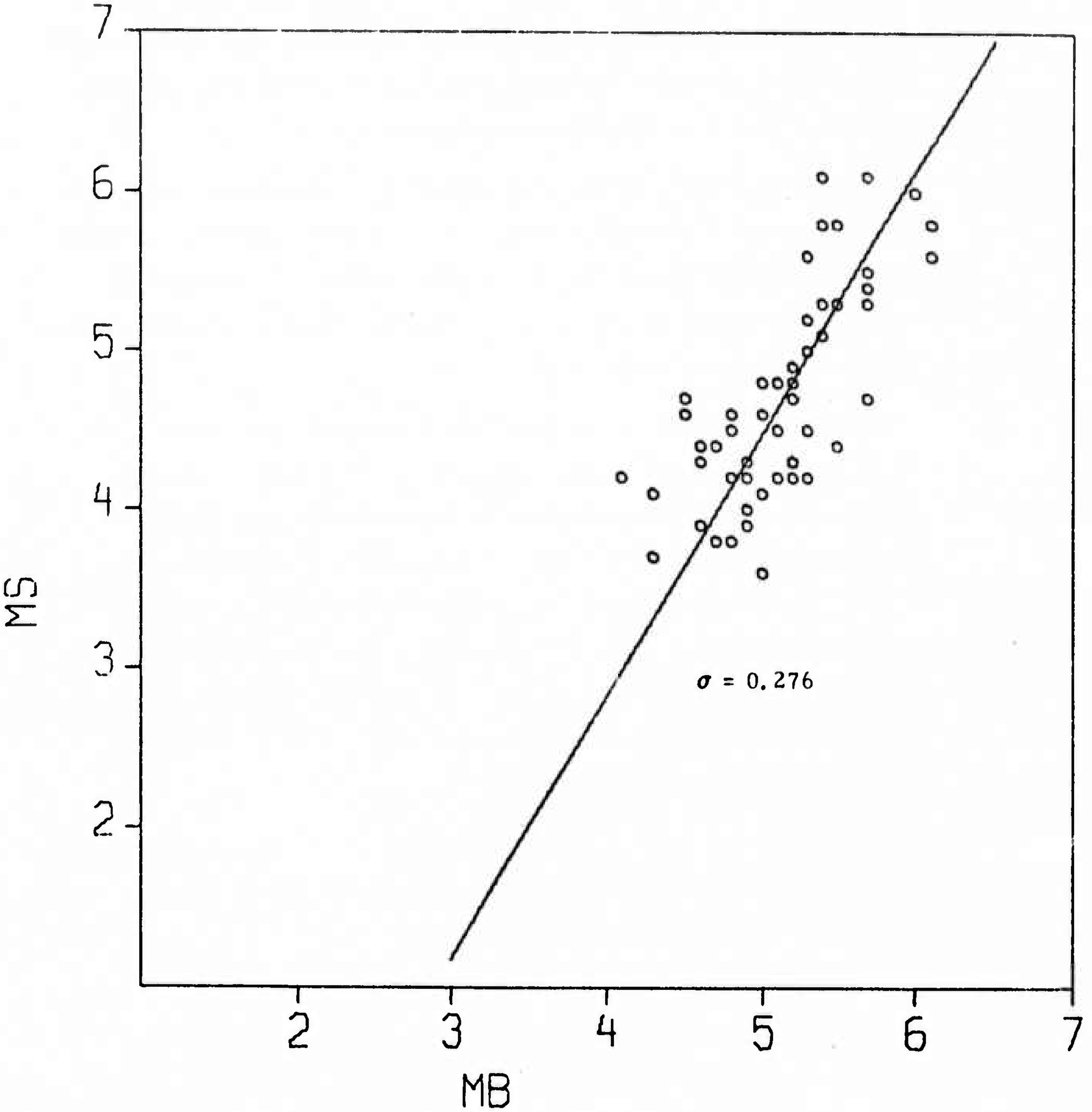

FIGURE II-13

SPECTRAL M_s ESTIMATE FROM BOTH RAYLEIGH AND LOVE WAVES

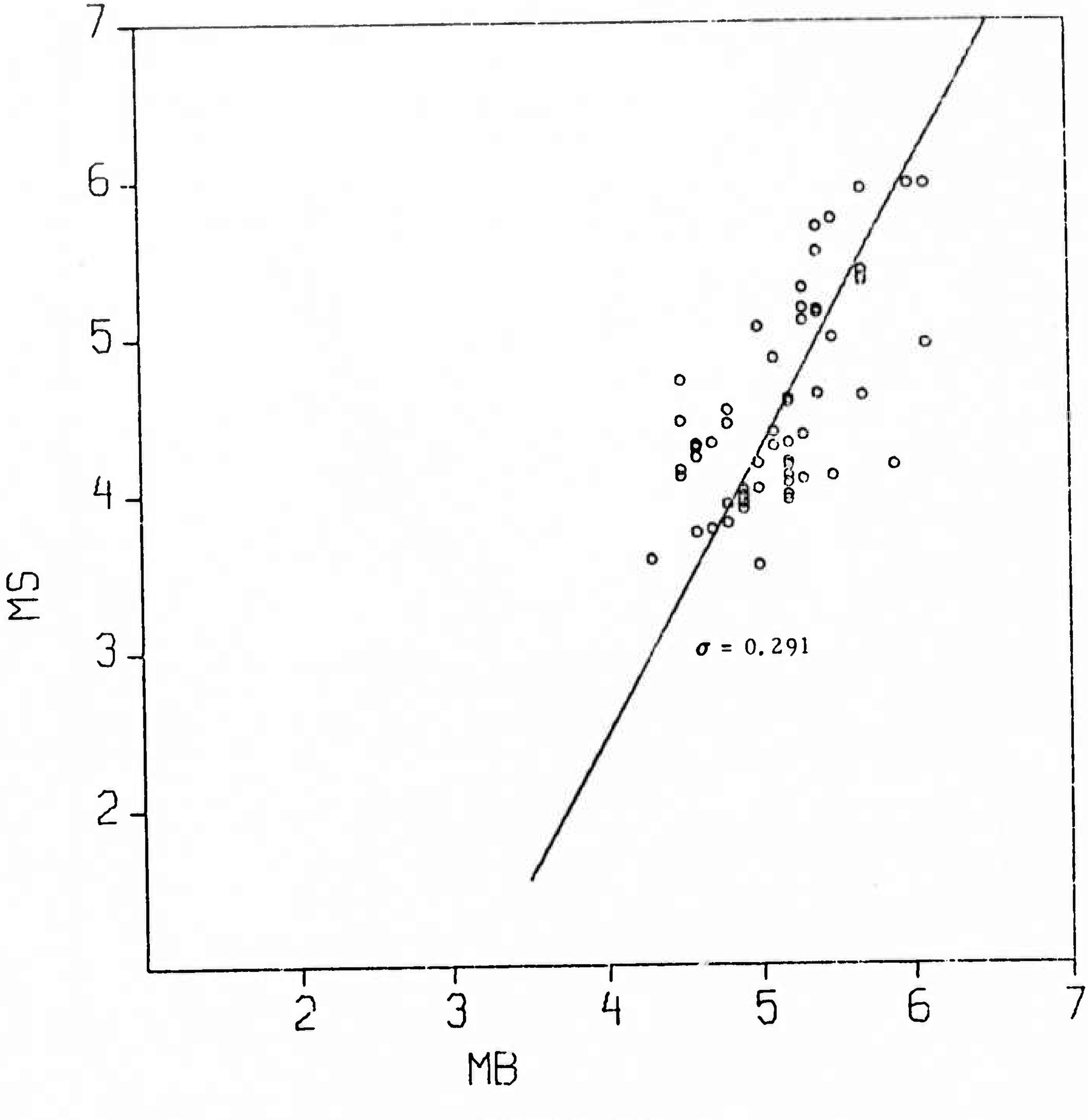

FIGURE II-14

DEMULTIPATHED M_s USING RAYLEIGH WAVE

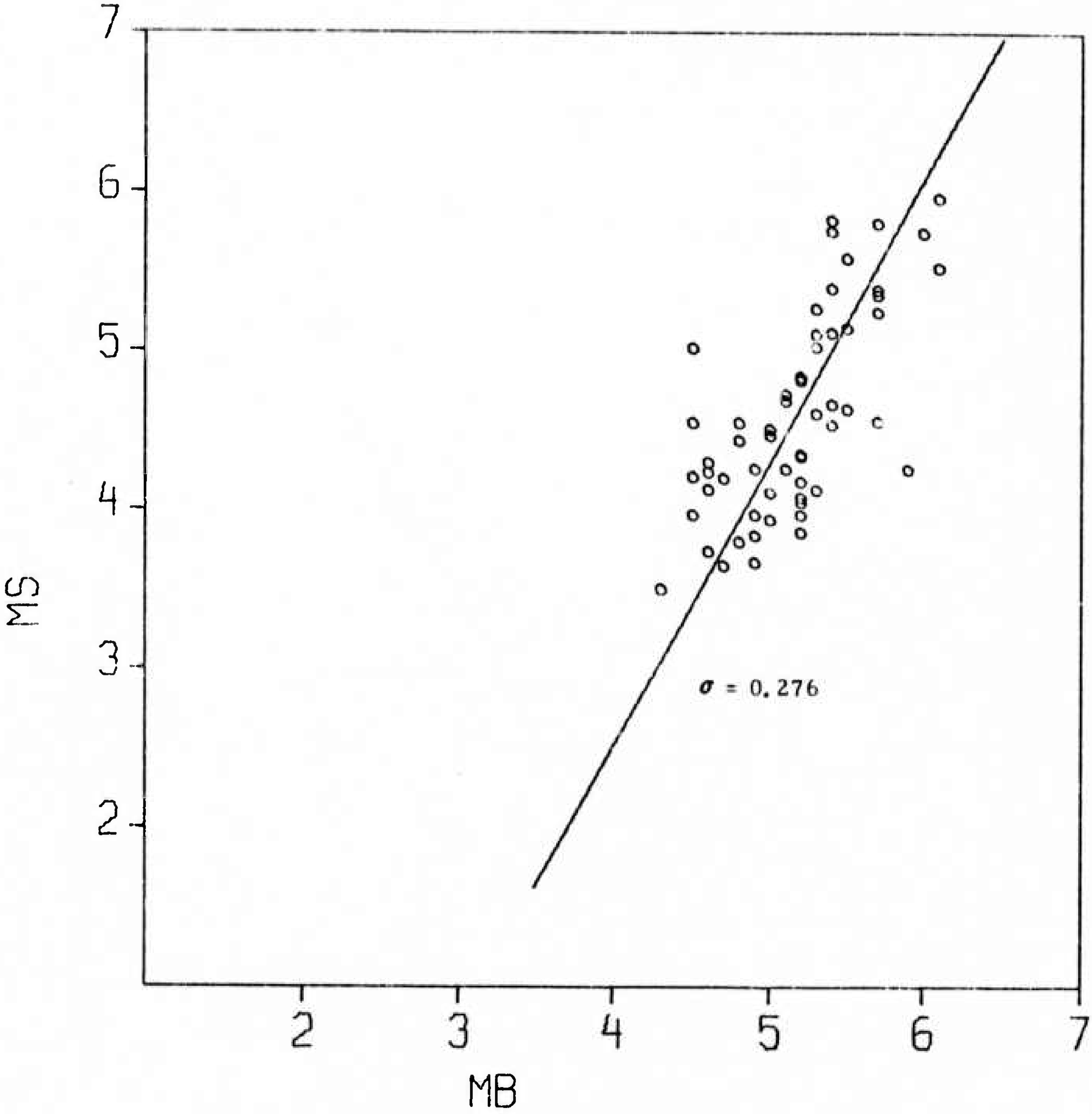

FIGURE II-15

DEMULTIPATHED M_s USING RAYLEIGH WAVE WITH HIGH AND LOW M_s VALUES REMOVED

removed, a standard deviation of approximately $\sigma = 0.28$ is the minimum for the data points of an M_s-m_b plot and cannot be reduced by attempting to reduce the variance in M_s. If any reduction in the scatter of these plots is to be achieved, it must be accomplished through reduction of the variance of m_b. It is suggested that this be attempted in the future by means of maximum likelihood estimation (Ringdal, 1975). The close agreement of the lines fitted to the M_s-m_b sets produced by the above methods and the similarity of the associated standard deviations indicates that the demultipathing method is a good way to determine M_s values. It has an advantage over the presently used manual measurement method in that it is not always possible to measure M_s at all of the desired periods manually, whereas these measurements can always be made by the demultipathing technique.

D. EXAMINATION OF THEORETICAL HIGHER MODE SPECTRA

Using the Harkrider (1964) formulation of a double couple source in a layered half space, theoretical first higher mode Rayleigh and Love wave spectra were generated. The objective of this study is to use higher mode information to determine depth and structure in the source region, especially for shallow events. We can summarize the properties of this spectra and its use as follows:

- Because the higher mode energy is greater at shorter periods, its spectra offers higher resolution than fundamental mode surface wave data for excitation differences between shallow, thin layers. As an example, the variation of this spectra with depth is shown in Figures II-16a and 16b for a vertical strike-slip fault. While the spectral shape is similar to that of the fundamental mode Rayleigh wave of longer periods, the higher mode Love wave spectra contains a great deal more character than its fundamental counterpart (Turnbull, et al., 1974a). Therefore, for the first higher mode, both Rayleigh and Love waves are diagnostic with source depth.

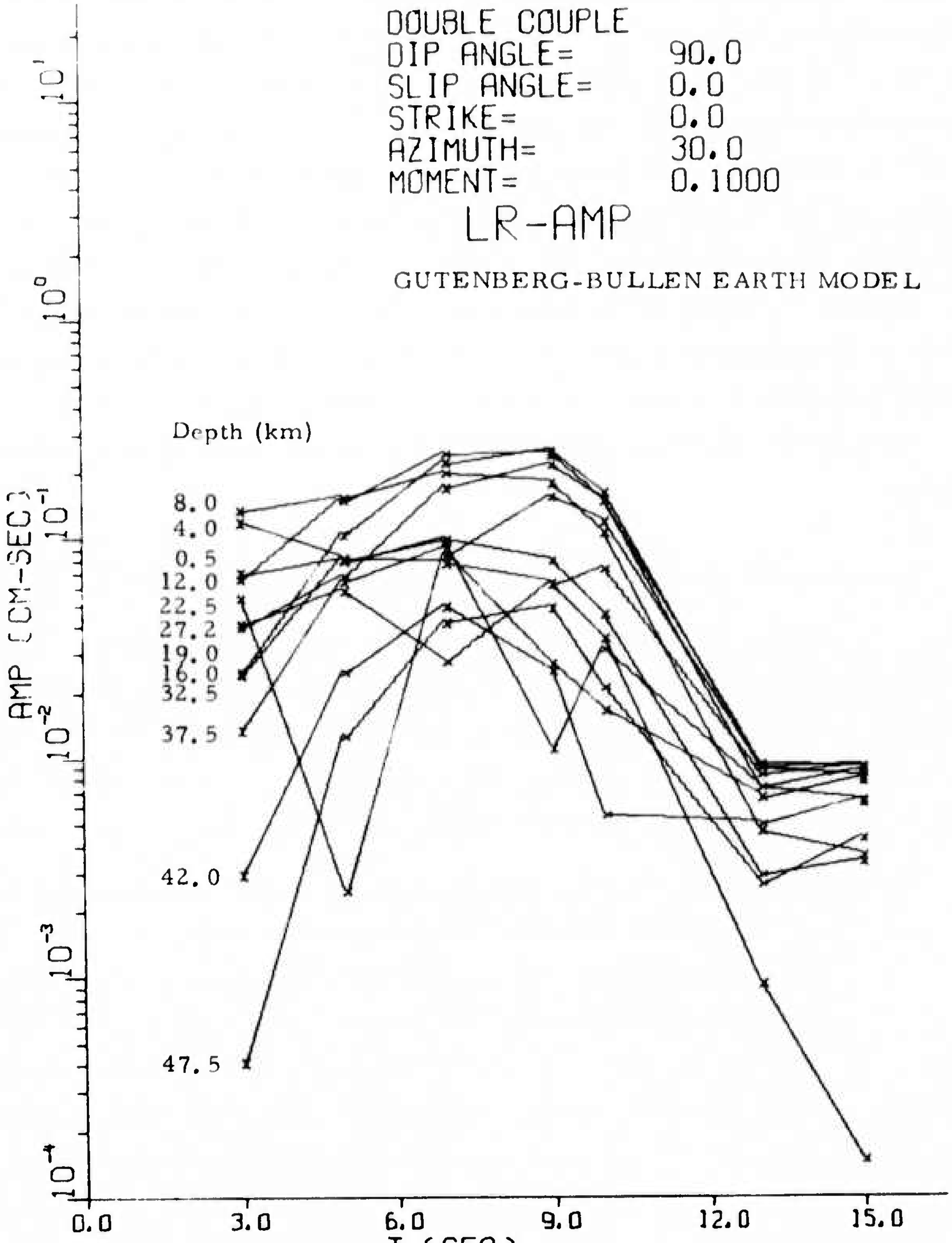

FIGURE II-16a

FIRST HIGHER MODE RAYLEIGH WAVE SPECTRA
FOR A VERTICAL STRIKE-SLIP FAULT

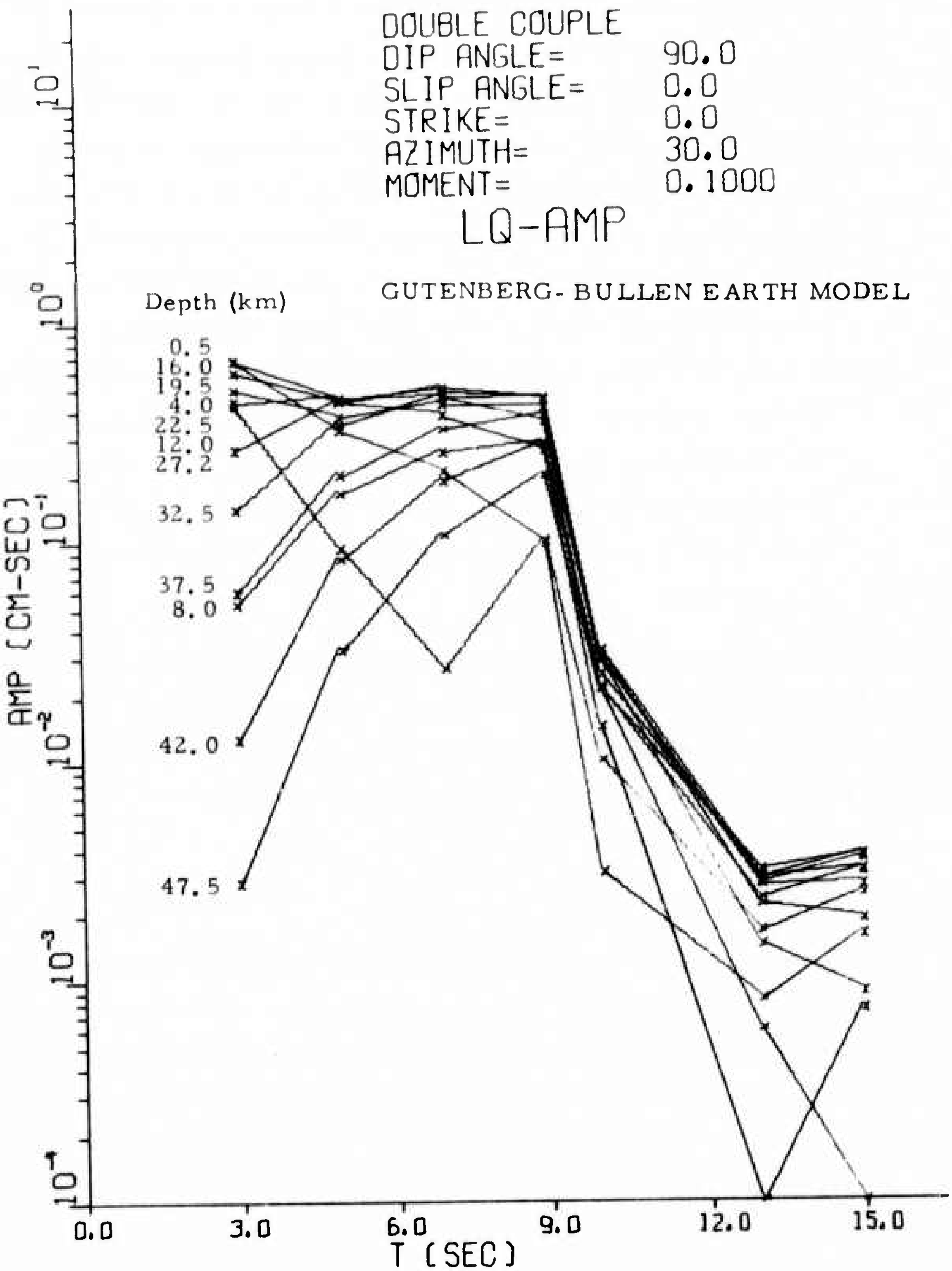

FIGURE II-16b

FIRST HIGHER MODE LOVE WAVE SPECTRA
FOR A VERTICAL STRIKE-SLIP FAULT

- There are several difficulties involved in the use of higher mode data. Because we are interested in shorter period energy (less than 15 seconds), attenuation and microseismic noise become a problem. Therefore, one is usually restricted to using data from very large earthquakes which generate long period higher mode energy. In the past, we have also been restricted by the instrument response, with very little energy recorded below 10 seconds period. Some of these difficulties will be eliminated though, when SRO, ILPA, and certain experimental LRSM data becomes available. These installations utilize new broadband instrumentation, with a flat response to below 3 seconds period. Employing filters for the microseismic noise and first zone events ($< 20^o$), higher mode data should be available over a range of magnitudes.

Our software for fitting fundamental mode surface wave spectra is presently being modified to handle higher mode data. When this is complete, and the broadband data is available, we will attempt to determine the source mechanism and source region structure using higher mode data.

E. CONCLUSION

Several tasks have been undertaken in our study of far-field spectra for source characteristics. Using spectral fitting procedures on fundamental mode surface wave data from two central California events, generally close agreement was obtained with source mechanism solutions from body waves. The spectral fits were of "average" quality at best, which was due to the relatively small azimuthal spread of stations and the gross approximation of source region structure. For the Bear Valley earthquake of June 22, 1973, the seismic moment obtained from the surface wave data was an order of magnitude smaller than that obtained from acceleration data. It is difficult to say whether this difference is a result of modeling inaccuracies or a real source property. For the central California earthquake of November 28, 1974, our solution was limited because of the availability of earth structure information. Future studies to these two events will involve implementation of more accurate earth structures for a definitive comparison with bodywave data.

In an attempt to reduce the scatter in M_s-m_b plots for an earthquake population, several attempts were made to reduce the variance in M_s. Using a demultipathing procedure as implemented for the radiation pattern with four station averages, produced no noticeable effect. If any reduction in the scatter of these plots is to be achieved, the variance of m_b must be reduced. Two byproducts of this investigation were the collection of enough source-station travel path data for a group velocity study of Eurasia, and an accurate method to determine M_s using the demultipathing procedure.

Finally, theoretical higher mode surface wave spectra have been generated for a double couple source in a layered half space. Both the Rayleigh and Love wave higher mode spectra vary shape to a higher degree as a function of source depth; they are quite sensitive to source depth and source region structure. Upon modification of our spectral fitting programs, and imminent availability of broadband data, we should obtain better depth resolution for shallow events.

SECTION III

REFERENCES

Barnard, T. E., 1975, The Maximum Entropy Spectrum and the Burg Technique, Internal Memorandum, Texas Instruments Incorporated, Dallas, Texas.

Brune, J. N., 1970, Tectonic Stress and the Spectra of Seismic Shear Waves, J. Geophysical Research, 75, 4997-5009.

Burg, J. P., 1967, Maximum Entropy Spectral Analysis, paper presented at 37 th Annual International SEG Meeting, Oklahoma City, Oklahoma.

Burg, J. P., 1968, A New Analysis Technique for Time Series Data, paper presented at NATO Advanced Study Institute on Signal Processing, Enschede, Netherlands.

Harkrider, D. G., 1964, Surface Waves in Multilayered Elastic Media; I. Rayleigh and Love Waves from Buried Sources in A Multilayered Elastic Half-Space, Bull. Seismol. Soc. Amer., 54, 627-679.

Helmberger, D. L., 1975, personal communication.

Johnson, L. R., 1975, personal communication.

King, W. R., William H. Swindell, and Leo J. O'Brien, 1974, Final Report on Development of a Curvilinear Ray Theory Model and Maximum Entropy Spectral Analysis, Final Report, Texas Instruments Report Number ALEX(03)-FR-74-01, Texas Instruments Incorporated, Dallas, Texas.

Lacoss, R. T., 1971, Data Adaptive Spectral Analysis Methods, Geophysics, Volume 36, 661-675.

Lambert, D. G., A. I. Tolstoy, and E. S. Becker, 1974, Seismic Detection and Discrimination Capabilities of the Very Long Period Experiment, Technical Report No. 7, Texas Instruments Report Number ALEX(01)-TR-74-07, AFTAC Contract Number F08606-74-C-0033, Texas Instruments Incorporated, Dallas, Texas.

Ringdal, F., 1975, Maximum Likelihood Estimation of Seismic Event Magnitude from Network Data, Texas Instruments Report No. ALEX(01)-TR-75-01, Contract Number F08606-75-C-0029, Texas Instruments Incorporated, Dallas, Texas.

Sax, R. L., 1975, personal communication.

Tsai, Y. B., 1972, Utility of Tsai's Method for Seismic Discrimination: Semiannual Technical Report No. 2, Texas Instruments, Incorporated, Dallas, Texas.

Turnbull, L. S., D. F. D. Sun, and J. S. Shaub, 1973, Determination of Seismic Source Parameters from Frequency Dependent Rayleigh and Love Wave Radiation Patterns, Semi-Annual Technical Report No. 1-Part C, Texas Instruments, Incorporated, Dallas, Texas.

Turnbull, Jr., L. S., and J. C. Battis, 1974, Interpretation of Strong-Motion Earthquake Accelerograms: The Bear Valley Event of 1973, Final Report, Texas Instruments Report Number ALEX(02)-FR-74-01, AFOSR Contract Number F44620-72-0073, Texas Instruments Incorporated, Dallas, Texas.

Turnbull, Jr., L. S., David Sun, and D. G. Black, 1974a, Determination of Seismic Source Parameters From Long-Period Teleseismic Waves, Semi-Annual Technical Report No. 2 - Part A, Texas Instruments Report Number ALEX(02)-TR-74-02-PART, AFOSR Contract Number F44620-73-C-0055, Texas Instruments Incorporated, Dallas, Texas.

Turnbull, Jr., L. S., James C. Battis, and David Sun, 1974b, Source Studies in the Near and Far Field, Semi-Annual Technical Report No. 3- Part A, Texas Instruments Report Number ALEX(02)-TR-74-03-PART A, AFOSR Contract Number F44620-73-C-0055, Texas Instruments Incorporated, Dallas, Texas.

Ulrych, T. J., 1972, Maximum Entropy Power Spectrum of Truncated Sinusoids, J. Geophys. Res., v. 77, p. 1396.

APPENDIX A

LONG-PERIOD SEISMOGRAMS FROM TWO CALIFORNIA EARTHQUAKES

In this appendix, the long-period seismograms used in the source mechanism determination of the 22 June, 1973 and the 28 November, 1974 central California earthquakes are displayed. Each of the figures represent copies of the signal displayed on the PDP-15 interactive graphics system (Turnbull, 1974b). The lines at the top of each figure give the event information and then the station identification. At the bottom of each figure, the amplitude of the trace is given in milli-microns (it is denoted by NM on the figure). The interval between scale marks on the baseline represents 100 seconds. The lines denoting S, LQ, LR, and LREND indicate arrival times generated from standard travel time curves, and are meant as an aid to the analyst rather than identification of the particular phases. The seismograms displayed are as follows:

- Bear Valley Earthquake - June 22, 1973

  Figures A-1-a, b, c: Vertical, transverse, and radial LP components as recorded at LASA

  Figures A-2-a, b, c: The three LP components as recorded at OGD

  Figures A-3-a, b, c: The three LP components as recorded at ALQ

- Central California Earthquake - November 28, 1974

  Figures A-4-a, b, c: Vertical, transverse, and radial LP components as recorded at LASA

  Figures A-5-a, b, c: The three LP components as recorded at NORSAR

Figures A-6-a, b, c: The three LP components as recorded at ALPA

Figures A-7-a, b, c: The three LP components as recorded at TLO

Figures A-8-a, b, c: The three LP components as recorded at KIP

Figures A-9-a, b, c: The three LP components as recorded at ZLP.

BEV/622/73LA 36.6N 121.2W 73/173/ 1.29.12.0
LAB 2 CP=1 46.7N 106.2W 73/173/ 1.33.35.0 A=-126 D= 15 S=2.00

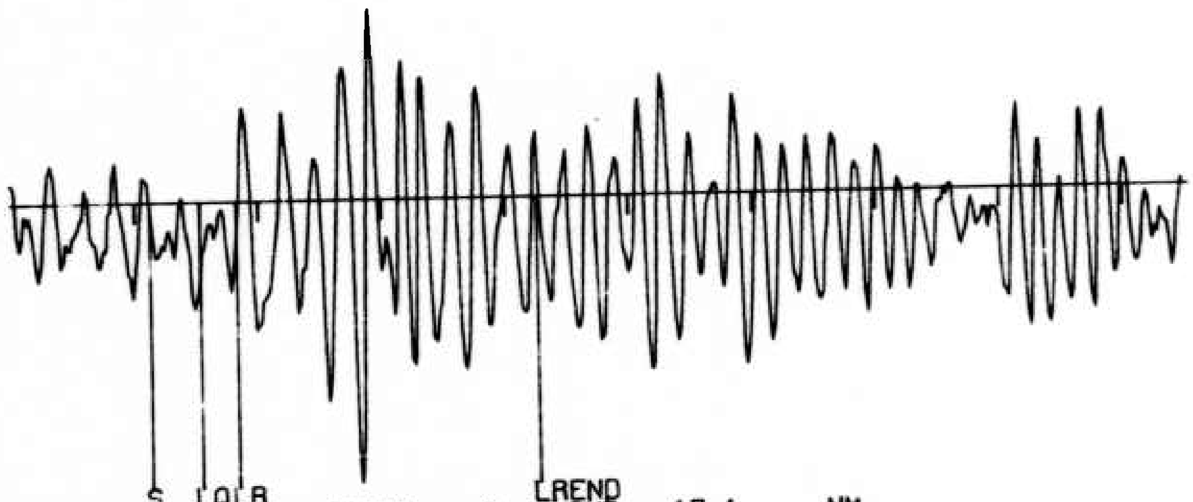

BP=0.000-10.000 CHIRP= 0. AMP= 17.1 NM

WORK TRACE = 1 CHIRP INCR = 100.

FIGURE A-1-a

THE LONG-PERIOD VERTICAL COMPONENT OF THE JUNE 22, 1973 BEAR VALLEY EARTHQUAKE AS RECORDED AT LASA

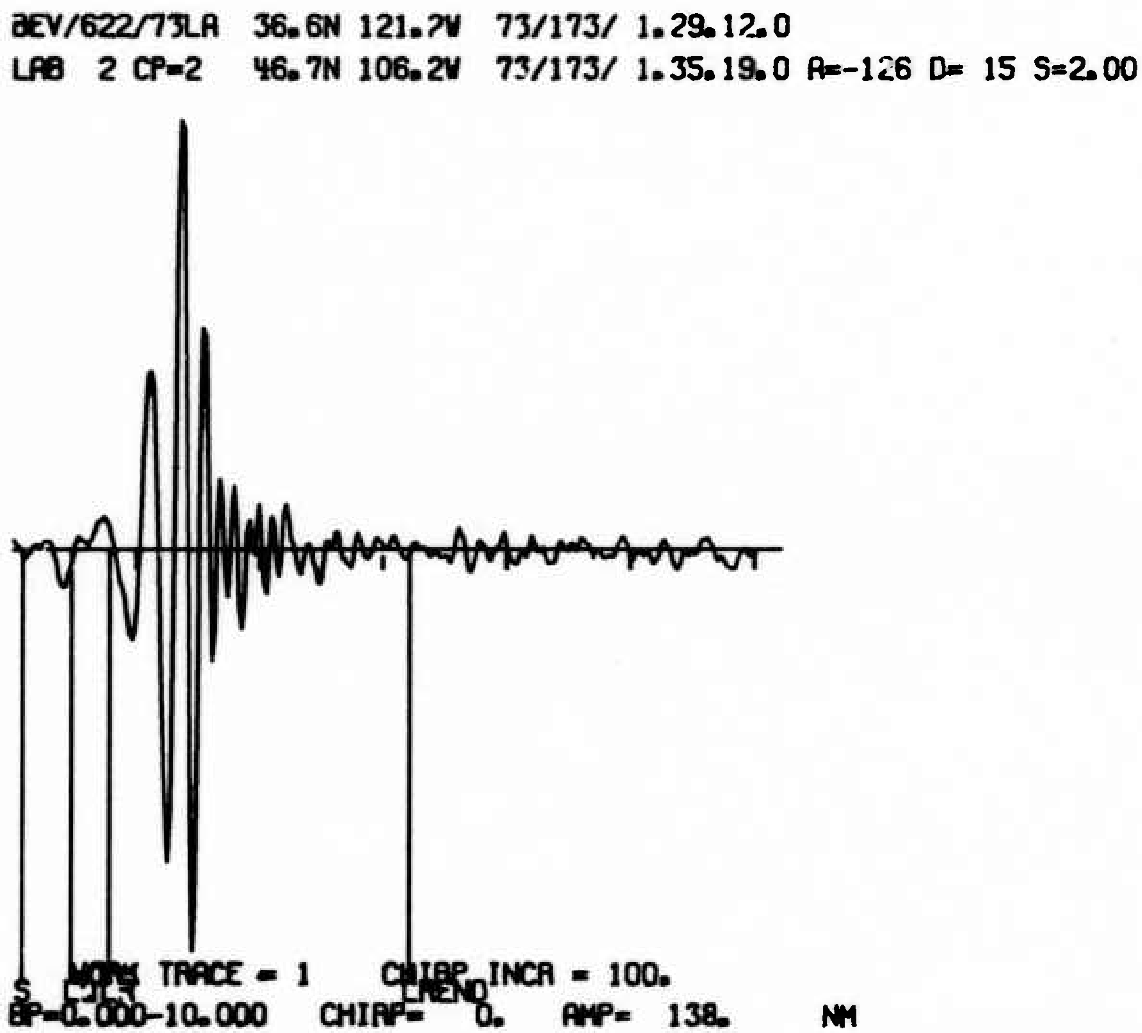

FIGURE A-1-b

THE LONG-PERIOD TRANSVERSE COMPONENT OF THE JUNE 22, 1973 BEAR VALLEY EARTHQUAKE AS RECORDED AT LASA

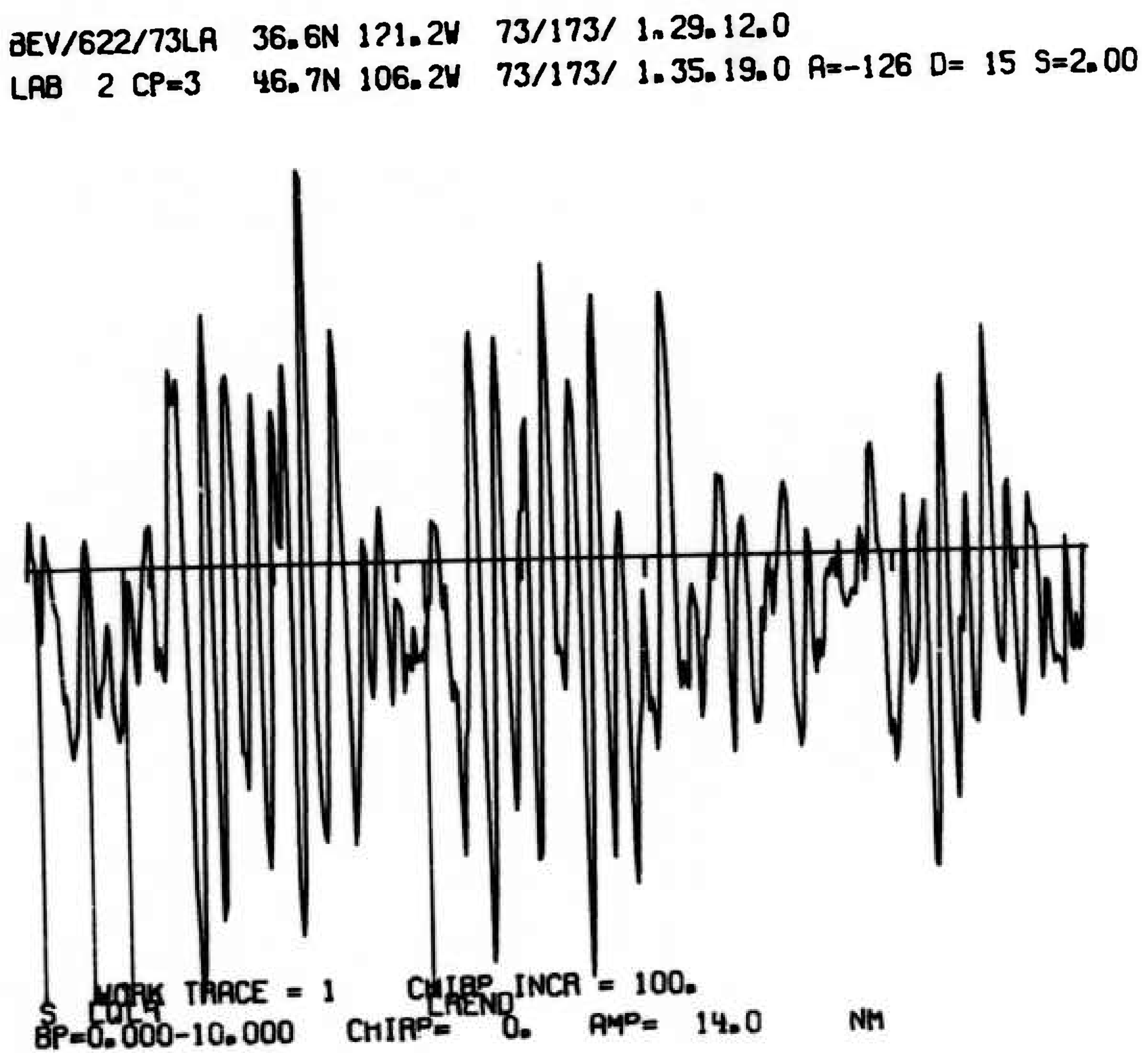

FIGURE A-1-c

THE LONG-PERIOD RADIAL COMPONENT OF THE JUNE 22, 1973
BEAR VALLEY EARTHQUAKE AS RECORDED AT LASA

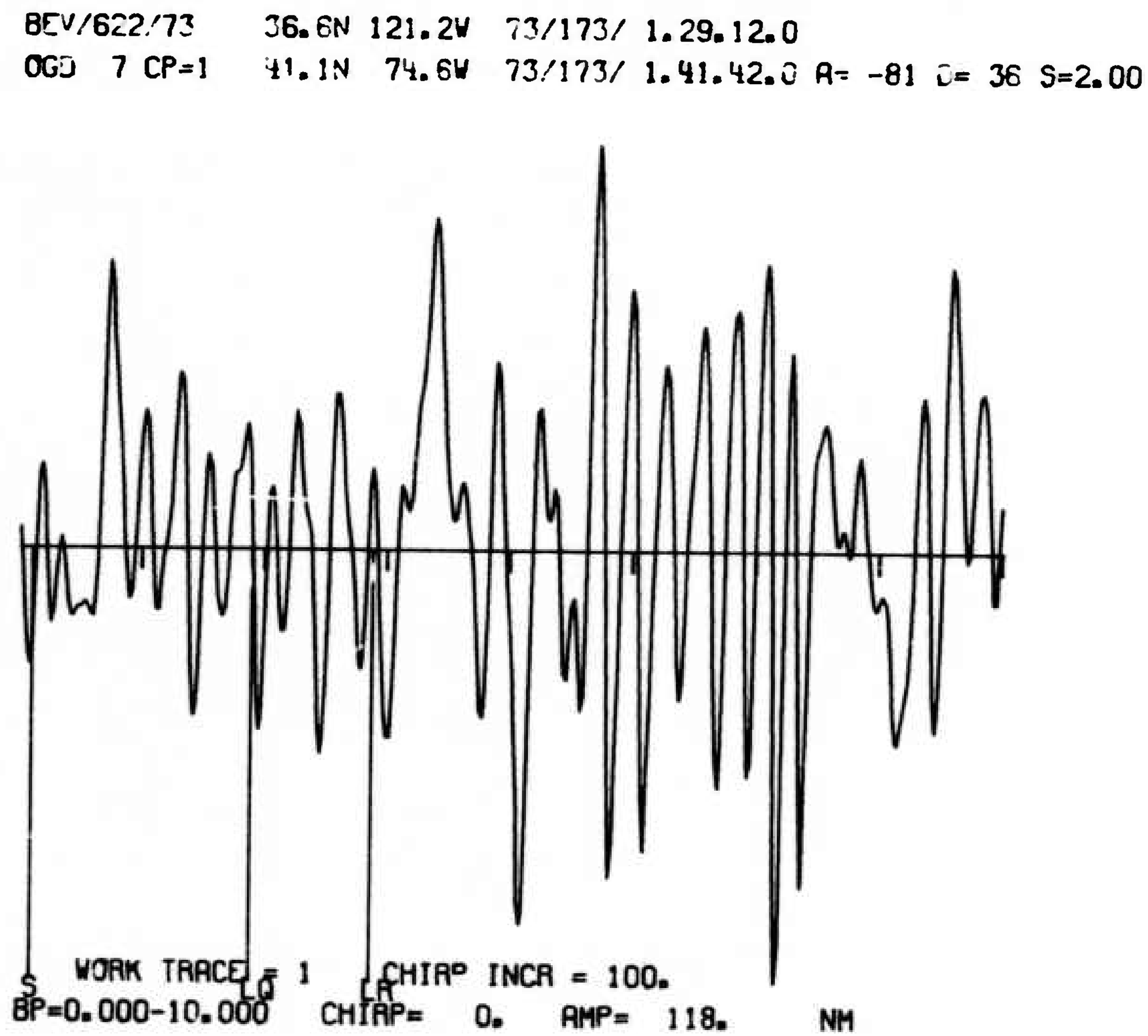

FIGURE A-2-a

THE LONG-PERIOD VERTICAL COMPONENT OF THE JUNE 22, 1973 BEAR VALLEY EARTHQUAKE AS RECORDED AT OGD

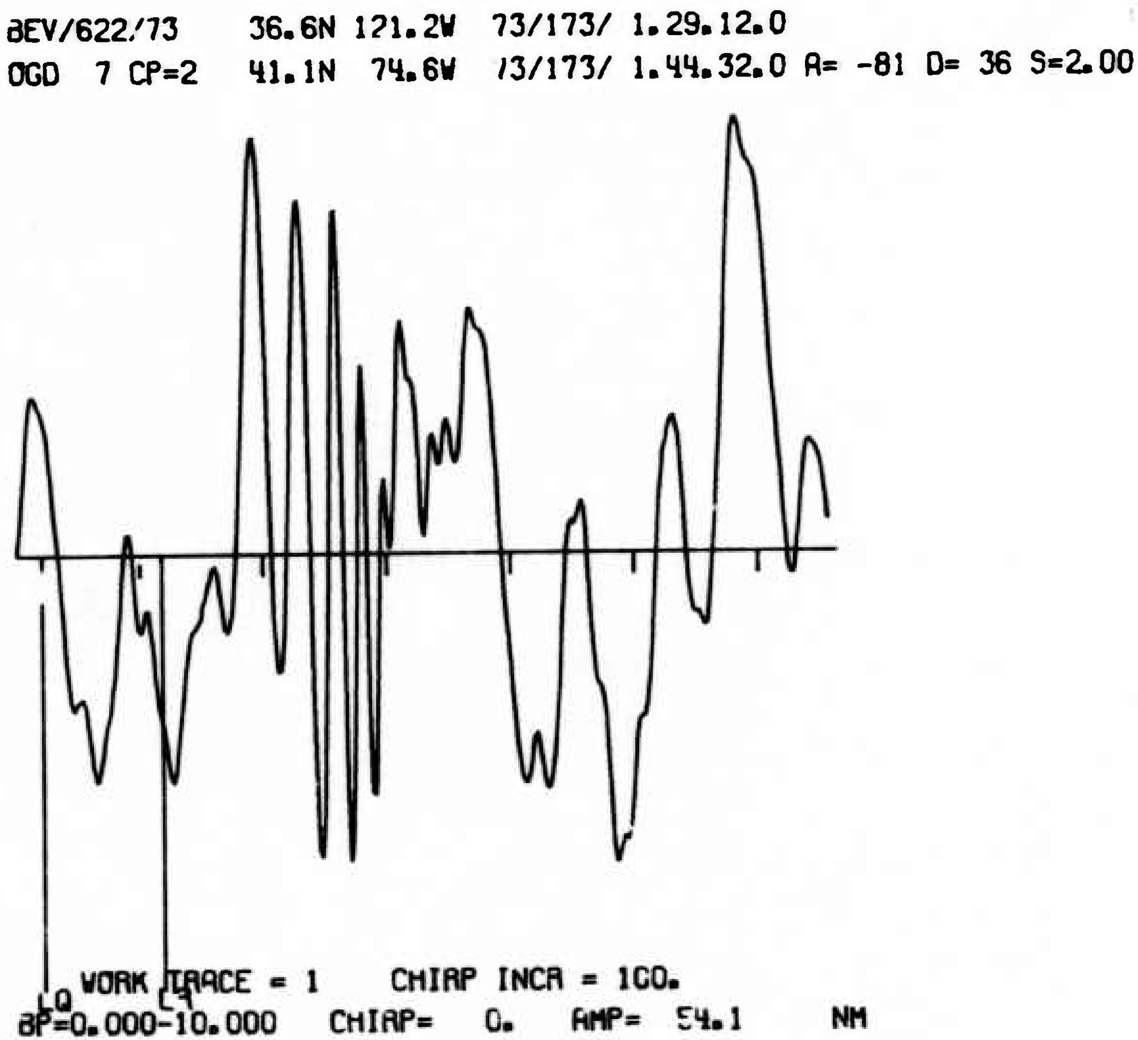

FIGURE A-2-b

THE LONG-PERIOD TRANSVERSE COMPONENT OF THE JUNE 22, 1973 BEAR VALLEY EARTHQUAKE AS RECORDED AT OGD

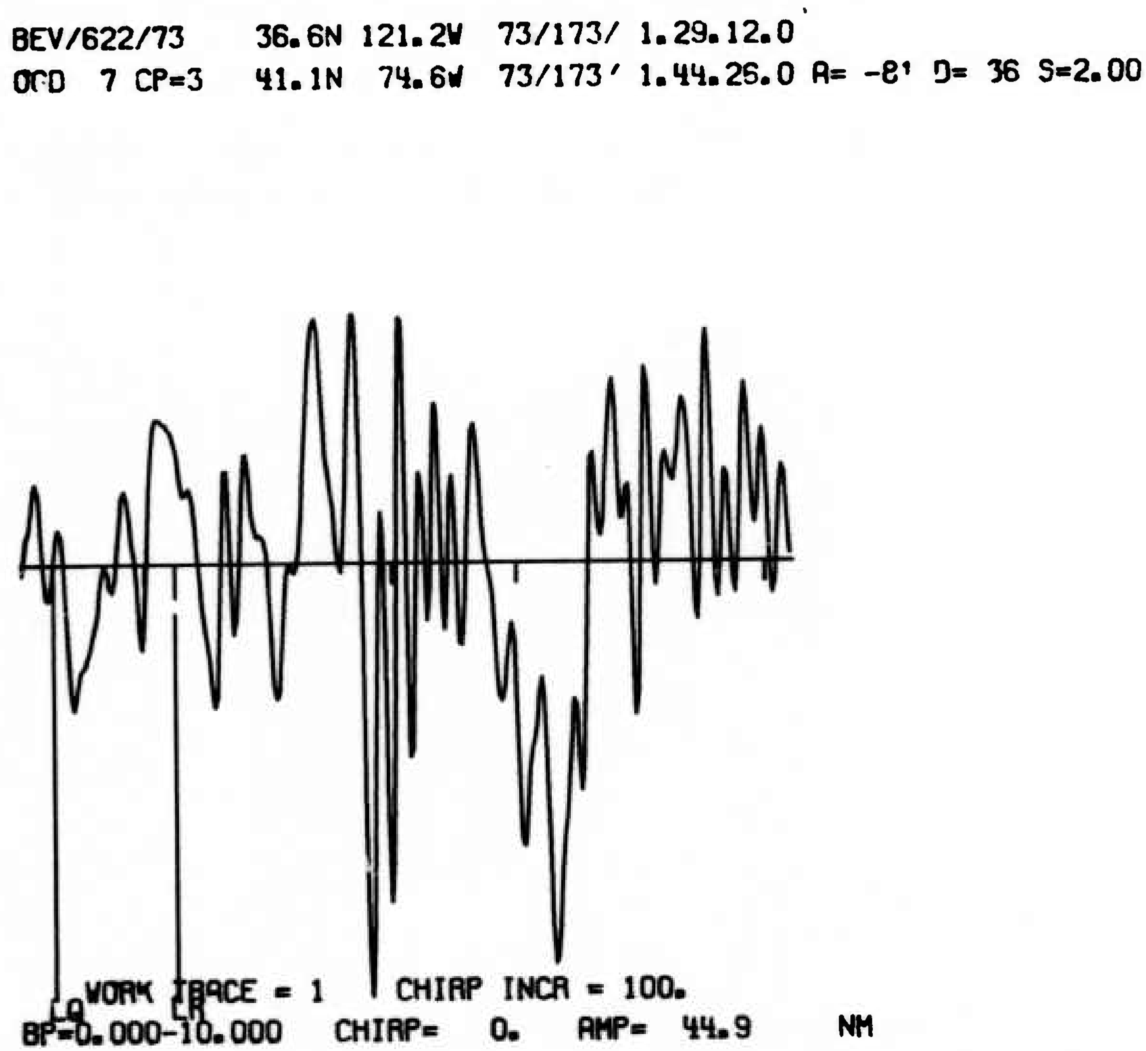

FIGURE A-2-c

THE LONG-PERIOD RADIAL COMPONENT OF THE JUNE 22, 1973
BEAR VALLEY EARTHQUAKE AS RECORDED AT OGD

FIGURE A-3-a

THE LONG-PERIOD VERTICAL COMPONENT OF THE JUNE 22, 1973 BEAR VALLEY EARTHQUAKE AS RECORDED AT ALQ

BEV/622/73   36.6N 121.2W   73/173/ 1.29.12.0
ALQ 9 CP=2   34.9N 1(6.5W   73/173/ 1.34.40.0 A= -77 D= 12 S=2.00

WORK TRACE = 1   CHIRP INCR = 100.
BP=0.000-10.000   CHIRP= 0.   AMP= 158.   NM

FIGURE A-3-b

THE LONG-PERIOD TRANSVERSE COMPONENT OF THE JUNE 22, 1973 BEAR VALLEY EARTHQUAKE AS RECORDED AT ALQ

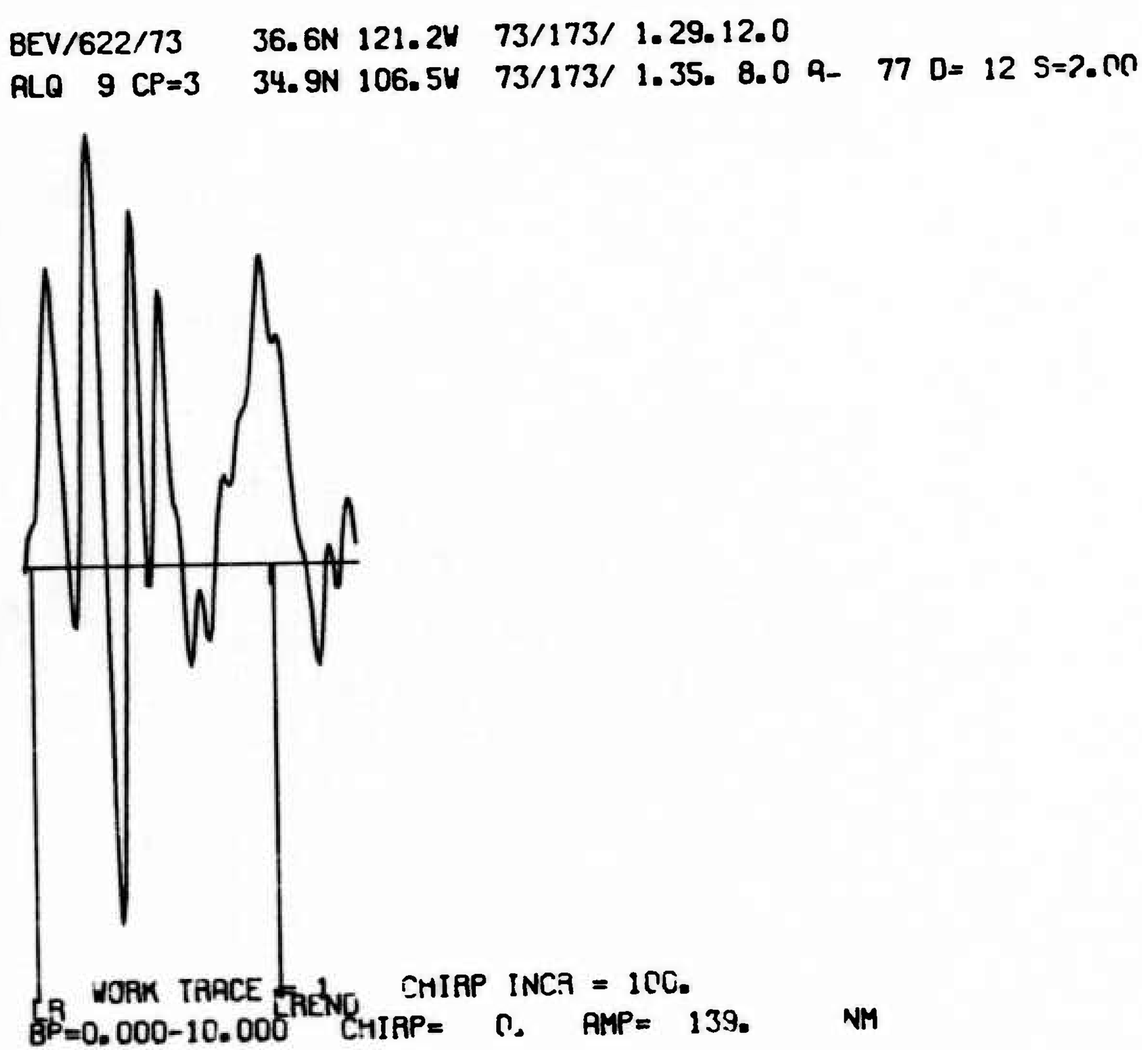

FIGURE A-3-c

THE LONG-PERIOD RADIAL COMPONENT OF THE JUNE 22, 1973 BEAR VALLEY EARTHQUAKE AS RECORDED AT ALQ

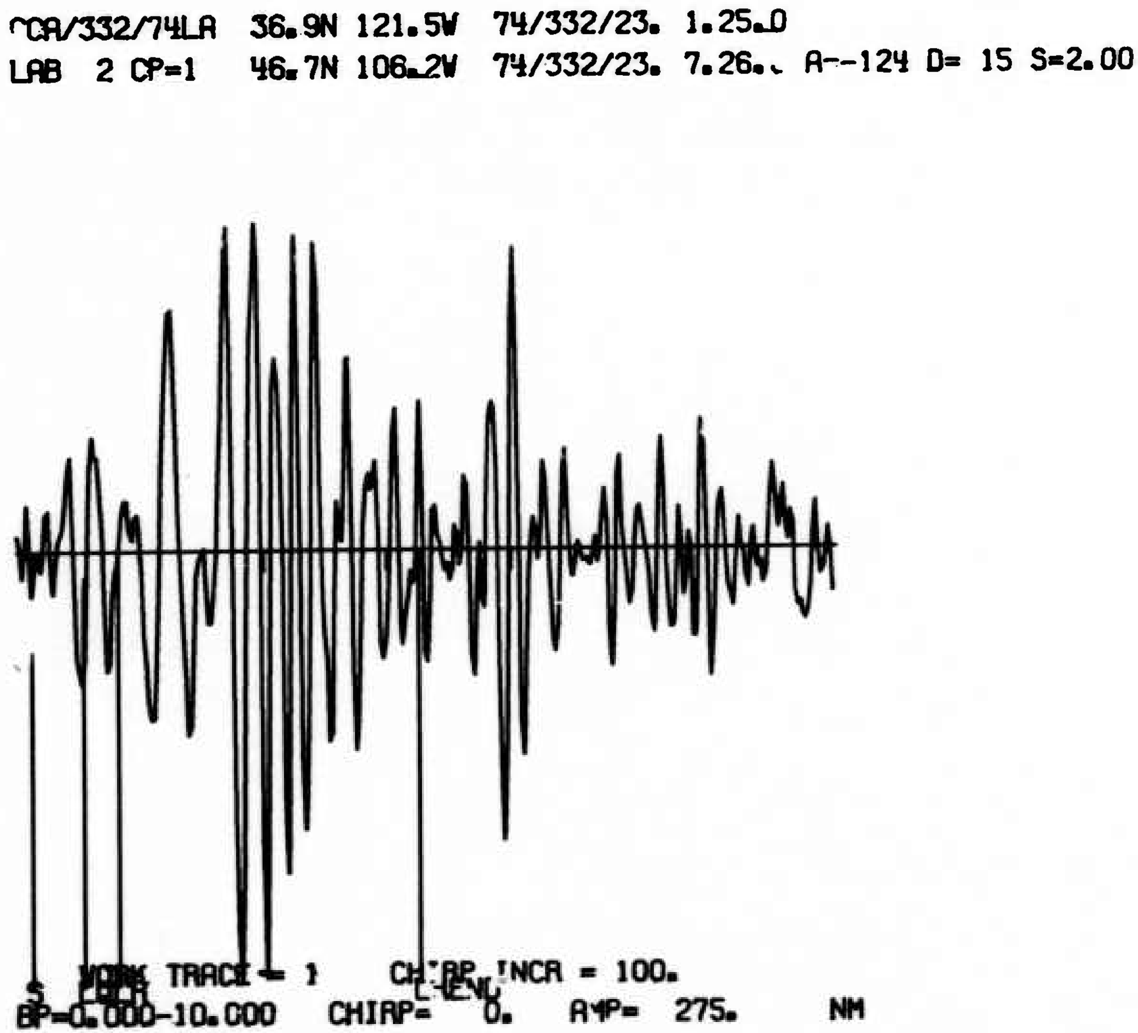

FIGURE A-4-a

THE LONG-PERIOD VERTICAL COMPONENT OF THE NOVEMBER 28, 1974 CENTRAL CALIFORNIA EARTHQUAKE AS RECORDED AT LASA

FIGURE A-4-b

THE LONG-PERIOD TRANSVERSE COMPONENT OF THE NOVEMBER 28, 1974 CENTRAL CALIFORNIA EARTHQUAKE AS RECORDED AT LASA

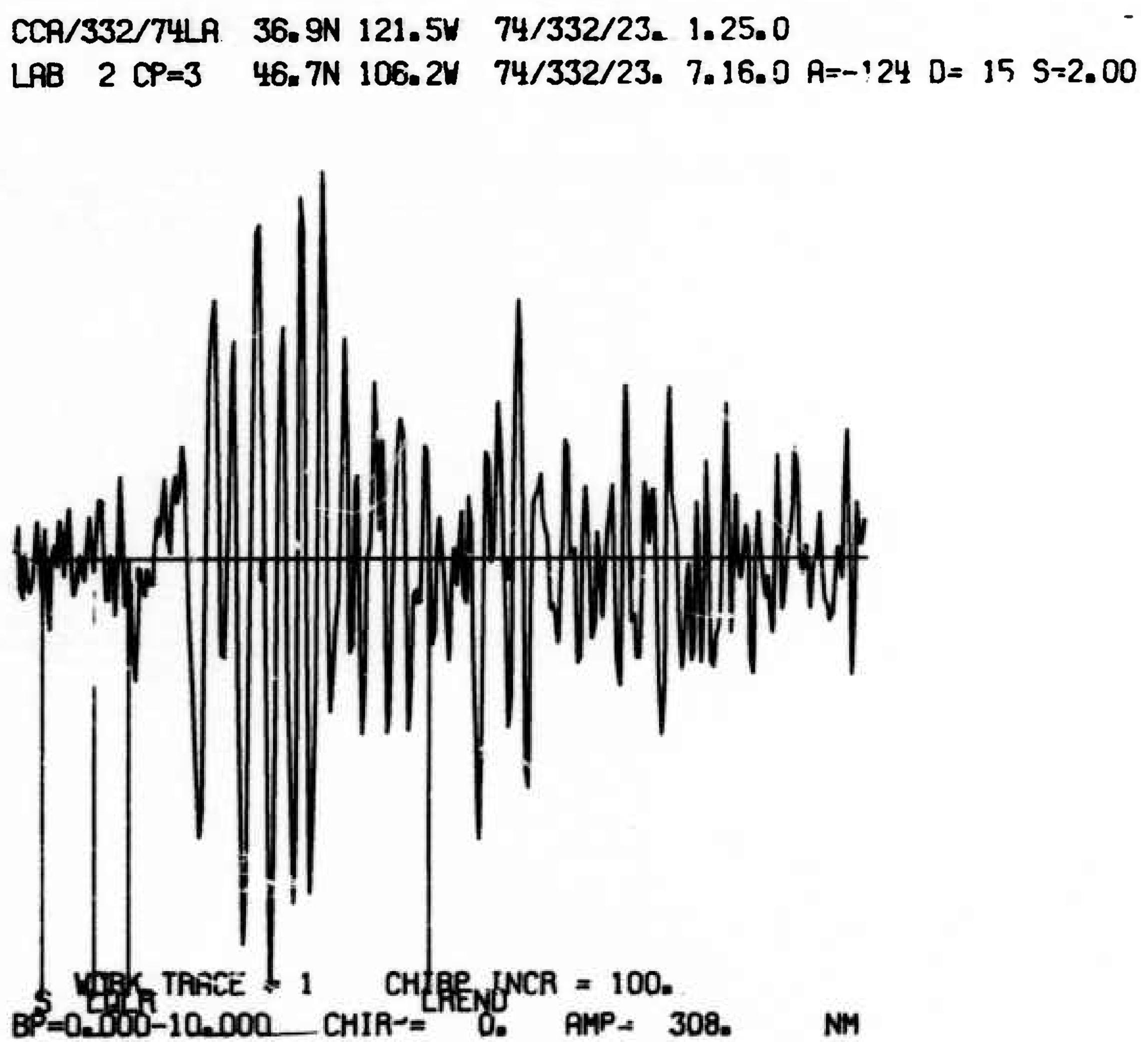

FIGURE A-4-c

THE LONG-PERIOD RADIAL COMPONENT OF THE NOVEMBER 28, 1974 CENTRAL CALIFORNIA EARTHOUAKE AS RECORDED AT LASA

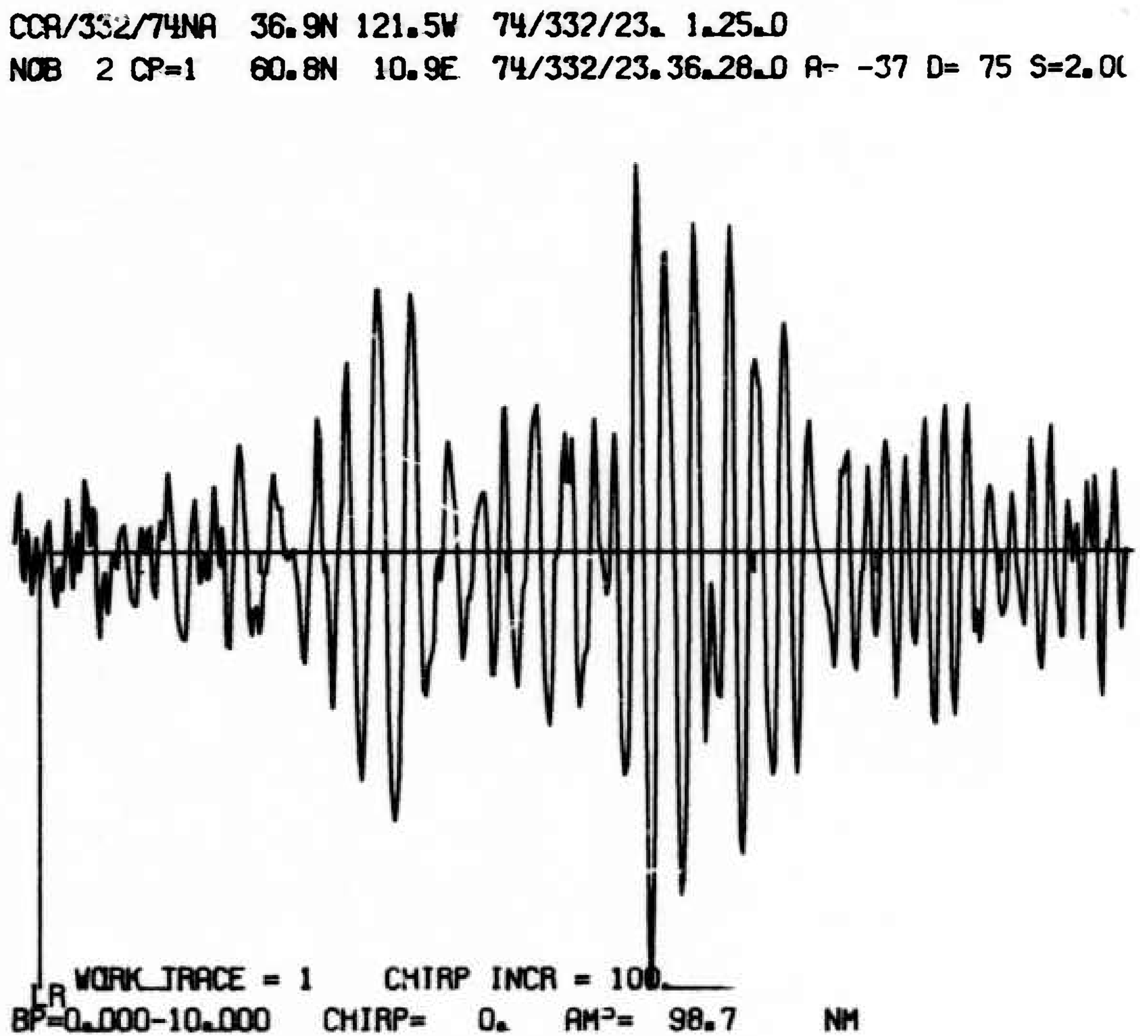

FIGURE A-5-a

THE LONG-PERIOD VERTICAL COMPONENT OF THE NOVEMBER 28, 1974 CENTRAL CALIFORNIA EARTHQUAKE AS RECORDED AT NORSAR

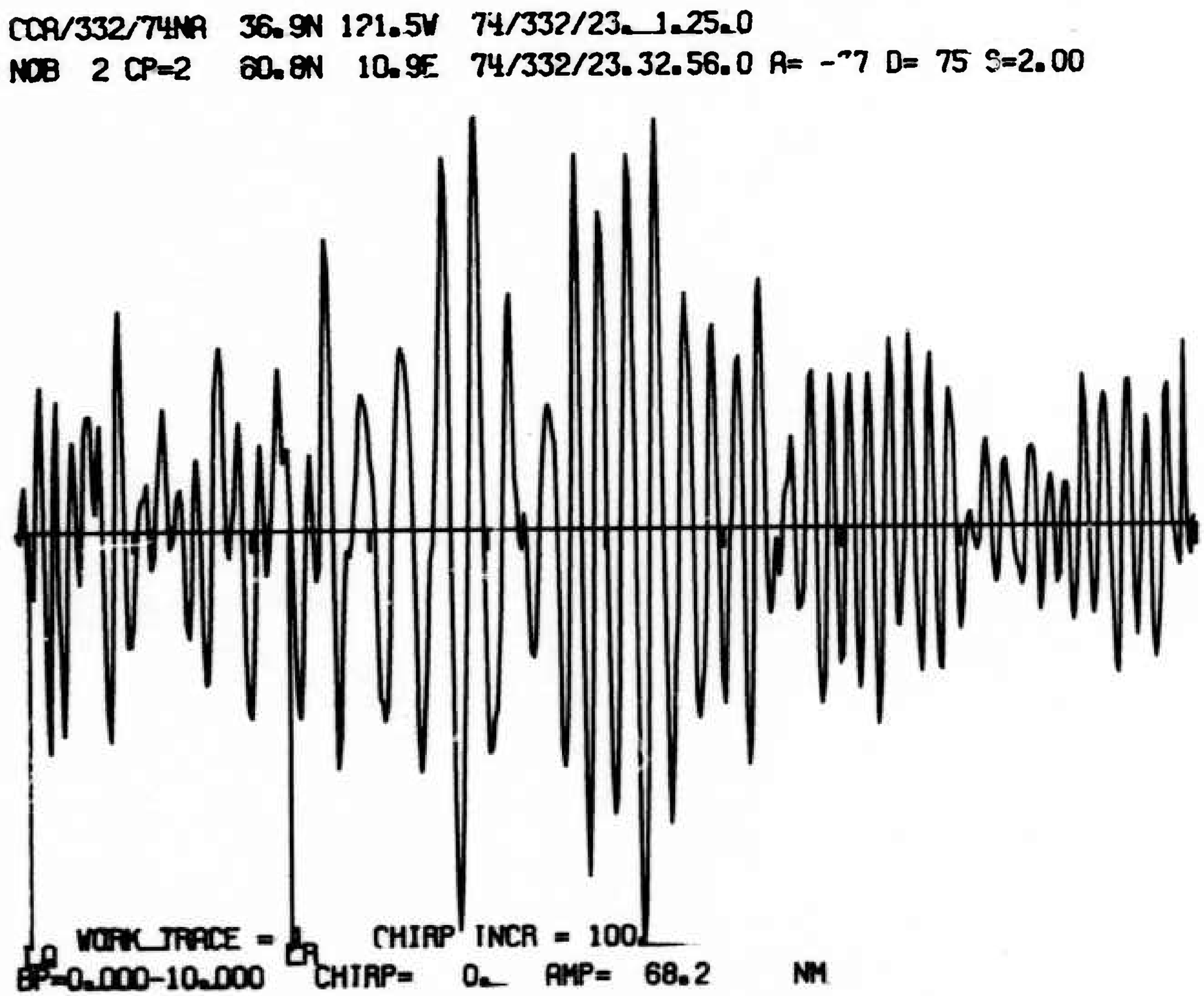

FIGURE A-5-b

THE LONG-PERIOD TRANSVERSE COMPONENT OF THE NOVEMBER 28, 1974 CENTRAL CALIFORNIA EARTHQUAKE AS RECORDED AT NORSAR

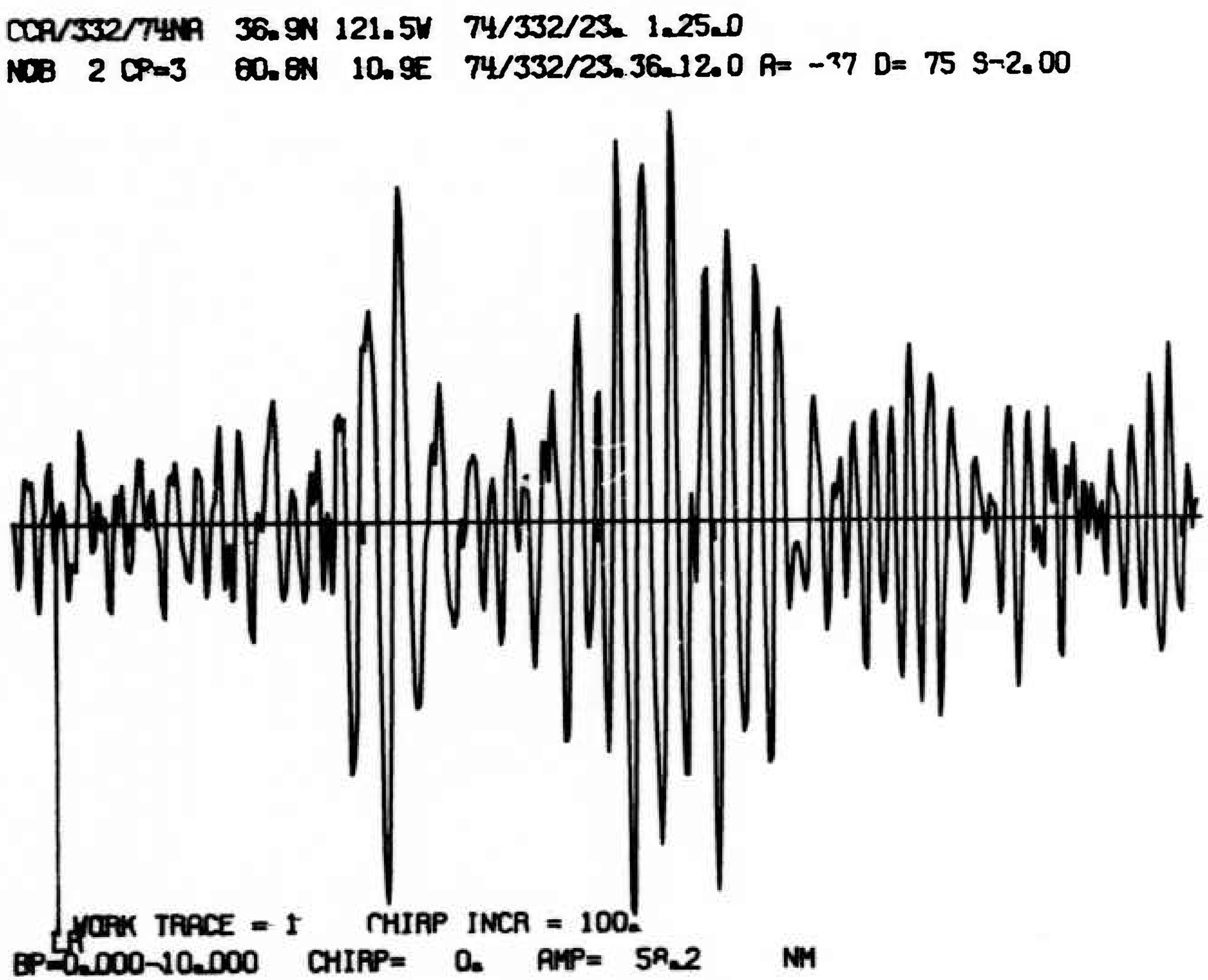

FIGURE A-5-c

THE LONG-PERIOD RADIAL COMPONENT OF THE NOVEMBER 28, 1974 CENTRAL CALIFORNIA EARTHQUAKE AS RECORDED AT NORSAR

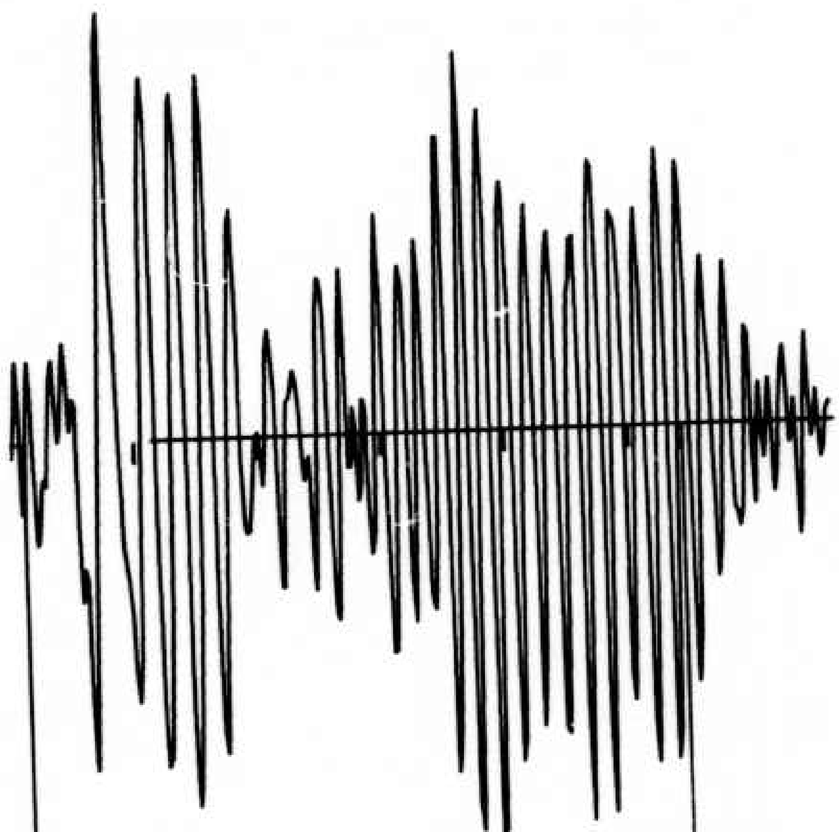

FIGURE A-6-a

THE LONG-PERIOD VERTICAL COMPONENT OF THE NOVEMBER 28, 1974 CENTRAL CALIFORNIA EARTHQUAKE AS RECORDED AT ALPA

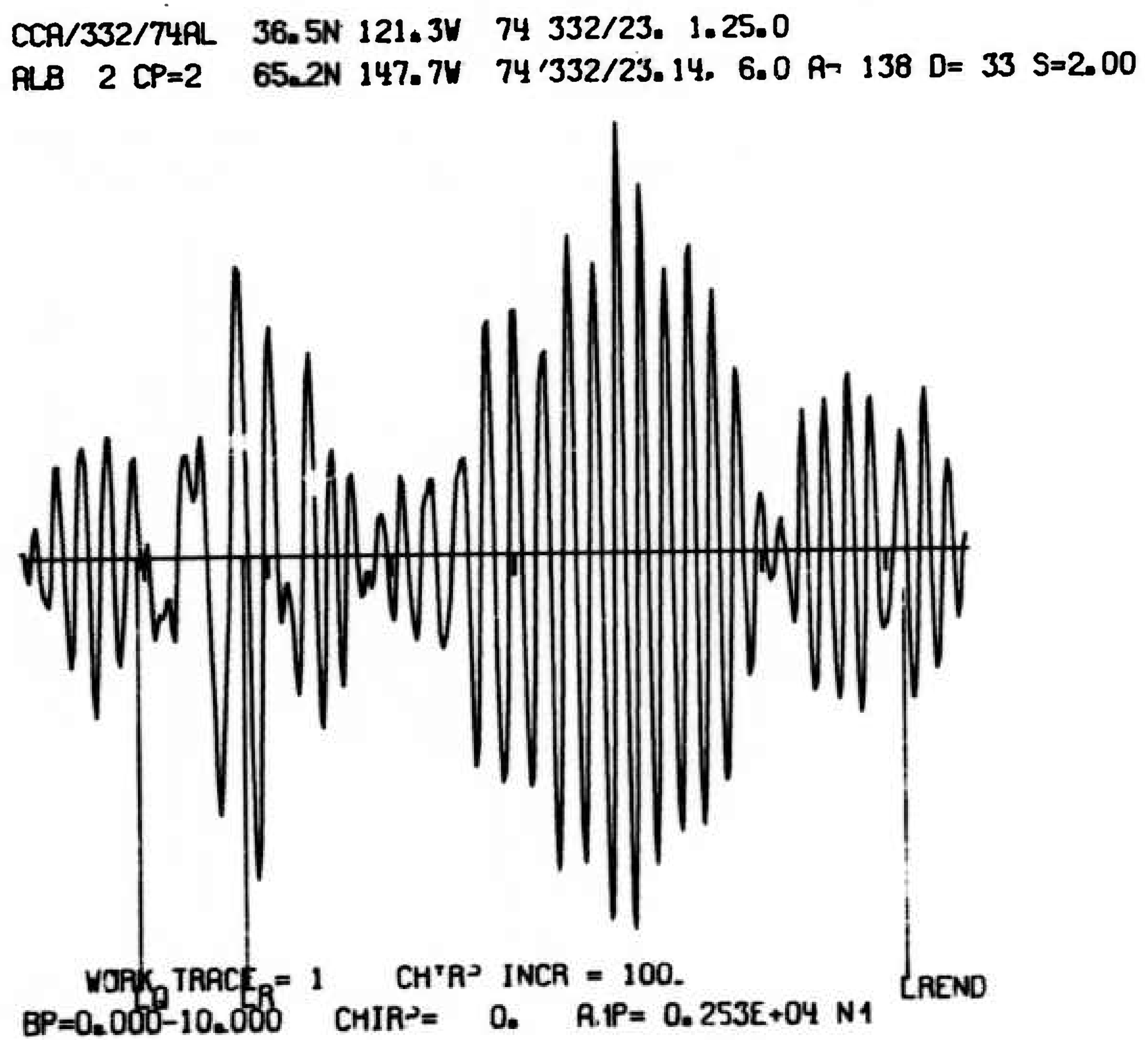

FIGURE A-6-b

THE LONG-PERIOD TRANSVERSE COMPONENT OF THE NOVEMBER 28, 1974 CENTRAL CALIFORNIA EARTHQUAKE AS RECORDED AT ALPA

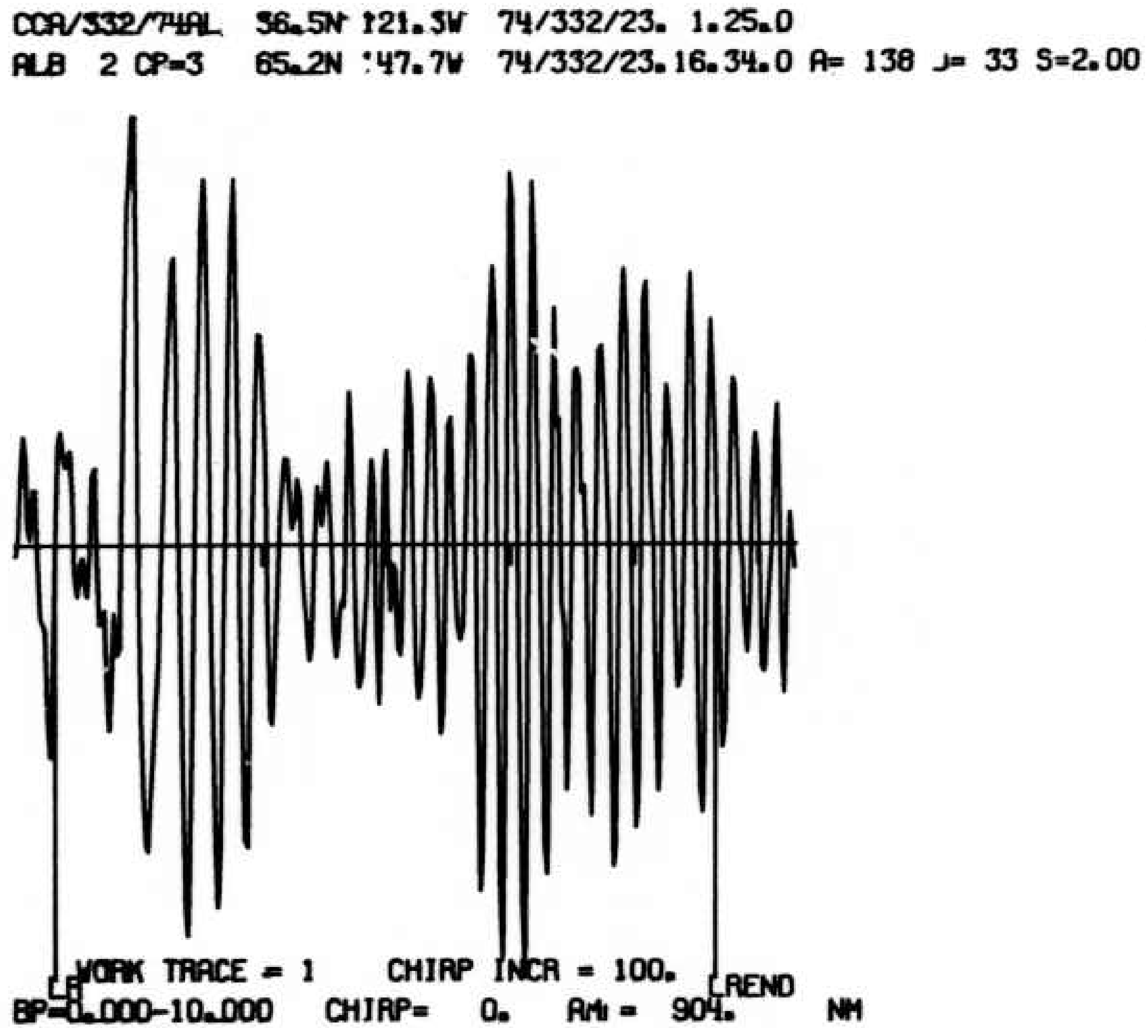

FIGURE A-6-c

THE LONG-PERIOD RADIAL COMPONENT OF THE NOVEMBER 28, 1974 CENTRAL CALIFORNIA EARTHQUAKE AS RECORDED AT ALPA

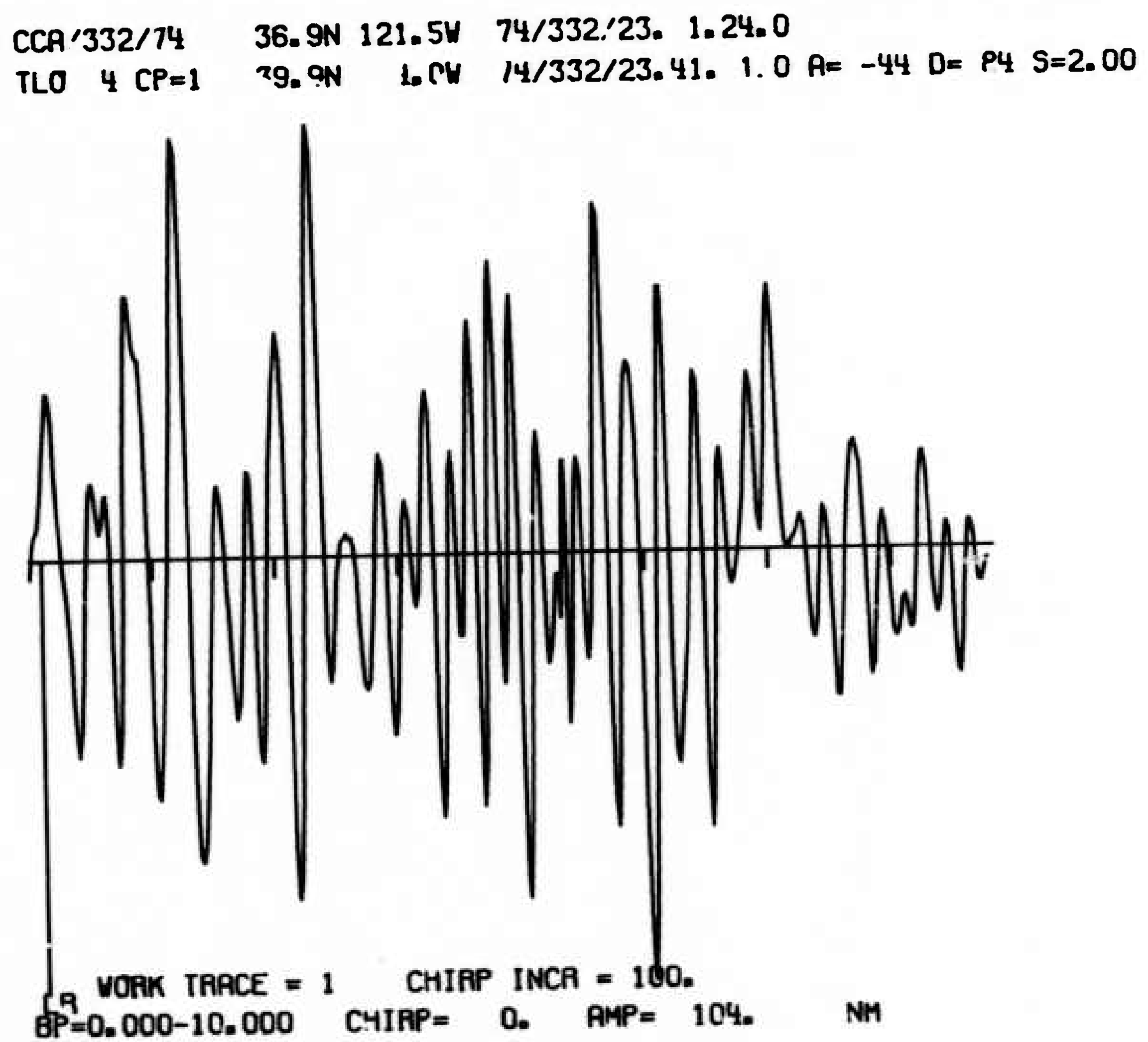

FIGURE A-7-a

THE LONG-PERIOD VERTICAL COMPONENT OF THE NOVEMBER 28, 1974 CENTRAL CALIFORNIA EARTHQUAKE AS RECORDED AT TLO

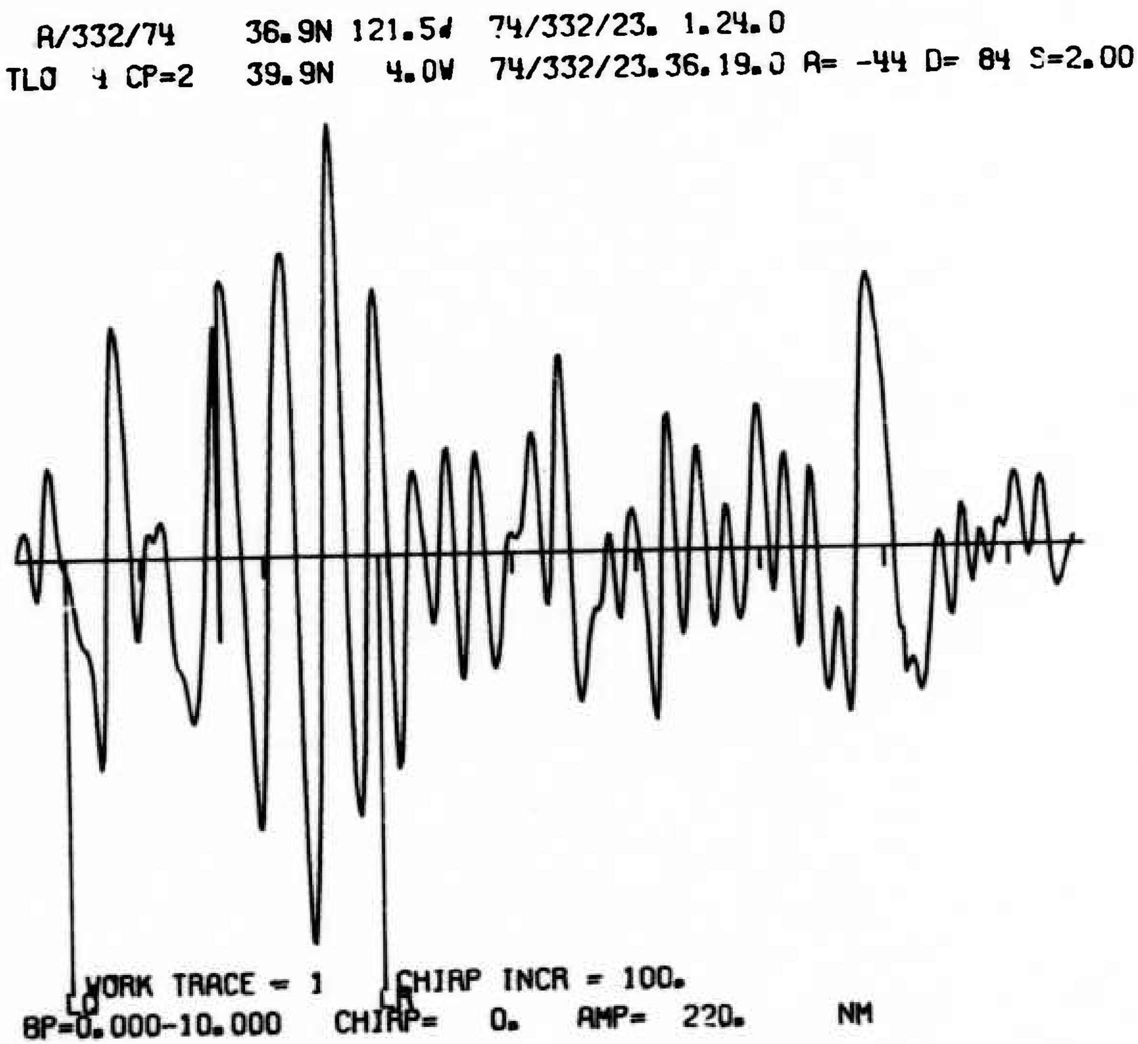

FIGURE A-7-b

THE LONG-PERIOD TRANSVERSE COMPONENT OF THE NOVEMBER 28, 1974 CENTRAL CALIFORNIA EARTHQUAKE AS RECORDED AT TLO

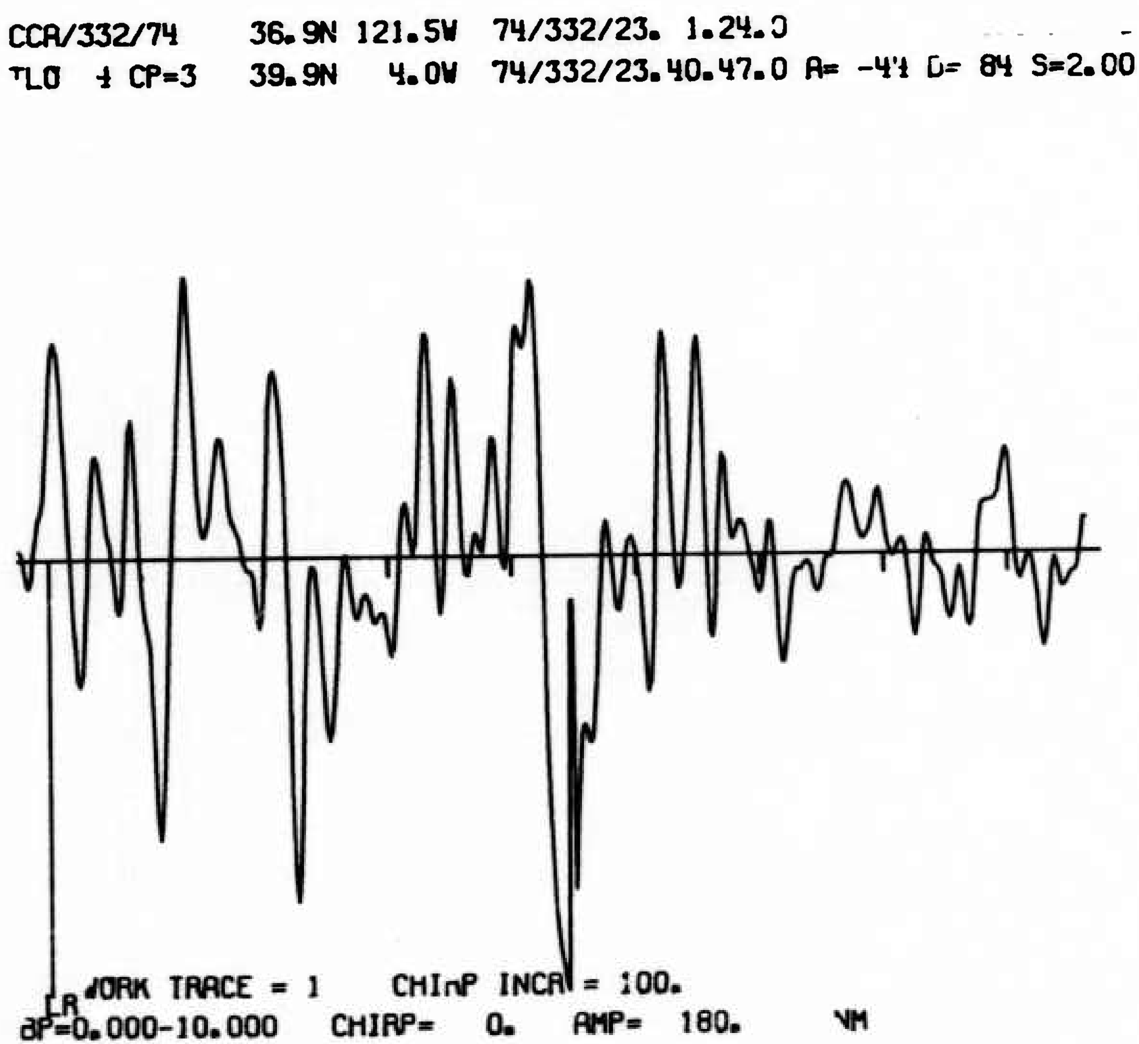

FIGURE A-7-c

THE LONG-PERIOD RADIAL COMPONENT OF THE NOVEMBER 28, 1974 CENTRAL CALIFORNIA EARTHQUAKE AS RECORDED AT TLO

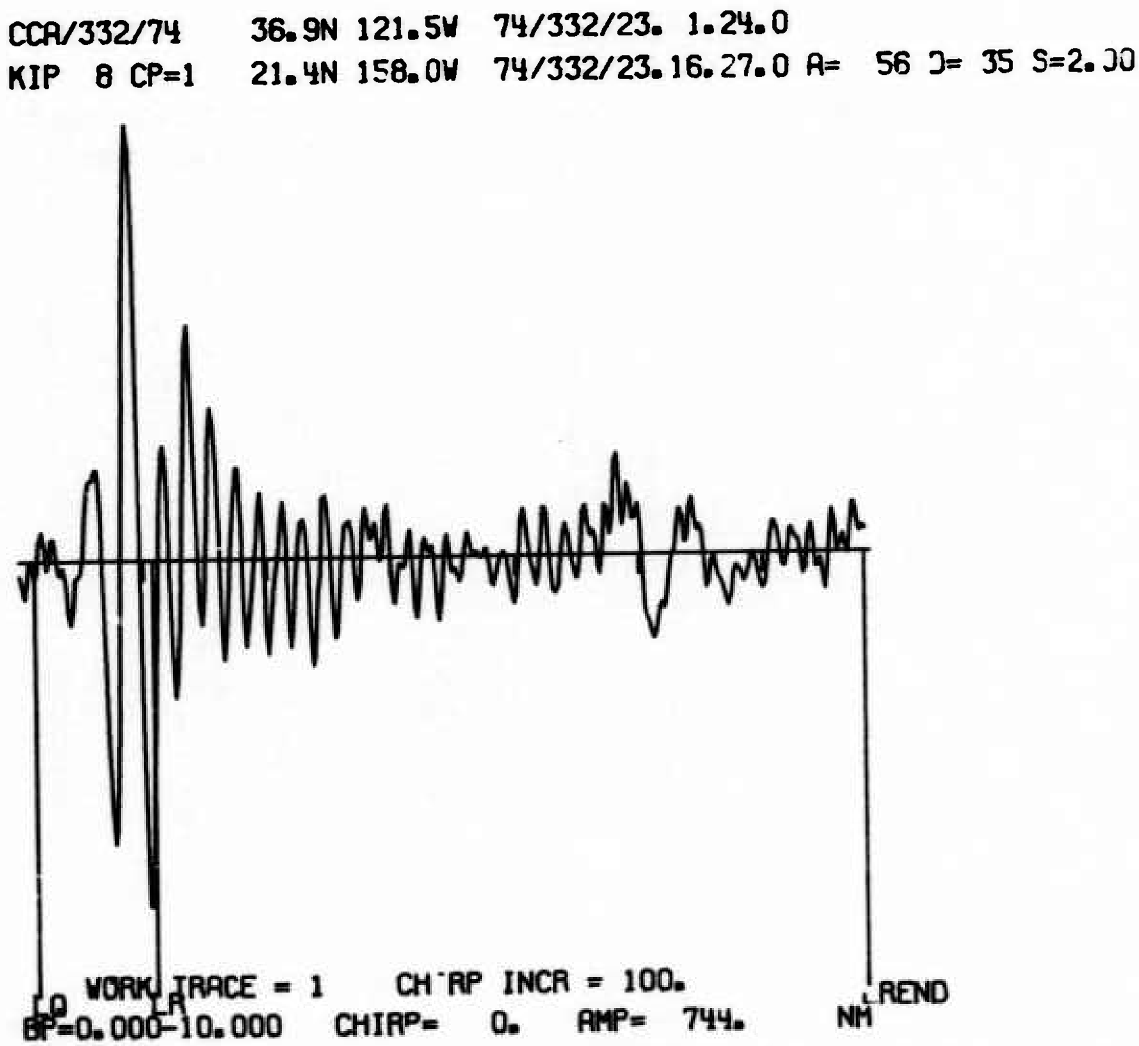

FIGURE A-8-a

THE LONG-PERIOD VERTICAL COMPONENT OF THE NOVEMBER 28, 1974 CENTRAL CALIFORNIA EARTHQUAKE AS RECORDED AT KIP

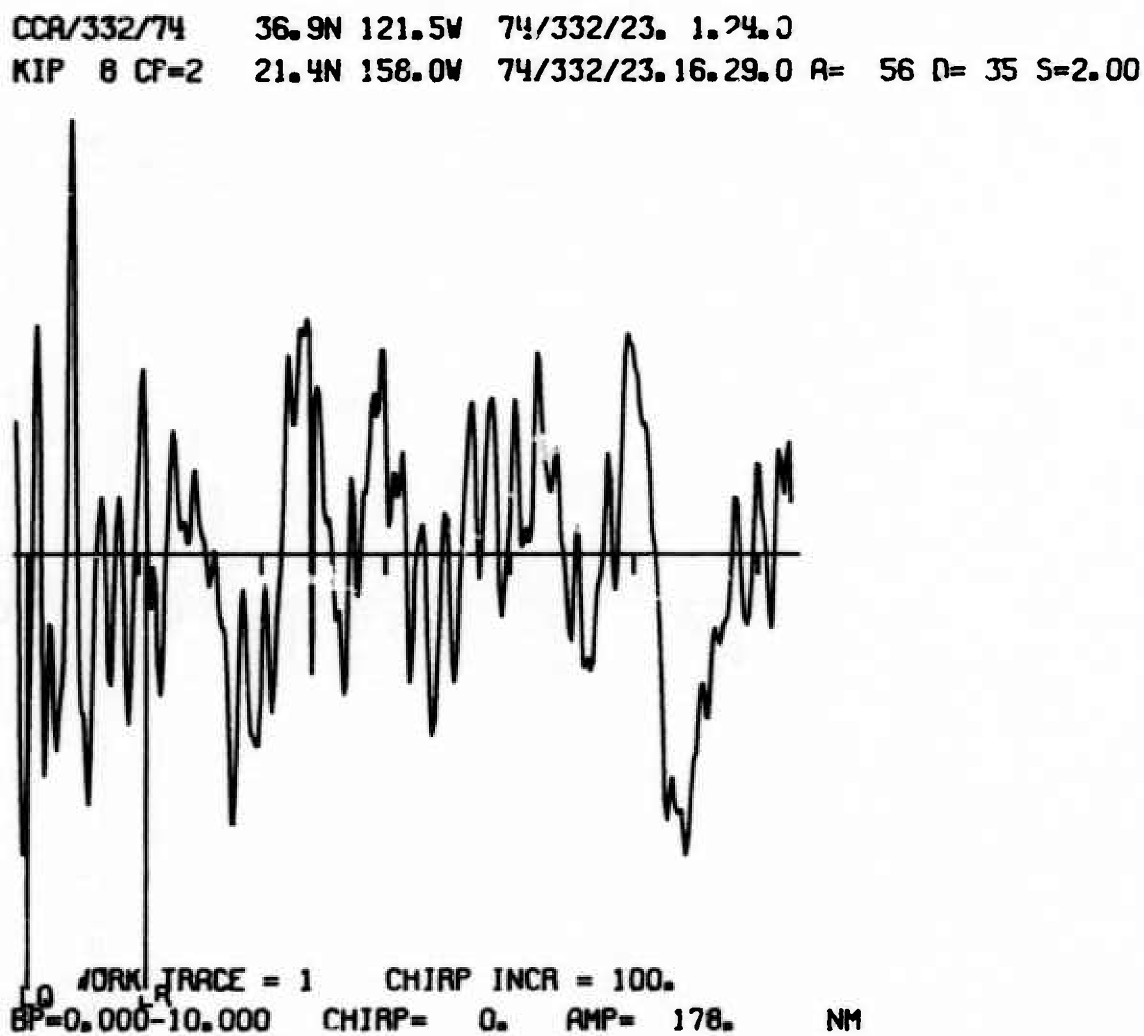

FIGURE A-8-6

THE LONG-PERIOD TRANSVERSE COMPONENT OF THE NOVEMBER 28, 1974 CENTRAL CALIFORNIA EARTHQUAKE AS RECORDED AT KIP

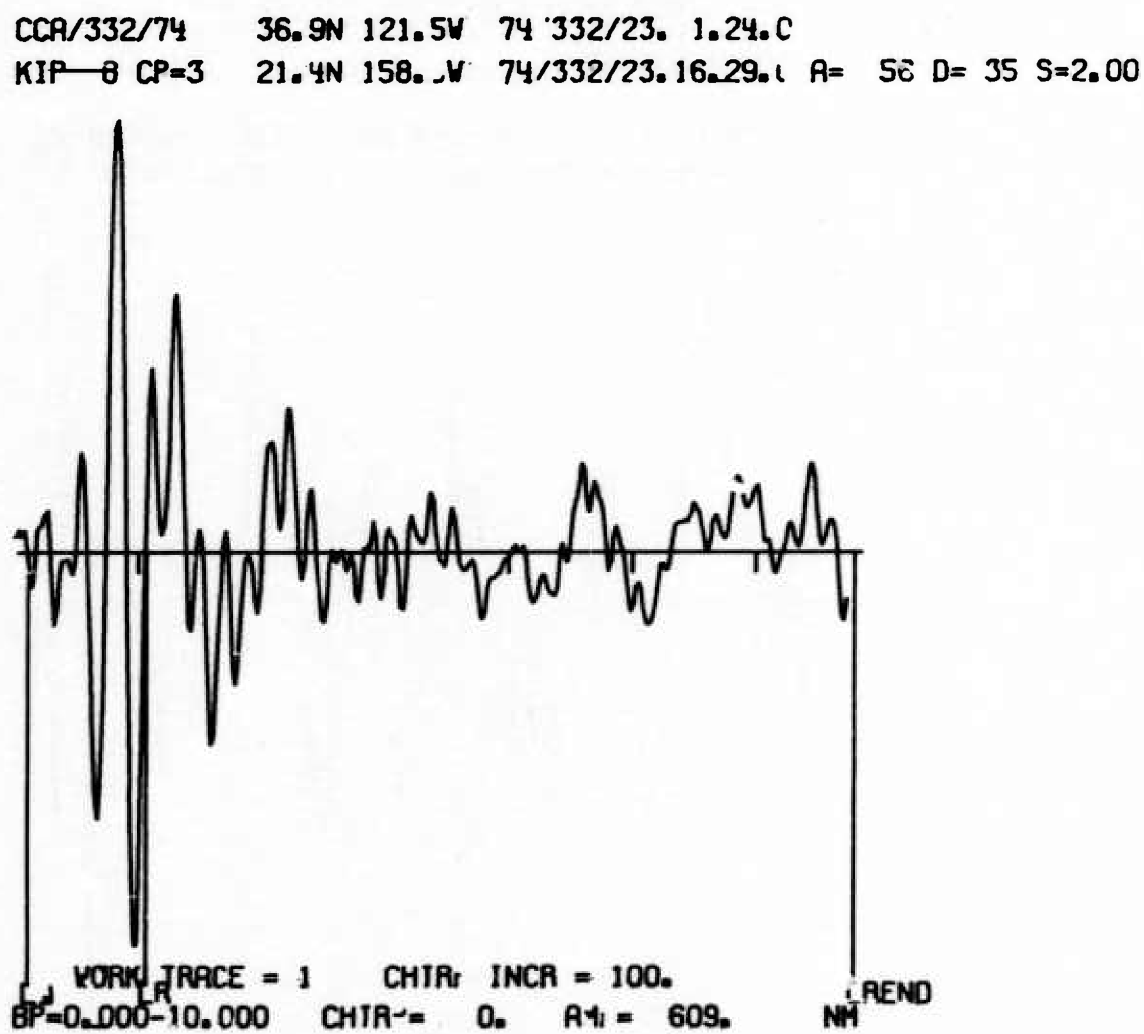

FIGURE A-8-c

THE LONG-PERIOD RADIAL COMPONENT OF THE NOVEMBER 28, 1974 CENTRAL CALIFORNIA EARTHQUAKE AS RECORDED AT KIP

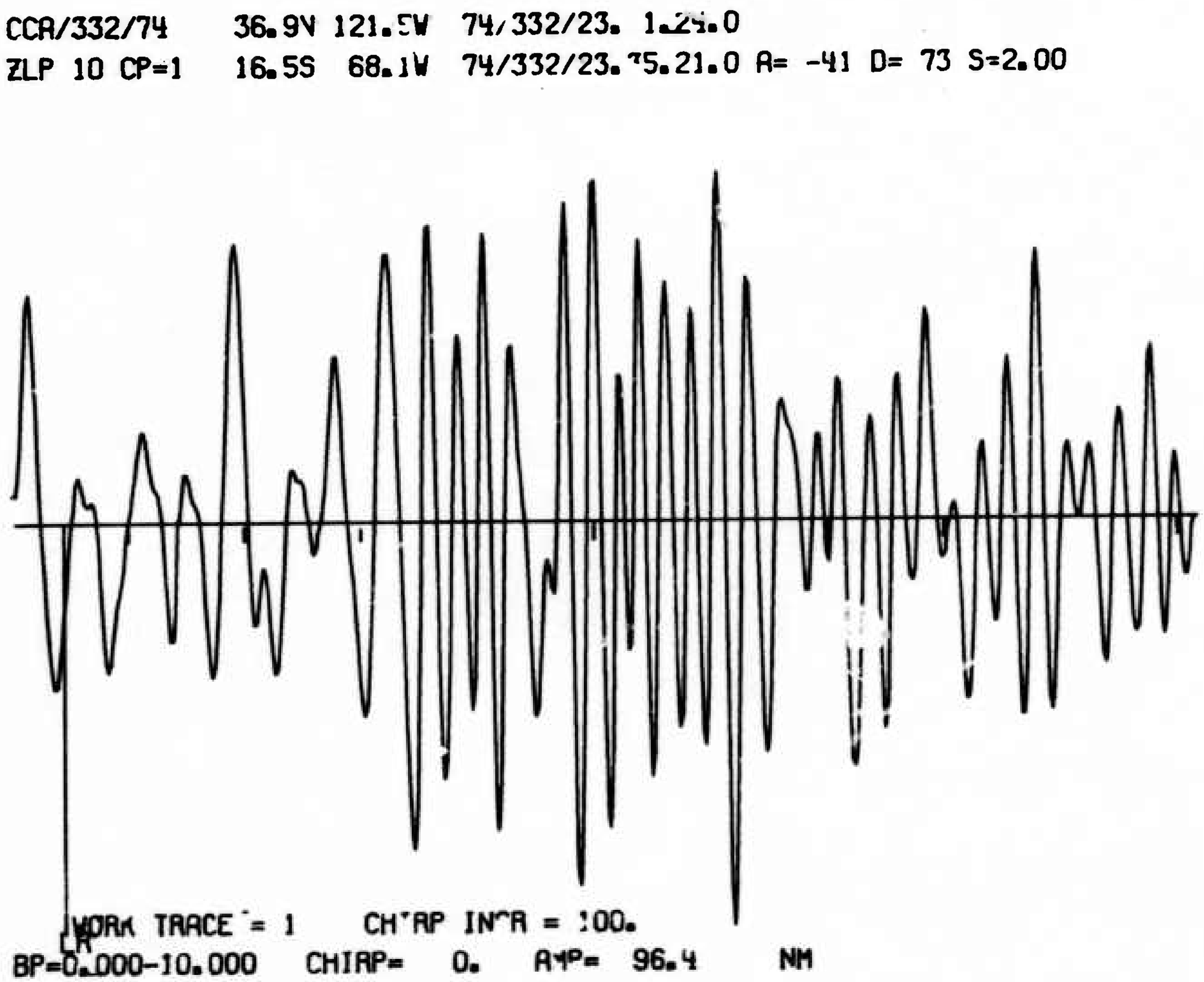

FIGURE A-9-a

THE LONG-PERIOD VERTICAL COMPONENT OF THE NOVEMBER 28, 1974 CENTRAL CALIFORNIA EARTHQUAKE AS RECORDED AT ZLP

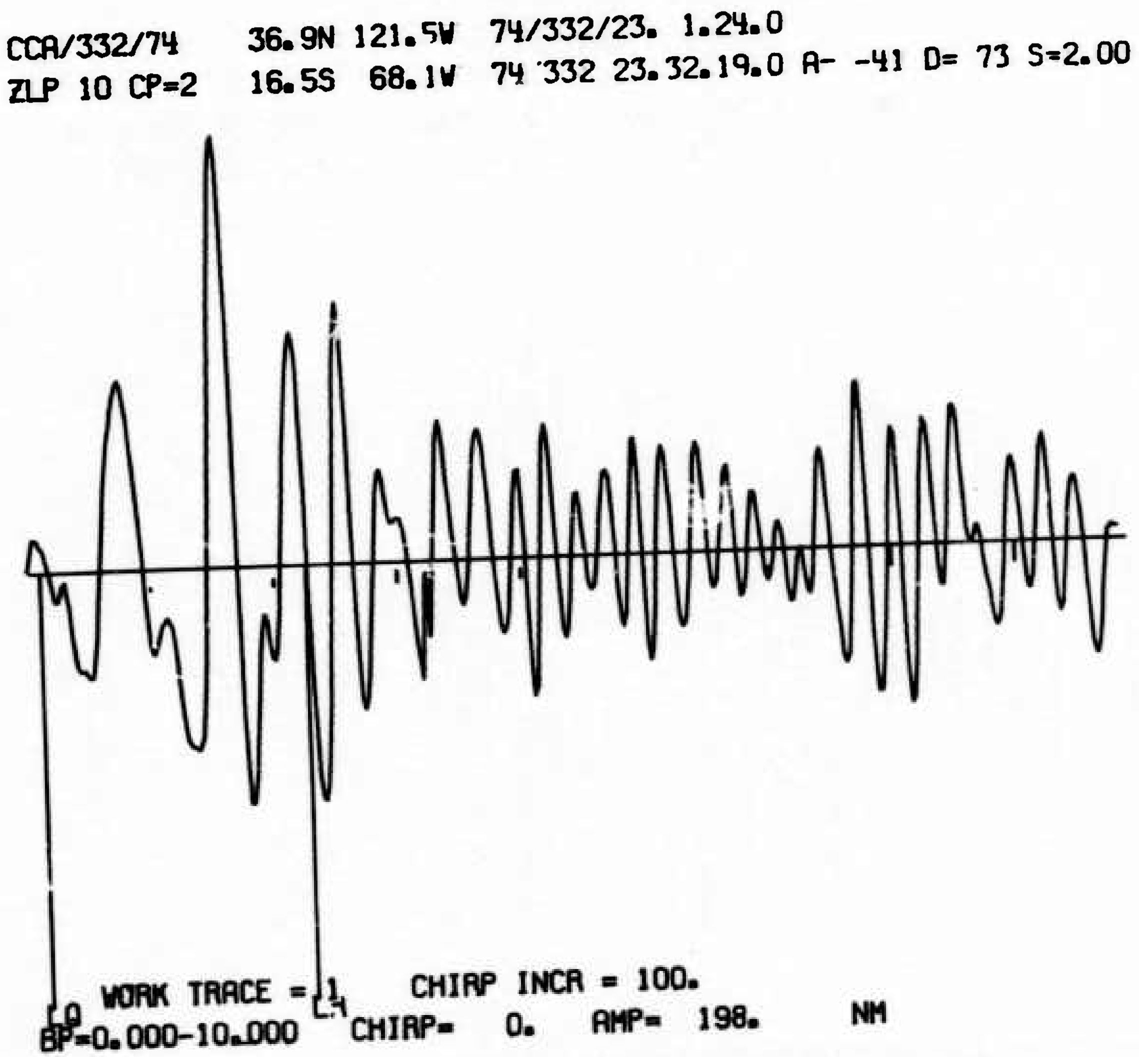

FIGURE A-9-b

THE LONG-PERIOD TRANSVERSE COMPONENT OF THE NOVEMBER 28, 1974 CENTRAL CALIFORNIA EARTHQUAKE AS RECORDED AT ZLP

CCA/332/74   36.9N 121.5W   74/332/23. 1.24 0
ZLP 10 CP=3   16.5S   68.1W   74 332/23.33.53.0 A= -41 D= 73 S=2.00

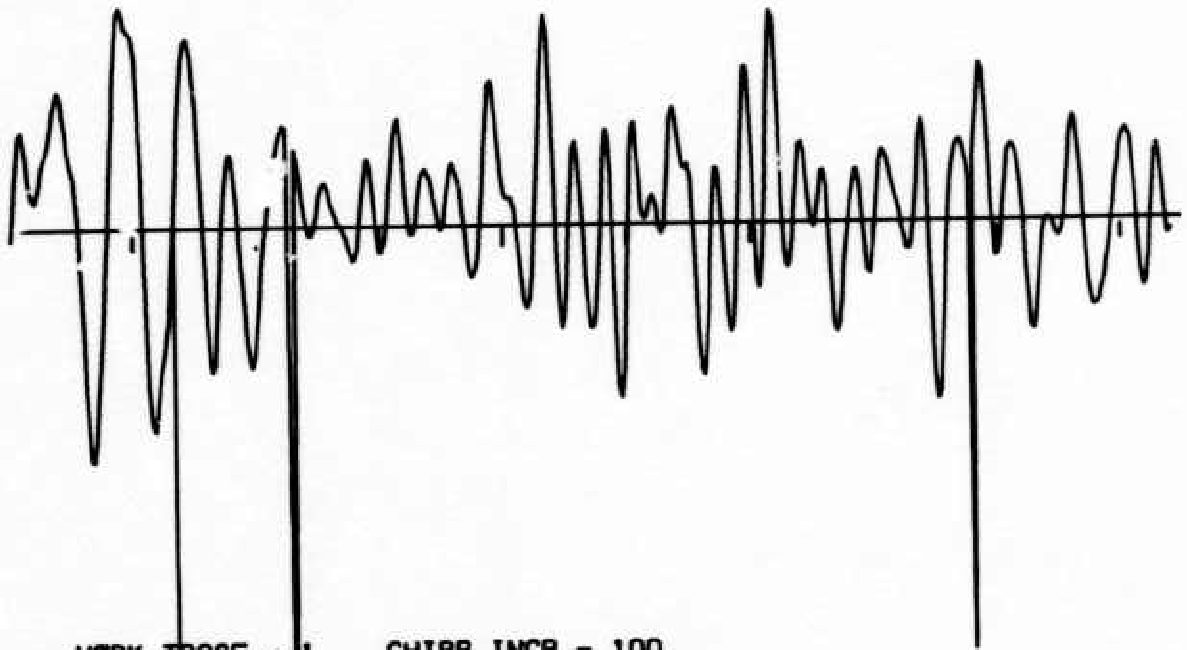

WORK TRACE = 1   CHIRP INCR = 100.
BP=0.000-10.000   CHIRP=   0.   AMP= 156.   NM

FIGURE A-9-c

THE LONG-PERIOD RADIAL COMPONENT OF THE
NOVEMBER 28, 1974 CENTRAL CALIFORNIA EARTHQUAKE
AS RECORDED AT ZLP

APPENDIX B

A PROCEDURE FOR DEMULTIPATHING SURFACE WAVES

As briefly described by Turnbull, et al. (1974b), a procedure for demultipathing surface waves has been implemented on the PDP-15 interactive graphics system. The motivation for implementing this procedure lies in obtaining path corrected spectral estimates, and possibly computing surface wave magnitudes (M_s). Figures B-1 through B-5 are reproductions of this procedure as displayed on the graphics system.

In Figure B-1, a Sinkiang earthquake as recorded at KON (vertical component) is shown. The heading on this figure and the others is as described in Appendix A. A series of narrow bandpass filters were run on the Rayleigh wave, and their effect is shown in Figures B-2-a and B-2-b. The center periods of these filters ranged from 10 seconds to 65 seconds, with 5 second increments. Next, a Hilbert transform was performed on each narrow bandpass filtered trace to obtain the envelope function (Figures B-3-a and B-3-b). The largest peaks of the envelope (up to four in quantity) were then chosen by the analyst. These picks, which represent group velocity arrivals at each period, are then compared to theoretical (oceanic and continental) group velocity dispersion curves (Figure B-3). The point at each period which most closely matched the trend of the appropriate dispersion curve is then chosen, and they form the corrected amplitude speccra (Figure B-5).

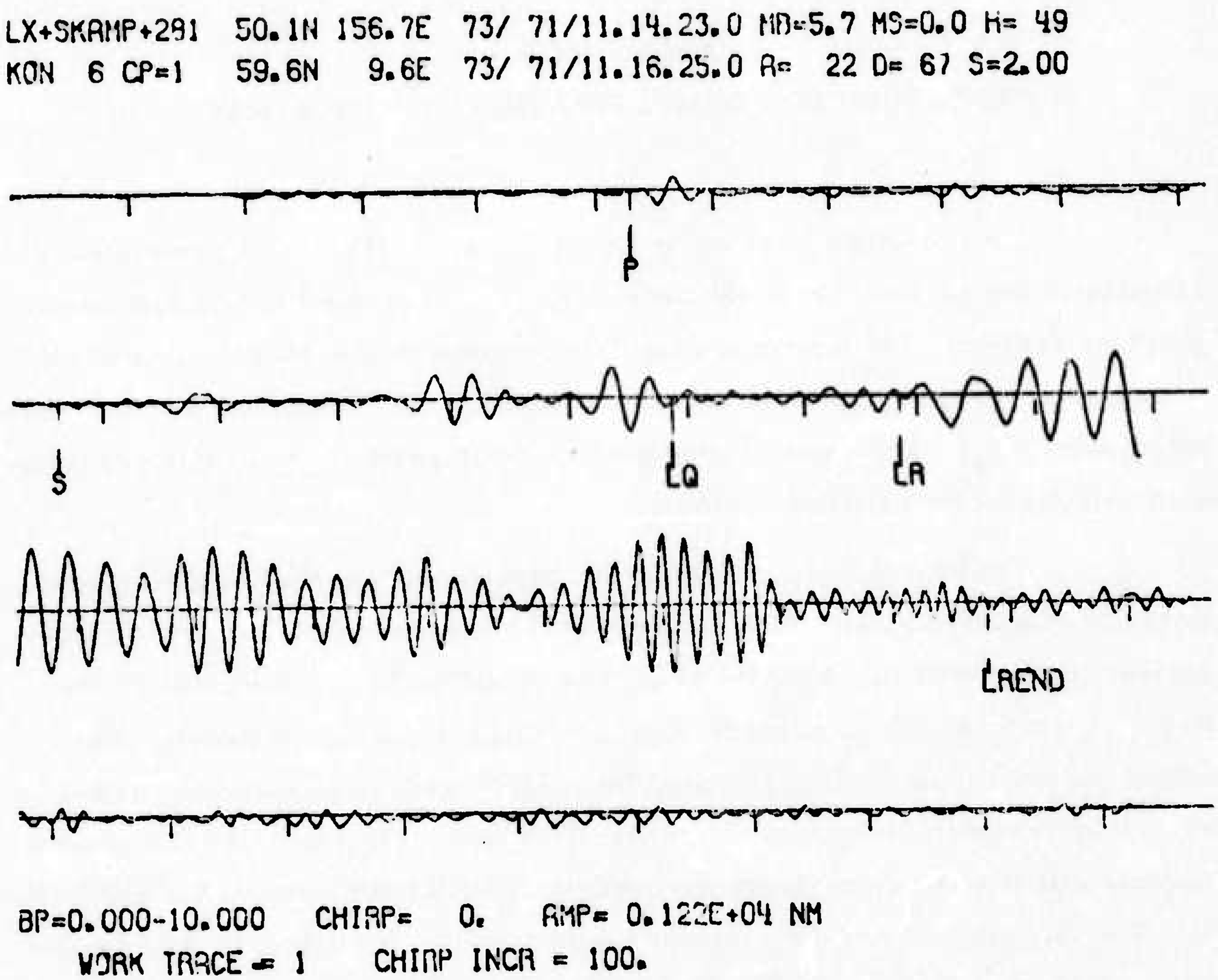

FIGURE B-1

DISPLAY OF A SINKIANG EARTHQUAKE AS RECORDED ON THE VERTICAL COMPONENT AT KON

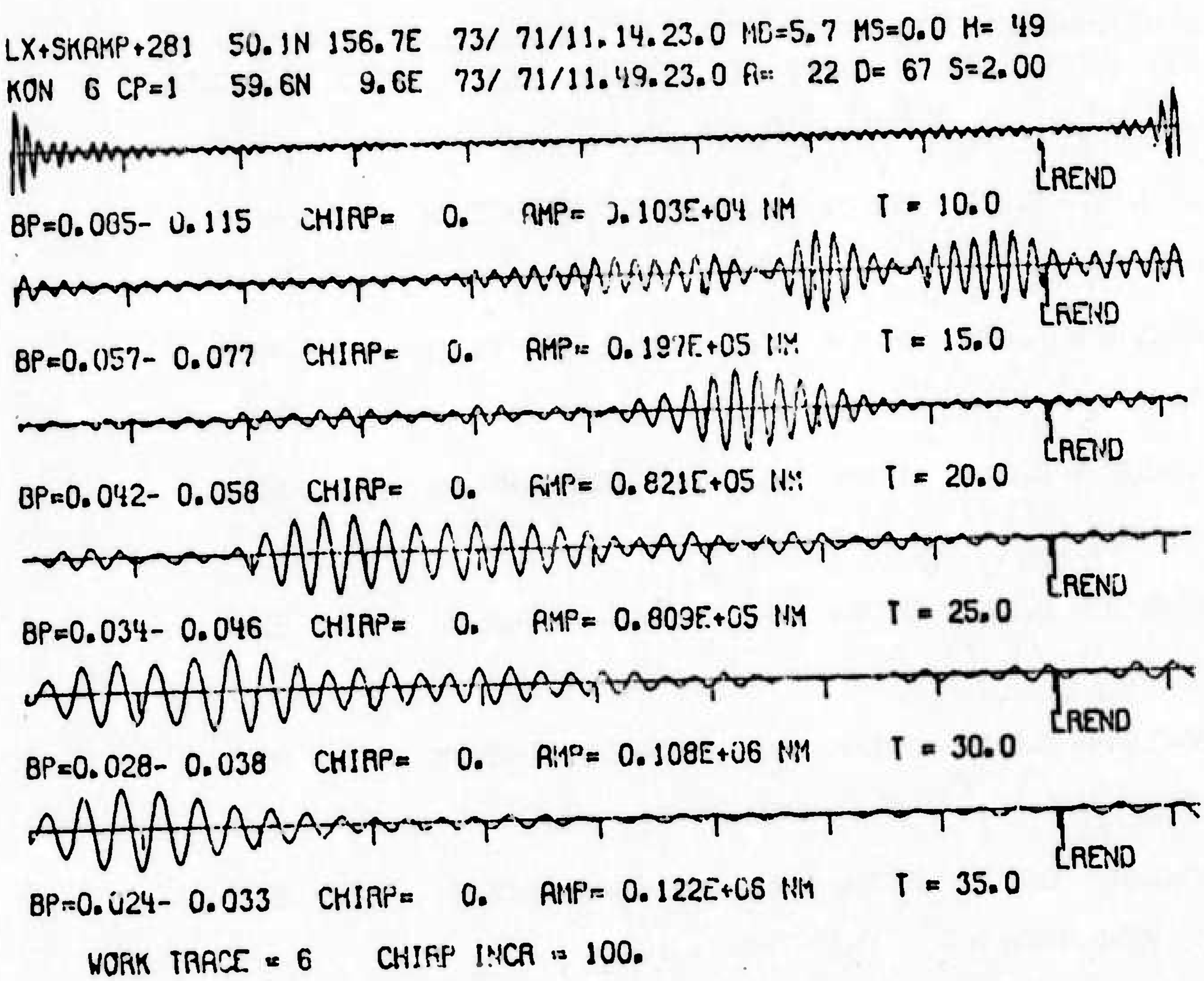

FIGURE B-2-a

THE EFFECT OF NARROW BANDPASS FILTERS ON THE RAYLEIGH WAVE ON THE SINKIANG EVENT: 10 TO 35 SECONDS PERIOD

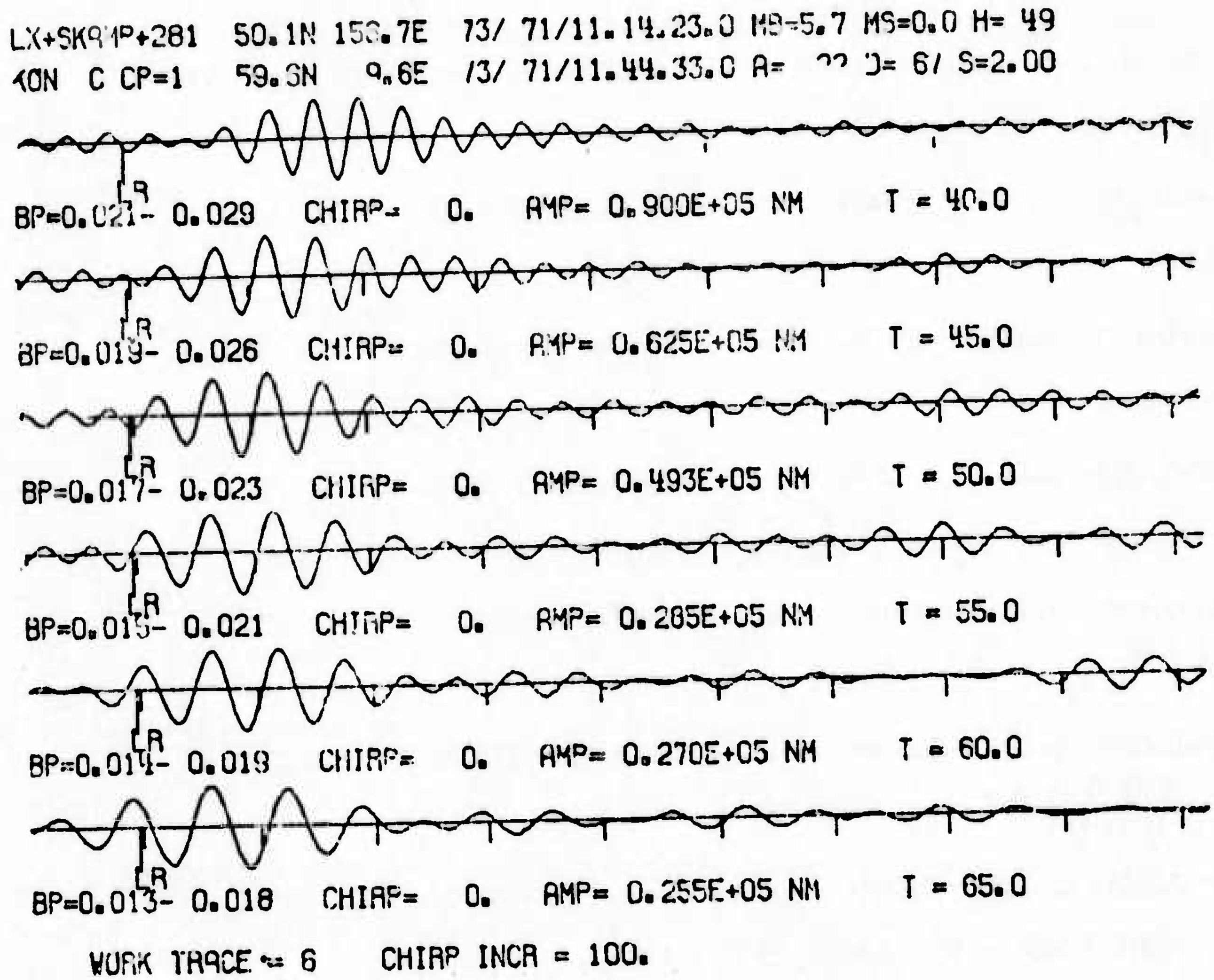

FIGURE B-2-b

THE EFFECT OF NARROW BANDPASS FILTERS ON THE RAYLEIGH WAVE ON THE SINKIANG EVENT: 40 TO 65 SECONDS PERIOD

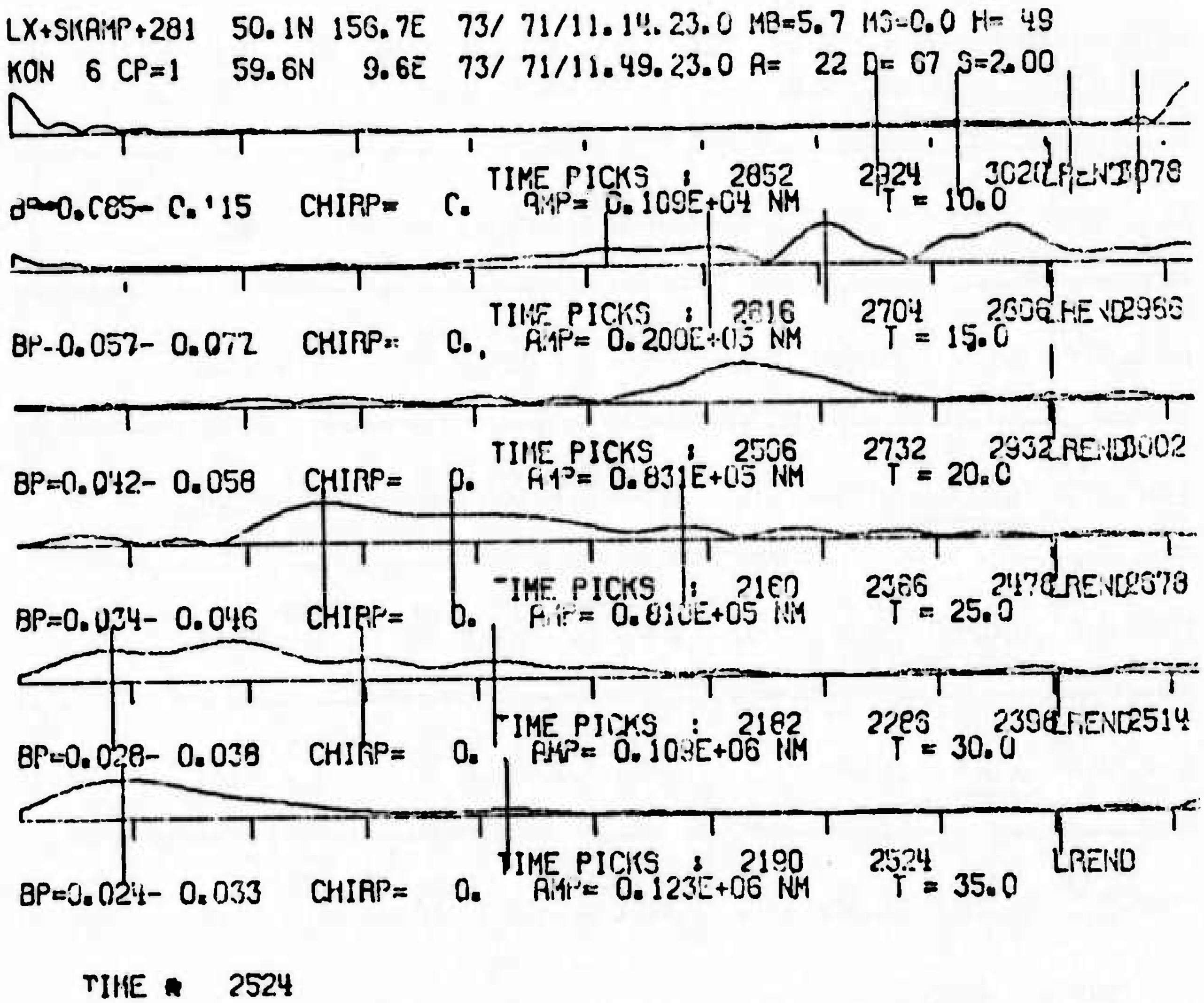

FIGURE B-3-a

THE ENVELOPE FUNCTION OF THE BANDPASS RESULTS WITH PEAK CHOICES: 10 TO 35 SECONDS PERIOD

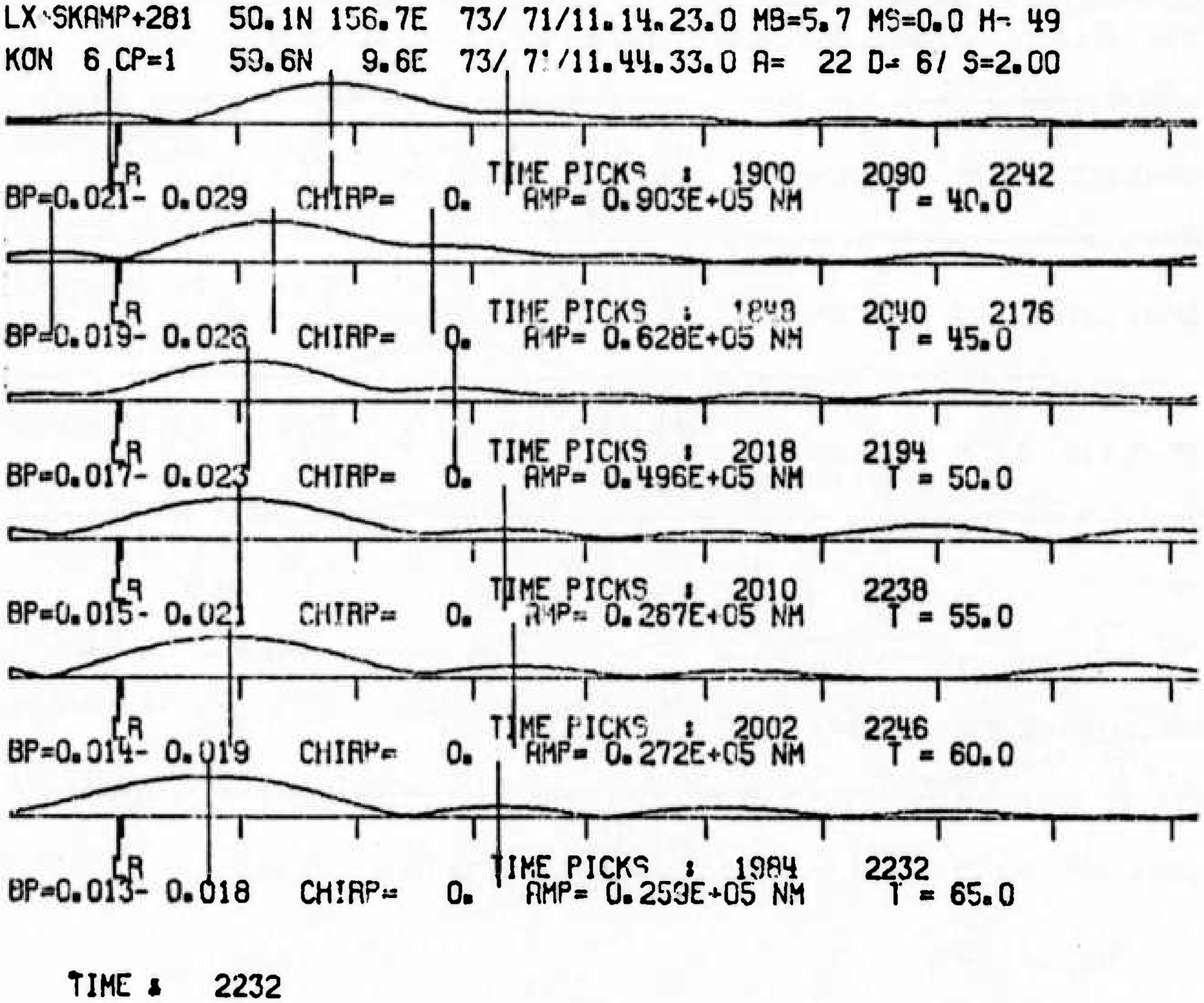

FIGURE B-3-b

THE ENVELOPE FUNCTION OF THE BANDPASS RESULTS WITH PEAK CHOICES: 40 TO 65 SECONDS PERIOD

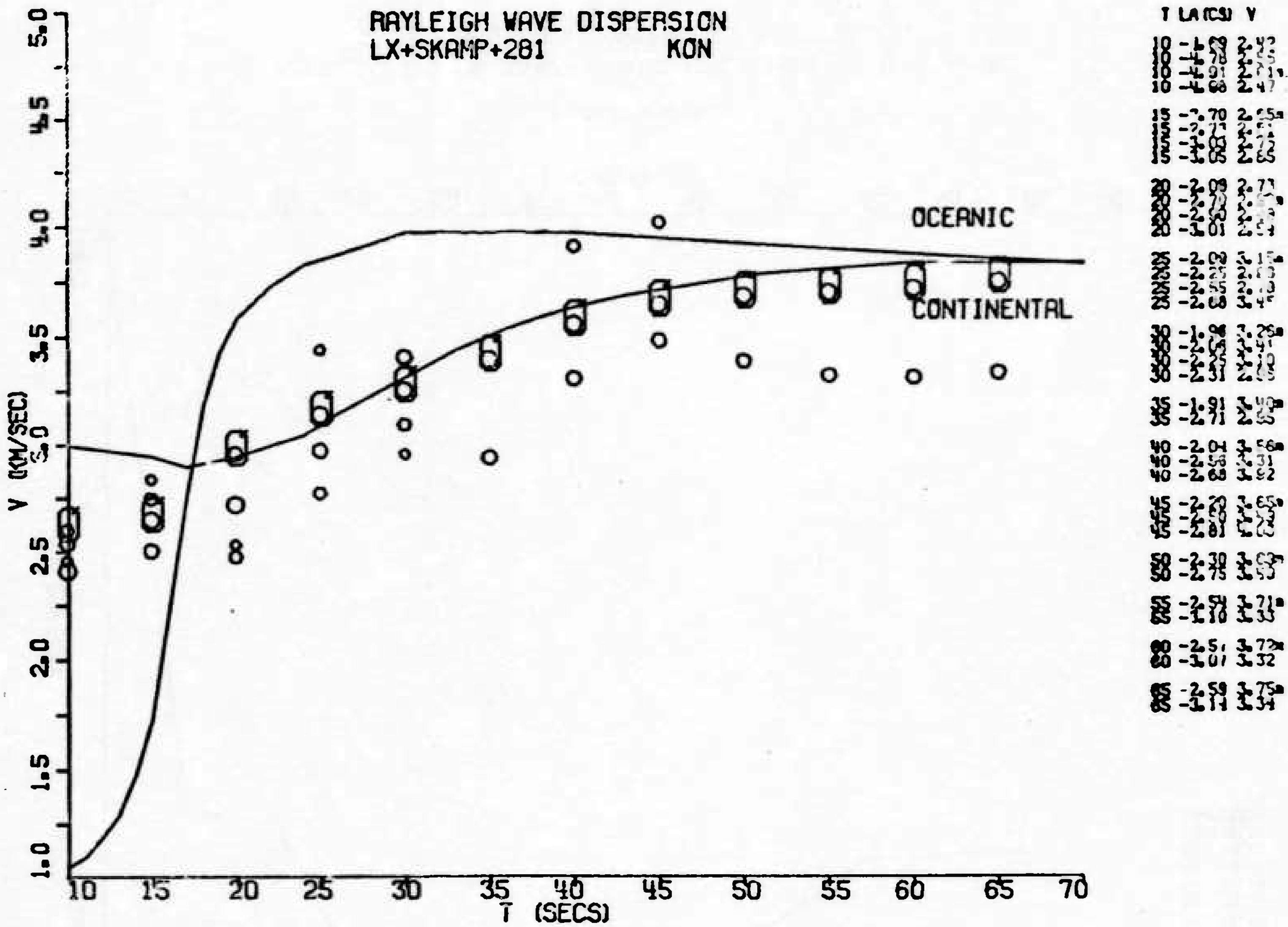

FIGURE B-4

GROUP VELOCITY PICKS (AS CHOSEN FROM ENVELOPE FUNCTION) DISPLAYED WITH THEORETICAL DISPERSION CURVES- FINAL PICKS INDICATED BY LARGE CIRCLES

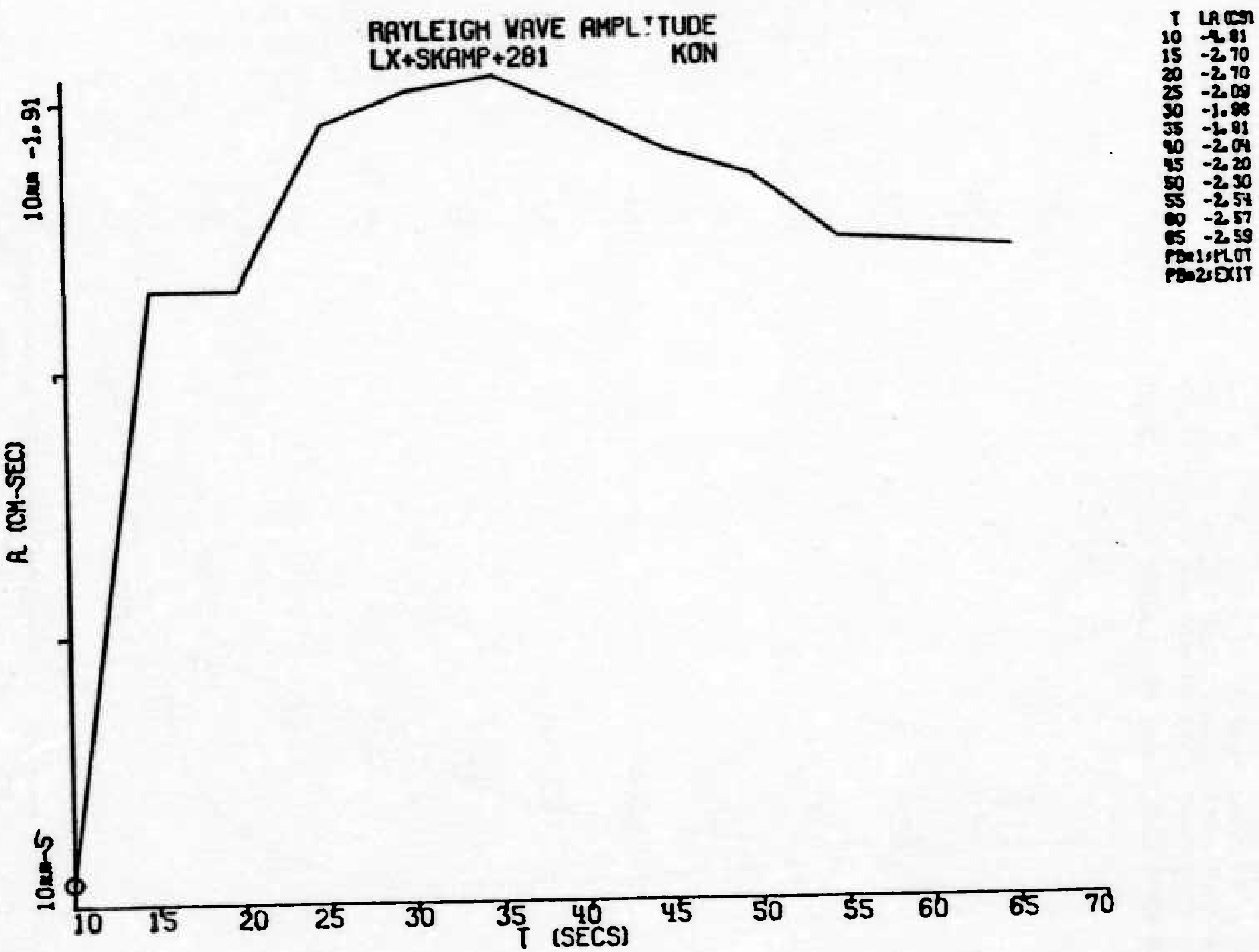

FIGURES B-5

RAYLEIGH WAVE AMPLITUDE SPECTRA AS OBTAINED
FROM DEMULTIPATHING PROCEDURE

UNCLASSIFIED

SECURITY CLASSIFICATION OF THIS PAGE (When Data Entered)

(19) REPORT DOCUMENTATION PAGE

READ INSTRUCTIONS BEFORE COMPLETING FORM

1. REPORT NUMBER (18) AFOSR - TR-75-1559

2. GOVT ACCESSION NO.

3. RECIPIENT'S CATALOG NUMBER

4. TITLE (and Subtitle) (6) SOURCE STUDIES IN THE NEAR- AND FAR-FIELD.

5. TYPE OF REPORT & PERIOD COVERED: Semi-Annual Technical

6. PERFORMING ORG. REPORT NUMBER (14) TI-ALEX(02)-TR-75-01-PART-A

7. AUTHOR(s) (10) Lawrence S. Turnbull, Jr., James C. Battis, David Sun [redacted] Alan C. Strauss

8. CONTRACT OR GRANT NUMBER(s) (15) F44620-73-C-0055, ARPA Order-1827

9. PERFORMING ORGANIZATION NAME AND ADDRESS: Texas Instruments Incorporated, Equipment Group, Dallas, Texas 75222

10. PROGRAM ELEMENT, PROJECT, TASK AREA & WORK UNIT NUMBERS: ARPA Program Code No. F10

11. CONTROLLING OFFICE NAME AND ADDRESS: Advanced Research Projects Agency, Nuclear Monitoring Research Office, Arlington, Virginia 22209

12. REPORT DATE (11) 30 May 1975

13. NUMBER OF PAGES 106

14. MONITORING AGENCY NAME & ADDRESS (if different from Controlling Office): Air Force Office of Scientific Research /NP, 1400 Wilson Boulevard, Arlington, Virginia 22209

15. SECURITY CLASS. (of this report) UNCLASSIFIED

15a. DECLASSIFICATION DOWNGRADING SCHEDULE

16. DISTRIBUTION STATEMENT (of this Report)

(12) 109p.

APPROVED FOR PUBLIC RELEASE, DISTRIBUTION UNLIMITED.

17. DISTRIBUTION STATEMENT (of the abstract entered in Block 20, if different from Report)

(9) Semi-annual technical rept. no. 4 (Part A), 1 Nov 74-30 Apr 75,

18. SUPPLEMENTARY NOTES

ARPA Order No. 1827

19. KEY WORDS (Continue on reverse side if necessary and identify by block number)

Seismology
Near-Field Spectra
Maximum Entropy Spectra
Demultipathing
Far-Field Spectra
Higher Mode Spectra

A005 786

20. ABSTRACT (Continue on reverse side if necessary and identify by block number)

Examination of the seismic source from both the near- and far-fields has been undertaken. Using a discrete Fourier transform (DFT) and a maximum entropy spectral estimator on near-field acceleration data produced corner frequency and low frequency level estimates. This latter estimator eliminates leakage, thereby obtaining more accurate values for the high frequency end, with better roll-off values and definition of side lobes. When the → over

DD FORM 1 JAN 73 1473 EDITION OF 1 NOV 65 IS OBSOLETE

UNCLASSIFIED 405 076

SECURITY CLASSIFICATION OF THIS PAGE (When Data Entered)

Cont'd

20. continued

maximum entropy spectral estimator was applied to data from the Parkfield earthquake and the Bear Valley event of June 22, 1973, the lower frequency level was lower than that from the DFT in all cases.

Using spectral fitting procedures on fundamental mode surface wave data from two central California events, generally close agreement was obtained with source mechanism solutions from bodywaves. For the Bear Valley earthquake of June 22, 1973, the seismic moment obtained from the surface wave data was an order of magnitude smaller than that obtained from acceleration data. In an effort to reduce the scatter in $M_s - m_b$ plots for an earthquake population, several attempts were made to reduce the variance in M_s. Both demultipathing and correcting for the radiation pattern had no effect. It was concluded that the variance of m_b is the controlling factor. Finally, theoretical higher mode surface wave spectra was generated for a double couple source in a layered half space. Both the Rayleigh and Love wave higher mode spectra were found to vary shape dramatically as a function of source depth.